AFRL-PR-WP-TR-2004-2099

HIGH-EFFICIENCY SILICON CARBIDE (SiC) CONVERTERS

Delivery Order 0001: Development of High-Temperature, High-Power, High-Efficiency, High-Voltage Converters Using Silicon Carbide

Janna R. Bonds and Michael S. Mazzola, Ph.D.

Mississippi Center for Advanced Semiconductor Prototyping
Dept. of Electrical & Computer Engineering
Box 9571
Mississippi State University, MS 39765-9571

MARCH 2004

Final Report for 15 May 2001 – 18 May 2002

Approved for public release; distribution is unlimited.

STINFO FINAL REPORT

PROPULSION DIRECTORATE
AIR FORCE MATERIEL COMMAND
AIR FORCE RESEARCH LABORATORY
WRIGHT-PATTERSON AIR FORCE BASE, OH 45433-7251

NOTICE

USING GOVERNMENT DRAWINGS, SPECIFICATIONS, OR OTHER DATA INCLUDED IN THIS DOCUMENT FOR ANY PURPOSE OTHER THAN GOVERNMENT PROCUREMENT DOES NOT IN ANY WAY OBLIGATE THE U.S. GOVERNMENT. THE FACT THAT THE GOVERNMENT FORMULATED OR SUPPLIED THE DRAWINGS, SPECIFICATIONS, OR OTHER DATA DOES NOT LICENSE THE HOLDER OR ANY OTHER PERSON OR CORPORATION; OR CONVEY ANY RIGHTS OR PERMISSION TO MANUFACTURE, USE, OR SELL ANY PATENTED INVENTION THAT MAY RELATE TO THEM.

THIS REPORT HAS BEEN REVIEWED BY THE OFFICE OF PUBLIC AFFAIRS (ASC/PA) AND IS RELEASABLE TO THE NATIONAL TECHNICAL INFORMATION SERVICE (NTIS). AT NTIS, IT WILL BE AVAILABLE TO THE GENERAL PUBLIC, INCLUDING FOREIGN NATIONALS.

THIS TECHNICAL REPORT HAS BEEN REVIEWED AND IS APPROVED FOR PUBLICATION.

/s/

JAMES D. SCOFIELD, Ph.D.
Project Engineer
Electrical Technology Branch
Power Division
AFRL/PRPE

/s/

JOSEPH A. WEIMER
Chief, Electrical Technology Branch
Power Division
AFRL/PRPE

/s/

CYNTHIA A. OBRINGER
Deputy Chief
Power Division
AFRL/PRP

If your address has changed, if you wish to be removed from our mailing list, or if the addressee is no longer employed by your organization, please notify AFRL/PRPE, Wright-Patterson AFB, OH 45433-7251 to help maintain a current mailing list.

Copies of this report should not be returned unless return is required by security considerations, contractual obligations, or notice on a specific document.

REPORT DOCUMENTATION PAGE

Form Approved
OMB No. 0704-0188

1. REPORT DATE *(DD-MM-YY)*	2. REPORT TYPE	3. DATES COVERED *(From - To)*
March 2004	Final	05/15/2001 – 05/18/2002

4. TITLE AND SUBTITLE
HIGH-EFFICIENCY SILICON CARBIDE (SiC) CONVERTERS
Delivery Order 0001: Development of High-Temperature, High-Power, High-Efficiency, High-Voltage Converters Using Silicon Carbide

5a. CONTRACT NUMBER
F33615-01-D-2103-0001

5b. GRANT NUMBER

5c. PROGRAM ELEMENT NUMBER
62173C

6. AUTHOR(S)
Janna R. Bonds and Michael S. Mazzola, Ph.D.

5d. PROJECT NUMBER
1660

5e. TASK NUMBER
P0

5f. WORK UNIT NUMBER
BE

7. PERFORMING ORGANIZATION NAME(S) AND ADDRESS(ES)

Mississippi Center for Advanced Semiconductor Prototyping
Dept. of Electrical & Computer Engineering
Box 9571
Mississippi State University, MS 39765-9571

8. PERFORMING ORGANIZATION REPORT NUMBER

9. SPONSORING/MONITORING AGENCY NAME(S) AND ADDRESS(ES)

Propulsion Directorate
Air Force Research Laboratory
Air Force Materiel Command
Wright-Patterson AFB, OH 45433-7251

10. SPONSORING/MONITORING AGENCY ACRONYM(S)
AFRL/PRPE

11. SPONSORING/MONITORING AGENCY REPORT NUMBER(S)
AFRL-PR-WP-TR-2004-2099

12. DISTRIBUTION/AVAILABILITY STATEMENT
Approved for public release; distribution is unlimited.

13. SUPPLEMENTARY NOTES

14. ABSTRACT

A design based on a self- aligned, gate-implanted, trenched source-gate junction FET was selected for its near term technological readiness and its long term manufacturability. This project concentrated on several key processes required for the realization of a viable VJFET fabrication technology, namely, 1) Development of silicon carbide dry (plasma) etches; 2) Development of appropriate edge termination technology; and 3) Development of implantation and annealing recipes core to the design. Semiconductor devices, principally the Schottky barrier diode and the PiN junction rectifier, were fabricated to test design assumptions and to evaluate new process steps. The principal accomplishments of the effort can be summarized as follows: 1) The completion of a design for a 600-V self-aligned, gate-implanted, trench VJFET, shown to deliver blocking voltages in excess of 800 V, an specific on resistance as low as 5 mohm-cm2; 2) The development of critical VJFET and rectifier device fabrication processes, and 3) The demonstration of a multi-wafer PiN diode lot of 1.5 kV PiN diodes.

15. SUBJECT TERMS
silicon carbide, power devices, VJFET, pilot production, prototyping, plasma etching, manufacturability

16. SECURITY CLASSIFICATION OF:			17. LIMITATION OF ABSTRACT:	18. NUMBER OF PAGES	19a. NAME OF RESPONSIBLE PERSON (Monitor)
a. REPORT	b. ABSTRACT	c. THIS PAGE			James D. Scofield, Ph.D.
Unclassified	Unclassified	Unclassified	SAR	152	19b. TELEPHONE NUMBER *(Include Area Code)* (937) 255-5949

Standard Form 298 (Rev. 8-98)
Prescribed by ANSI Std. Z39-18

TABLE OF CONTENTS

CHAPTER Page

LIST OF TABLES

LIST OF FIGURES

FIGURE Page

FIGURE Page

FIGURE Page

EXECUTIVE SUMMARY

Contract F33615-01-D-2103 was awarded on 19 April 2001 as an Indefinite Delivery, Indefinite Quantity (IDIQ) contract with a ceiling of $13,553,119 and an anticipated expiration date of 31 October 2004. Multiple delivery orders were expected to be awarded under the IDIQ contract. Delivery Order no. 1, the subject of this final report, was awarded on 15 May 2001 and eventually funded to $1,553,478 with amendments.

The effort funded by this contract encompassed two principal objectives:

1. The continuation of a project funded by Contract F33615-00-C-2030, which created a silicon carbide semiconductor device prototyping capability at Mississippi State University known as the Mississippi Center for Advanced Semiconductor Prototyping (MCASP).
2. The extension of the earlier work, which demonstrated a power Schottky barrier diode (SBD) prototyped in pre-production lot size (i.e., many more parts than is typical of research), to a unipolar silicon carbide semiconductor power switch, the Vertical Junction Field Effect Transistor (VJFET).
3. The continued involvement by a direct commercialization partner, namely SemiSouth Laboratories, Inc., in the development of a realistic path to system insertion for the technology funded by this contract and its predecessor (F33615-00-C-2030), via a public/private partnership involving technology licensing and subcontracting.

The two larger objectives, the development a viable power semiconductor switch and the creation of a realistic commercial path to DoD system integrators (the large defense prime contractors) can not be accomplished in one delivery order. Delivery Order no. 1 begins at the beginning, namely the development of critical processes within the

previously established MCASP semiconductor processing facilities that support the VJFET design. A design based on a self-aligned, gate-implanted, trenched source-gate junction FET was selected for its near term technological readiness and its long term manufacturability. Delivery Order no. 1 concentrated on several key processes:

- Development of trenching-free silicon carbide dry (plasma) etches.
- Development of appropriate edge termination technology.
- Development of implantation and annealing recipes core to the design.

Semiconductor devices, principally the Schottky barrier diode and the PiN junction rectifier, were fabricated to test design assumptions and to evaluate new process steps.

This final report will focus on the single most important process resulting from this work, namely, the development of etch recipes suitable for use in the Lam 9400 Inductively Coupled Plasma (ICP) etcher for which all subsequent device work (funded by later delivery orders) has been based. The principal investigators of this project wish to acknowledge Ms. Janna Rea Bonds (now Janna R. B. Casady) for the report that follows, which was largely authored by her in partial fulfillment of the degree requirements for her Master of Science in Electrical Engineering at Mississippi State University. However, the activities funded by Delivery Order No. 1 required the dedicated effort of a team of engineers, technicians, and students at Mississippi State University and SemiSouth Laboratories, Inc.

The principal accomplishments of the effort funded by this contract can be summarized as follows:

- The completion of a design for a 600-V self-aligned, gate-implanted, trench VJFET with approximate active area of 0.55 mm^2. (In later delivery orders, this design is

shown to deliver blocking voltages in excess of 800 V, specific on resistance as low as 5 mΩ-cm^2, and multi-ampere current per die).

- The development of critical VJFET and rectifier device fabrication processes specific to large scale production capable equipment within MCASP. (Critical etch recipes are the principal accomplishment documented in this report).
- The demonstration through the fabrication of a multi-wafer PiN diode lot of 1.5 kV PiN diodes using implanted anode and guard-ring based edge terminations that have been adopted in the VJFET design.

The MCASP concept is continuing under subsequent delivery orders of F33615-01-D-2103, which have now reached five in number. In the spirit of the effort documented here, every effort will be made to introduce this device technology through the normal supplier chain so as to fulfill the promised benefits of SiC semiconductors into relevant DoD systems.

CHAPTER I

INTRODUCTION

Introduction to SiC Material Properties and Benefits

Silicon carbide (SiC) has been a material of growing interest over the past decade. Compared to more traditional semiconductors such as silicon (Si) and gallium arsenide (GaAs), SiC has much higher electric breakdown strength, thermal conductivity, saturated electron drift velocity, and much wider bandgap. These material properties make SiC very appealing for high-power, high-temperature, and high-frequency applications.

Structurally, SiC exhibits a one-dimensional polymorphism called polytypism [1,2,3]. It is the most prominent of a family of materials capable of this behavior [3]. Over 200 polytypes of SiC have been discovered with some of the more common shown in Table 1.1 [2]. SiC's basic structures (referred to as a bilayer) consist of a tetrahedron bond of four carbon (C) atoms with a Si atom in the middle [1]. The C-C or Si-Si and Si-C bond lengths are approximately 3.08 Å and 1.89 Å, respectively [1]. The individual binding energies and atomic structure of each polytype are similar; therefore, the distinguishing factor between the polytypes is the stacking sequence of the bilayers [3]. With respect to the lattice, bilayers can be positioned in one of three possible positions (arbitrarily assigned the notation A, B, or C) [3] and have a zinc-blende (cubic) or wurtzite (hexagonal) nature between Si and C atom bonds in adjacent bilayer planes [3].

Table 1.1

Lattice Structure Properties of Selected SiC Polytypes

After [2]

Polytype	Lattice Structure	Lattice constant ***a*** (Å)	Lattice constant ***c*** (Å)
3C-SiC	face-centered cubic	4.3590	-
2H-SiC	Hexagonal	3.0817	5.0394
4H-SiC	Hexagonal	3.079	10.254
6H-SiC	Hexagonal	3.0817	15.1183
8H-SiC	Hexagonal	3.079	20.146
15R-SiC	Rhombohedral	3.079	37.78
21R-SiC	Rhombohedral	3.079	52.88
27R-SiC	Rhombohedral	3.079	67.995
33R-SiC	Rhombohedral	3.079	83.10
51R-SiC	Rhombohedral	3.079	128.434
75R-SiC	Rhombohedral	3.079	188.867
84R-SiC	Rhombohedral	3.079	211.539
87R-SiC	Rhombohedral	3.079	219.094

Neighboring bilayers are rotated 60° with respect to one another in zinc-blende structures and are mirror images in wurtzite structure [3]. SiC is named according to its bilayer periodicity and structure by using a number to designate the number of bilayers in a period and a letter to denote overall structural symmetry. For example, 3C-SiC, commonly referred to as beta (β) SiC, has a three bilayer periodicity (ABCABC) and is cubic in structure. 2H-SiC has a two bilayer periodicity (ABAB) and is hexagonal in structure. 3C-SiC and 2H-SiC are the only two pure cubic and heaxagonal structures, respectively [3]. 4H-SiC and 6H-SiC have an overall crystal symmetry that is considered hexagonal, but in reality they possess a mixture of cubic and hexagonal bonds in a ratio of 1:1 in 4H-SiC and 2:1 in 6H-SiC [3]. The hexagonal family is commonly referred to as alpha (α) SiC [3]. Figure 1.1 shows the crystal structure of 3C-, 4H-, and 6H-SiC. Rhombohedral structure polytypes also exist with the most common being 15R.

Table 1.2 shows the mechanical, thermal, optical, and room temperature electrical properties of various SiC polytypes. Some properties (particularly electrical properties, such as effective mass, carrier mobility, and bandgap) vary widely between polytypes [2]. 3C-SiC is an appealing polytype because is has the smallest bandgap (~2.4eV) and one of the largest electron mobilities (~800 $cm^2/V*s$ in low doped material) and saturated drift velocity of all the known SiC polytypes [2], resulting from its reduced photon scattering due to high symmetry [3]. Generally speaking, the greater the wutzite component, the larger the bandgap [3]. Therefore, it is understandable that the bandgap is 2.4 eV [2], 3.26 eV [2], 3.02 eV [2], and 3.3 eV [3] for 3C-SiC, 4H-SiC, 6H-SiC, and 2H-SiC, respectively. The downfall of 3C-SiC is that it is not commercially available, unlike 4H-SiC and 6H-SiC, in bulk single-crystalline form suitable for homoepitaxy.

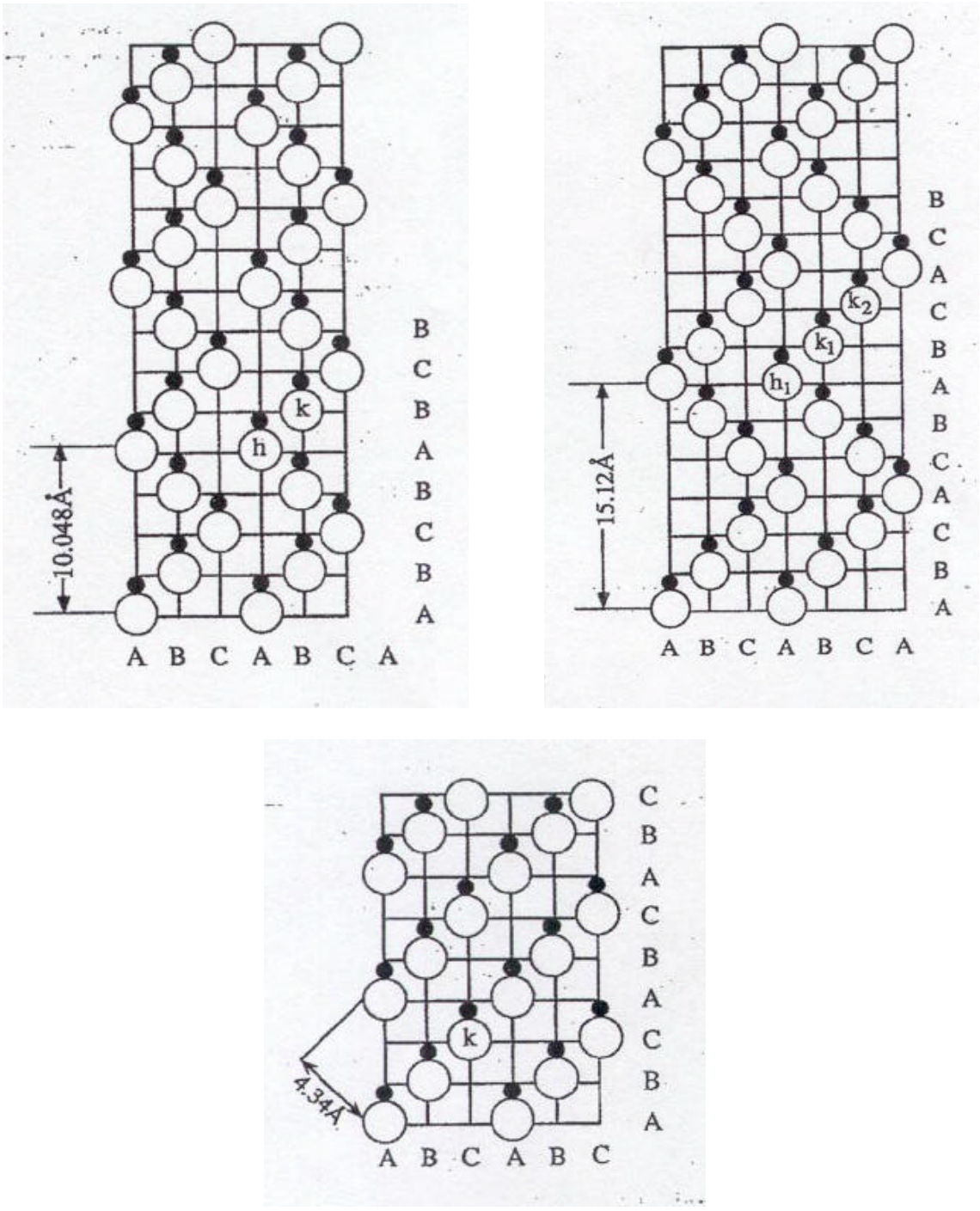

Figure 1.1 Crystal structure of 4H-, 6H-, and 3C-SiC After [3]

Table 1.2

Mechanical, Thermal, Optical and RT Electrical Properties of SiC Polytypes

After [1]

Type	**Property**	**Polytype**	**Value**	**Comments**
Mech.	Young's modulus (GPa)	3C	392-448	RT (≈300K)
	Mohs hardness	3C	≈ 9	
	Acoustic velocity (ms^{-1})	3C	12,600	RT, polycry.
Ther.	Thermal conductivity ($Wcm^{-1}K^{-1}$)	3C	4.9	RT
	Thermal expansion coefficient (K^{-1})	3C	$2.9x10^{-6}$	RT
	Decomposition temperature (°C)	3C	2839±40	35 atm
Opti.	Optical bandgap (eV)	3C	2.60, 2.4	LT (2-8K)
	Optical bandgap (eV)	3C	2.2	RT
	Exciton energy gap (eV)	3C	2.39	LT
Opti.	Exciton energy gap (eV)	2H	3.33	LT
Mech.	Mohs hardness	4H	≈ 9	
	Acoustic velocity (ms^{-1})	4H	13,730	20 K
Ther.	Thermal conductivity ($Wcm^{-1}K^{-1}$)	4H	4.9	⊥ c-axis
Opti.	Exciton energy gap (eV)	4H	3.265	LT
Elec.	Saturated electron drift velocity ($cm\ s^{-1}$)	4H	$2.0x10^{7}$	
	Breakdown electric field ($V\ cm^{-1}$)	4H	$2.2x10^{6}$	|| c-axis
Mech.	Bulk modulus (GPa)	6H	97	RT
	Mohs hardness	6H	≈ 9	
	Acoustic velocity (ms^{-1})	6H	13,260	RT
Ther.	Thermal conductivity ($Wcm^{-1}K^{-1}$)	6H	4.9	RT, ⊥ c-axis
	Thermal expansion coefficient (K^{-1})	6H	$4.68x10^{-6}$	700K,||c-axis
Opti.	Optical bandgap (eV)	6H	2.86	RT
	Exciton energy gap (eV)	6H	3.023	LT
Elec.	Saturated electron drift velocity ($cm\ s^{-1}$)	6H	$2.0x10^{7}$	|| c-axis
	Breakdown electric field ($V\ cm^{-1}$)	6H	$2.5x10^{6}$	|| c-axis
Opti.	Exciton energy gap (eV)	15R	2.986	LT

As mentioned elsewhere [2], it is important to note that material properties of SiC are often unreliable in the literature due to the lack of examination of temperature, test methods, material quality (mixed polytype material can easily be obtained), dopant concentration and dopant species for which many properties are highly dependant. An example of this problem is observed with thermal conductivity values reported for 6H-SiC as shown in Figure 1.2 along with 4H-SiC and 3C-SiC values. Table 1.3 summarizes the properties of 3C-SiC, 4H-SiC, 6H-SiC, and Si after examining the above factors. It is obvious that SiC has advantages over Si and GaAs in terms of thermal conductivity, electric field breakdown strength, bandgap, and velocity saturation when considering high-temperature, high-power, and high-frequency operation [2]. The electron velocity versus electric field intensity of GaAs, Si, and SiC are compared in Figure 1.3. SiC has larger optical phonon energies resulting in larger saturation velocities [3] and obviously performs well at high electric fields (300 kV/cm) [2].

Temperature influences all of the quantities shown in Table 1.3. In the following section mobility, intrinsic carrier concentration, bandgap, and thermal conductivity will be examined. Electron mobility (μ_e) and hole mobility (μ_h) are carrier velocity per unit drift field [2] and can vary widely depending on crystallographic orientation. The ratio of the electron mobility perpendicular to the c-axis over the electron mobility parallel to the c-axis [$(\mu_\perp)/(\mu_\parallel)$] for 4H-SiC is 0.7 at 300K compared to 6 for 6H-SiC which makes 4H-SiC a much more isotropic material [2]. As well as being temperature dependant, mobility is doping density dependant. Figure 1.4 shows mobility at room temperature as a function of total doping density for n and p-type Si (used as a reference), 4H-SiC, and 6H-SiC.

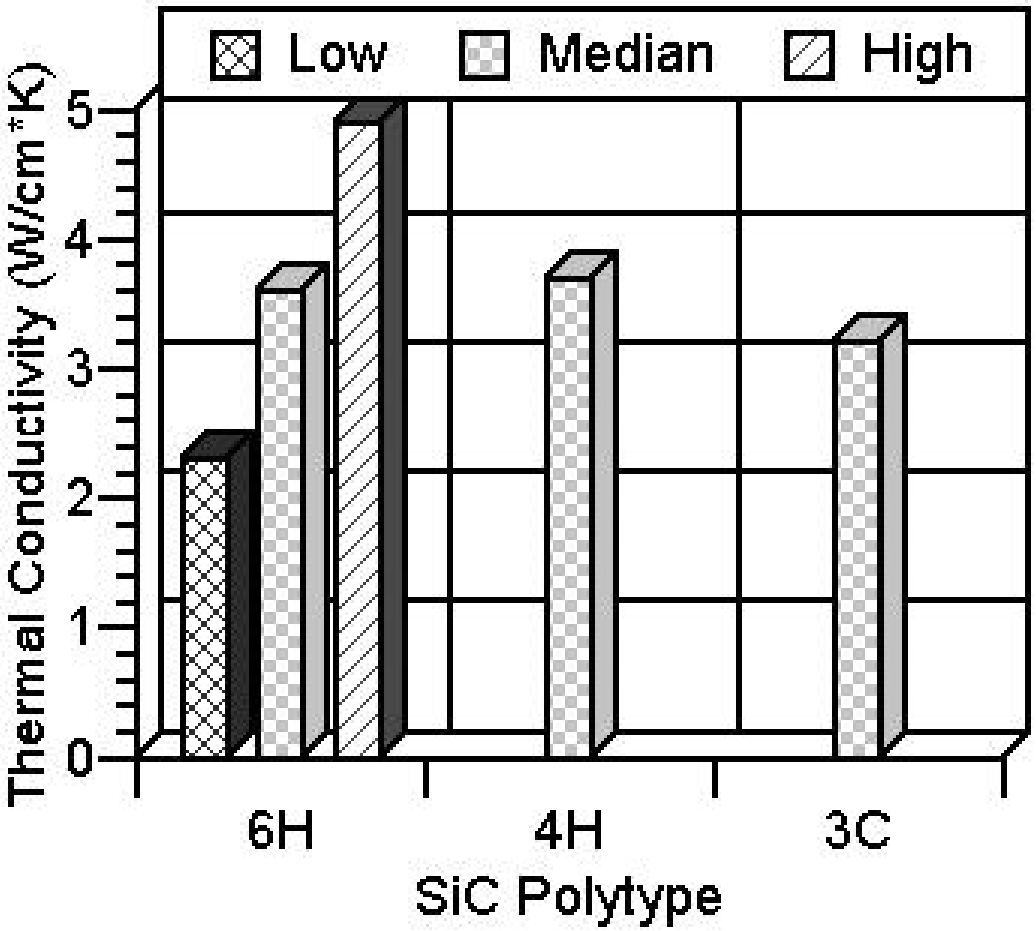

Figure 1.2 Thermal conductivity for different SiC polytypes After [2]

Table 1.3

Material Properties of Selected SiC Polytypes

After [2]

QUANTITY	**3C-SiC**	**4H-SiC**	**6H-SiC**	**Si**
E_g (eV) at T < 5 K	2.40	3.26	3.02	1.12
E_{crit} (MV/cm)	2.12	2.2	2.5	0.25
E_{crit} (N_D) (kV/cm)			$10.64 \bullet N_D^{0.142}$	
Θ_K (W/cm·K) at 300 K (doped at ~10^{17} cm^{-3})	3.2	3.7	4.9	1.5
n_i (cm^{-3}) at 300 K (doped at ~10^{17} cm^{-3})	$1.5x10^{-1}$	$5x10^{-9}$	$1.6x10^{-6}$	$1.0x10^{10}$
v_{sat} (cm/s) [parallel to *c*-axis]		$2.0x10^7$	$2.0x10^7$	$1.0x10^7$
μ_e (cm^2/Vs)	800	1000	400	1400
$\mu_\perp/\mu_{||}$ at 300 K		0.7-0.83	6	
μ_h (cm^2/Vs)	40	115	101	471
χ (eV) at 300 K		2.70	2.95	3.15
Refractive index (n)	2.7	2.712	2.7	3.5
ε_S	9.72		9.66	11.7

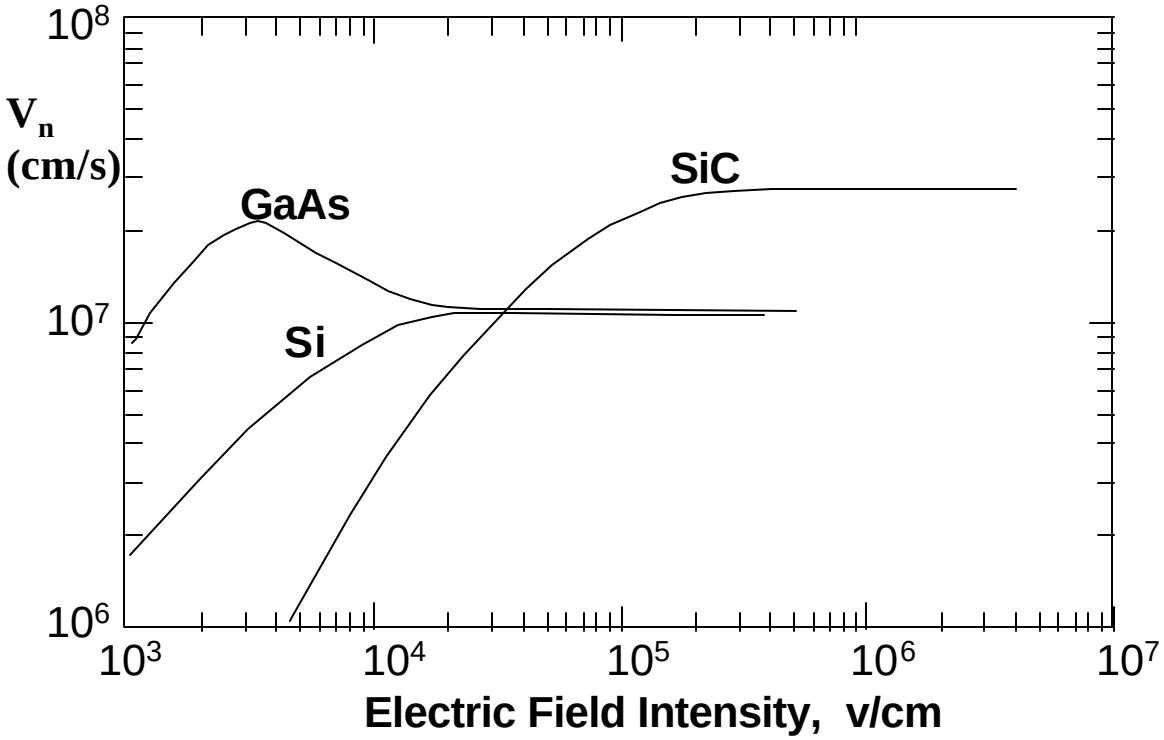

Figure 1.3 Electron velocity versus electric field intensity for GaAs, Si, and SiC
After [2]

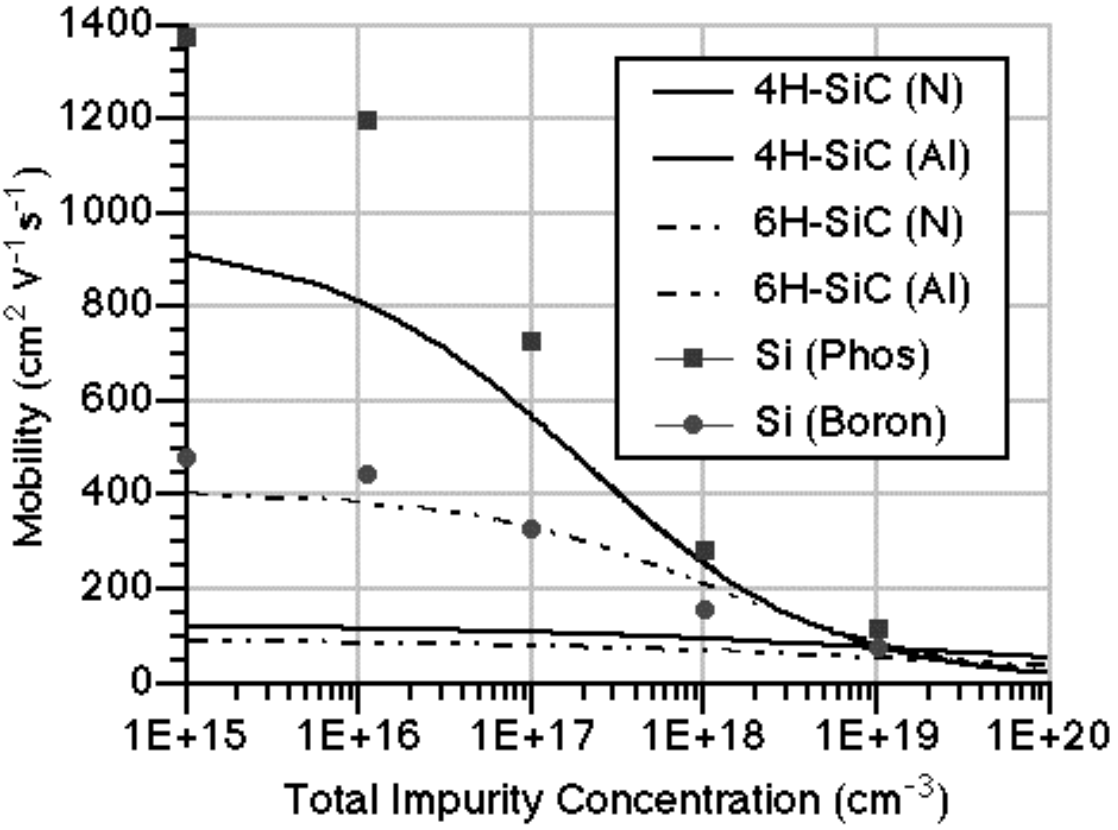

Figure 1.4 Electron and hole mobilites in silicon and silicon carbide at room temperature as functions of total dopant concentration. Mobilities for SiC were least squared fits (of experimental data taken in the basal plane) to an empirical relation for mobility in silicon After [2]

The conduction band density of states (N_C) and valence band density of states (N_V) have an empirical temperature ($T^{3/2}$) dependence [2]. Therefore, the intrinsic carrier concentration (n_i), which is defined in Equation 1.1 and shown to be directly proportional to N_c and N_v, is also temperature dependent.

$$n_i = \sqrt{N_C \cdot N_V}\exp^{(-Eg/2kT)} \tag{1.1}$$

While N_c and N_v are empirically dependent on temperature, n_i is instead exponentially dependent on temperature, as well as the energy bandgap (E_g) [2]. Device operation in excess of 1500°C is theoretically possible in 4H-SiC, as illustrated in Figure 1.5 where n_i as a function of reciprocal temperature is shown [2]. PN junction leakage currents in devices are normally proportional to n_i or n_i^2 when diffusion currents dominate the total leakage current; therefore, n_i is important in high-temperature device applications [2].

Figure 1.6 shows the temperature dependence of E_g for 2H-, 4H-, 6H-, 15R-, 21R-, 8H-, and 3C-SiC. Photoluminescence studies performed at liquid helium (He) temperatures (~4.2 K) under very low pressures (~10^{-11} T) are typically used to determine E_g values.

Dopants in semiconductors are intentional impurities occupying vacant lattice sites which are electrically activated. Dopants used in SiC are nitrogen (N), phosphorous (P), and arsenic (As) for n-type material and aluminum (Al), boron (B), beryllium (Be), gallium (Ga), oxygen (O), and scandium (Sc) for p-type material, with N and Al being the most common [2]. Typically residual nitrogen is present and results in undoped SiC being n-type. The specific polytype determines the color of the material which is slightly green in tint for 6H-SiC and slightly gray in tint for 4H-SiC. Donor activation energies are often found to vary over a wide range depending upon measurement technique,

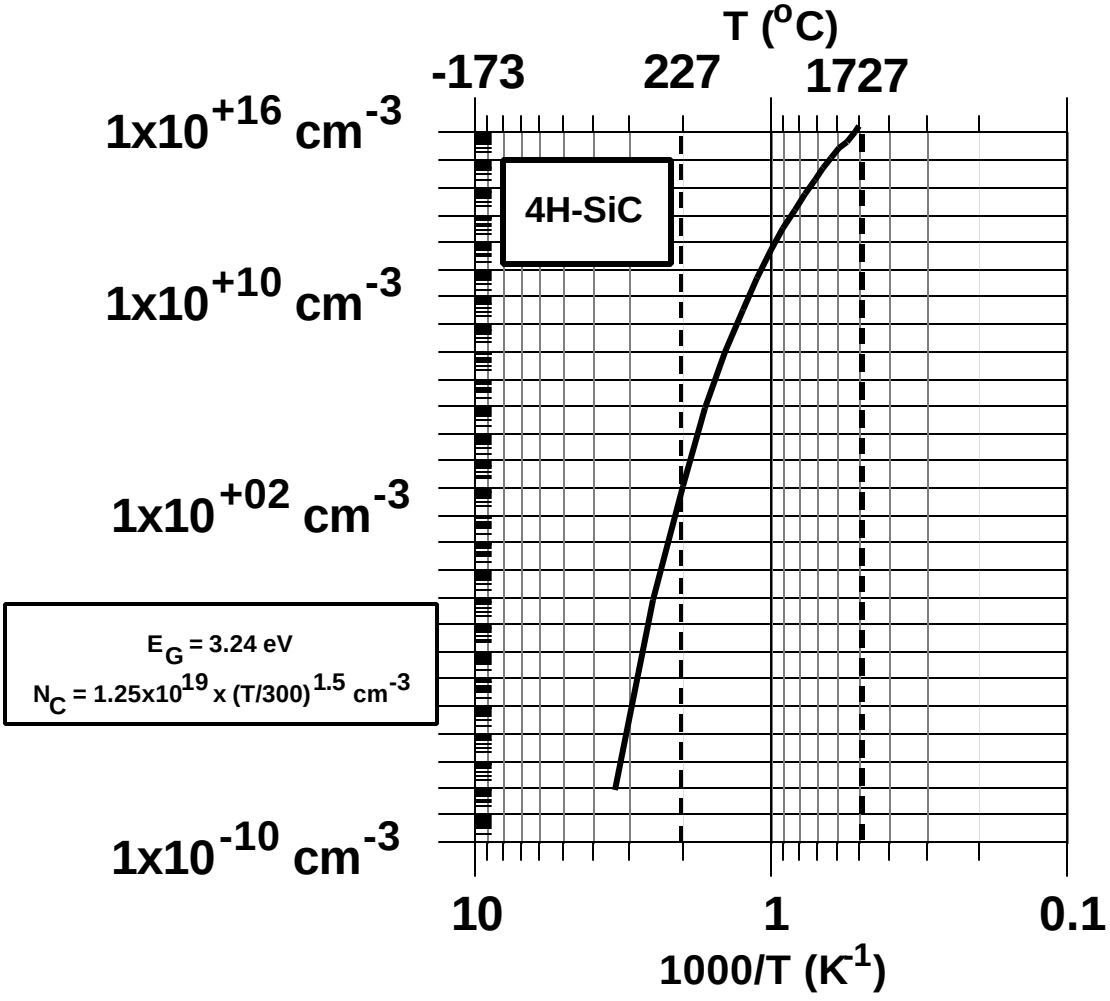

Figure 1.5 Intrinsic carrier concentration as a function of reciprocal temperature (1000/T) in units of inverse Kelvin for 4H-SiC After [2]

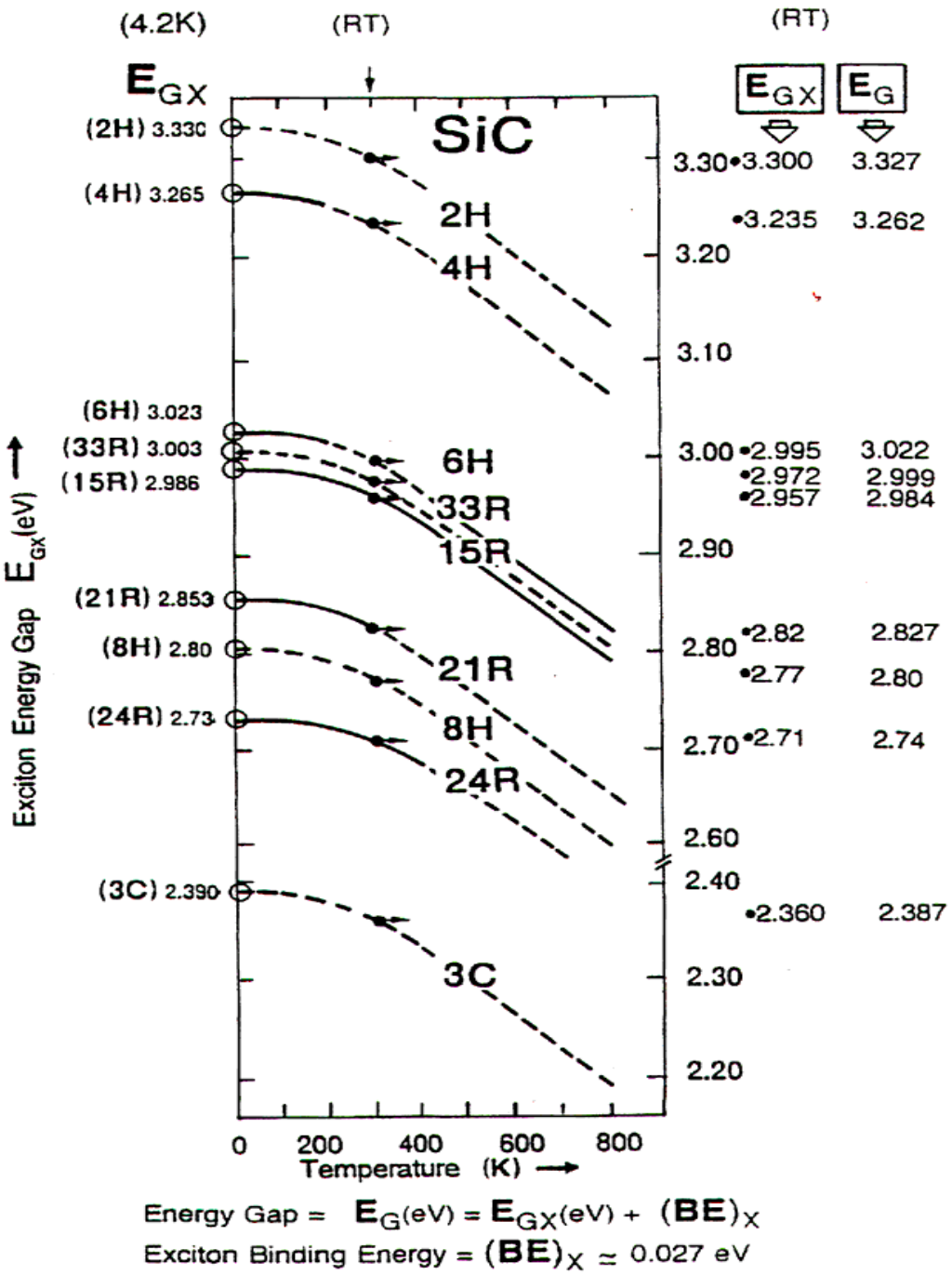

Figure 1.6 Temperature-dependent bandgap values for different polytypes of SiC After [2]

material quality, polytype, dopant concentrations, and the substitutional site occupied in the lattice (cubic or hexagonal) [2]. Nitrogen activation energies for n-type 3C-SiC range from 18 to 48 meV [2]. In 4H-SiC and 6H-SiC, two donor levels have been found depending upon the two occupancy sites: site 1 (hexagonal site) and site 2 (cubic site). Site 1 activation energy is 45 meV and 84 to 100 meV, respectively for 4H-SiC and 6H-SiC [2]. Site 2 activation energy is 100 meV and 125 to 150 meV, respectively for 4H-SiC and 6H-SiC [2]. The thermal energy (kT/q) for SiC at room temperature is only ~25.9 meV. This fact explains partial carrier freeze-out in SiC at room temperature. In addition, most dopant levels are deeper in SiC than those found comparably in silicon. Regardless of this fact, lower temperature operation of devices is feasible due to carriers being ionized by electric fields which has been demonstrated in the operation of a SiC junction field effect transistor (JFET) down to temperatures as low as 77 K[2].

SiC Technology Status

SiC is available in bulk wafer form for the 4H and 6H polytypes. Commercial wafers were released in 1991 from Cree Research, Inc. (now Cree, Inc.). Currently, low resistivity (10^{-3} Ω cm) to insulating (10^{15} Ω cm, 4H-SiC) wafers are available. Crystals up to 100 mm in diameter have been demonstrated [4], but because of high defect densities are only commercially available up to 75 mm in diameter from Cree and 50 mm from Sterling Semiconductor, SiCrystal AG, Nippon Steel, Okmetic and others.

The two major forms of defects in wafers are micropipes and dislocations (screw and edge). With recent efforts, micropipe densities have been decreased but high densities (on the order of 10^{3}-10^{4} cm^{-2}) of elemental screw and edge dislocations still

exist [4]. Commercial wafers can currently be purchased with less than 15 average micropipes per cm^2, but the number of dislocations remains unclassified. New approaches for bulk growth are being developed, one being the use of high temperature CVD (chemical vapor deposition) [4]. Crystals are being grown on the $(11\bar{2}0)$ face, instead of the typical {0001} face, resulting in micropipe-free substrates with much lower concentrations of stacking faults [4].

The growth of epitaxial layers is a critical step for designing devices in SiC due to the fact that essentially no diffusion occurs in the material. The propagation of defects, surface morphology, step bunching, and precise dopant control are key issues. SiC epitaxy growth is reportedly performed in various types of reactors, such as horizontal hot-wall, horizontal cold-wall, vertical hot-wall, vertical cold-wall, planetary for multiwafers, high-temperature CVD, and planetary hot-wall at temperatures of 1500-1600 ^oC [4]. The Si and C sources are typically silane (SiH_4) and propane (C_3H_8) with hydrogen being the carrier gas. N-type and p-type dopants include nitrogen (N_2) and trimehtylaluminum (TMA) or diborane (B_2H_6), respectively [4]. Unintentional doping (n-type) has been a problem in epilayers with donor concentrations of 10^{14}–10^{15} cm^{-3} being measured, but increased C/Si ratios (on the Si face, no sensitivity has been observed on the C face) has showed donor concentrations in the low 10^{13} cm^{-2} and below [4]. On both faces an increase in N_2 flow rates proportionally increases the n-type donor concentration [4]. For p-type material the dopant concentration is enhanced under carbon rich conditions [4]. Growth is typically performed on the {0001} Si and C face of 3.5^o off-axis 6H-SiC and 8^o off-axis 4H-SiC toward the $[11\bar{2}0]$ direction [4]. Repeatable

growth of 3C-SiC has also been realized on silicon substrates through the utilization of carbonization of silicon before CVD [4]. As a result 0.2 mm free-standing 3C-SiC wafers up to 150 mm in diameter are available following a wet etch to remove the silicon host substrate [4].

Other issues of concern with SiC technology include ion implantation and activation, ohmic contact formation, oxidation, and etching. The high thermal properties of SiC require that much higher processing temperatures be used in comparison to silicon technology. Because of the lack of diffusion in SiC, ion implantation is important for selective doping, but requires a 1600-1700 ^{o}C anneal to get activation greater than 90% which results in less design flexibility since it must be done early in the fabrication process [4]. Low sheet resistances (290 or 51 Ω/ð for high-dose N^{+} and P^{+} implants, respectively) can be achieved for n^{+}-SiC formation using lower implant temperatures (~1200-1400 ^{o}C), but higher temperatures are necessary to reduce crystal damage [4]. P^{+}-SiC, however, still maintains higher sheet resistances (5–10 kΩ/ð) using hot implantation [4]. These problems can be overcome by the development of lower temperature activation anneal processes and better p^{+}-SiC epilayer growth techniques.

High processing temperatures are also needed for ohmic contact formation. Currently resistances of $8x10^{-7}$ Ω cm^2 and $5x10^{-6}$ Ω cm^2 for n-type and p-type highly doped ($>10^{19}$ cm^{-3}) SiC layers, respectively, have been achieved, but long term stability (above 200 ^{o}C) has not been established [4].

SiC has an advantage over other wide bandgap materials of having a native oxide (SiO_2), but many problems exist with the SiO_2/SiC interface. Many techniques [re-

oxidation anneals, hydrogen (H_2) treatments, and nitrous oxide (NO) gas anneals] show improvement in the interface, but much work remains.

Another area where much work has been done but where much more still needs to be done is dry etching. Dry etching of SiC is very important because there are no room temperature wet etches available for the material due to its high bond strength. Because of this property, dry etch techniques also take careful planning due to mask erosion and micromasking effects. A thorough literature review of SiC etching will be provide in the following section and a detailed discussion of dry etching provided in Chapter 2.

SiC Etching Literature Review

Since modern SiC development in the early 1960's [5], much work has been done in the area of etching SiC. Groups have examined wet etch methods and dry etch methods using both reactive ion etch (RIE) and inductively coupled plasma (ICP) systems.

Wet etching of SiC has been accomplished using molten salts at high temperatures but is unfeasible because of the damage done to most masking materials, such as metal, oxide, and photoresist, and the low aspect ratios achievable with this approach [6], but new approaches are being developed. Song and Shin report on the use of a photoelectrical process which uses a UV light to generate holes to etch 4H-SiC and 6H-SiC using several electrolytes different from previous attempts, such as hydrogen fluoride based acids, hydrogen peroxide (H_2O_2), and mixtures of the two [7]. They found that the best surface roughness obtainable was only 27 Å. The surface roughness of the etched SiC layer is important to achieve good morphology, channel widths of submicron

features, and device mobility (which suffers with roughness if the etched area is in contact with the channel of the device) [6]. Shor, et.al, have also reported on the wet etching of SiC using photoelectrochemical (PEC) etching [8]. They were able to selectively etch n-type β–SiC over p-type β–SiC which is practical since it has been widely reported that PEC etching of semiconductors depends on the carrier concentration and dopant types [8].

Even though new wet etch approaches are being developed, much work still needs to be done in the area and dry etching is still considered the method of choice. Yih, et. al., reviewed SiC etching in fluorinated plasmas [5]. The bonding energy of SiC is

$$Si - C = 1.34 x Si - Si = 4.52 eV , \tag{1.2}$$

and for C-C bonds it is 6.27 eV. The much higher bonding strength of the C-C atoms compared to the Si-C atoms helps explain the enhanced etching of SiC compared to C in fluorinated plasmas [5]. C atoms are removed by C-F reactions or C-O reactions when O_2 is added to the plasma. The specific affects of adding O_2 to a fluorinated plasma are discussed in Chapter 2. At low percent O_2, carbon is removed by C-F reactions and by C-O reactions at high percent O_2, but SiC etch rates decrease as percent O_2 increases above a certain level indicating that C-O reactions are not as efficient as C-F reactions [5]. High etch rates at low percent O_2 in carbon tetrafluoride (CF_4), nitrogen trifluoride (NF_3), and sulfur hexafluoride (SF_6) were observed because these gases produce high fluorine intensity [5]. In low fluorine intensity gases, such as trifluoromethane (CHF_3), high etch rates were obtained at high percent O_2 (60 to 80%) [5]. They also observed that highly anisotropic profiles in CHF_3/O_2 is not achievable but is possible in all other fluorinated plasmas [5].

RIE of SiC has been studied extensively. Kothardaraman, et. al., reported on the etching of 6H-SiC in a parallel-plate, aluminum-electrode (area of 720 cm^2) RIE system using a SF_6/O_2 gas mixture [9]. They achieved a peak etch rate of 360 Å/min. at 30 mTorr and 200 W (0.28 W/cm^2) with a gas flow of 10 sccm and gas ratio of 1:1. It was suggested that a higher etch rate is possible, but their results were limited to avoid damaging their system.

Yih and Steckl examined various gas mixtures in order to obtain residue-free etches with high etch rates [10,11]. They reported the etching of 6H-SiC in a Plasma-Therm PK1241 parallel plate RIE system with Al electrodes using mixtures of fluorinated gases [10]. They set the pressure to 20 mTorr, the power to 200 W (0.4 W/cm^2) and total gas flow to 20 sccm. In SF_6/CHF_3 and NF_3/CHF_3 gas mixtures, all of their etches were contaminated with a residue. The residue results from Al that is sputtered off the electrode and redeposited onto the etch sample. In a CF_4/CHF_3 plasma, residue-free etches were obtained at 85% or higher CHF_3 concentration. The peak etch rate obtained was 153 Å/min. at 300 W with 85% CHF_3. Using the same system and parameters, they examined H_2 addition to various fluorinated gas and O_2 mixtures for etching β-SiC [11]. In a $NF_3/10\%O_2$ plasma, a peak etch rate of 830 Å/min. was observed but all samples etched in >10% O_2 concentration had residue on the surface. The addition of H_2 at a minimum of 10 sccm in a 2 sccm of NF_3 and 18 sccm O_2 plasma was needed to prevent residue formation but resulted in a reduction of the etch rate from 399 to 44 Å/min. In a CHF_3/O_2 plasma, small amounts of H_2 (~10%) was found to prevent residue at all concentrations of O_2. The highest etch rates (obtained at 20 mTorr) were 330 Å/min. in a $CHF_3/50\%O_2$ plasma with 2 sccm of H_2 added, and 400 Å/min. in a $CHF_3/80\%O_2$ plasma

with no H_2 added. In a $CF_4/20\%O_2$ plasma, an etch rate of 350 Å/min. was obtained but significant residue was observed with all concentrations of O_2. A residue-free etch was obtained at 30 mTorr with 7.5 sccm of H_2 added to a $CF_4/50\%O_2$ plasma. In a $SF_6/20\%O_2$ plasma, an etch rate of 450 Å/min. was obtained but again all samples had significant residue at all concentrations of O_2. A residue-free etch demonstrating an etch rate of 175 Å/min. was obtained at 30 mTorr with 10 sccm of H_2 added to a $SF_6/50\%O_2$ plasma. For all cases except CHF_3, the amount of H_2 needed to prevent or reduce residue formation increases with O_2 concentration and reaches a maximum at 10% O_2. They found that the use of a graphite or a Kapton sheet to cover the electrode prevented residue formation in all cases but that the graphite sheet cracked during long etches and the Kapton sheet etched away in NF_3/O_2 plasmas [11].

Casady, et. al., reported the etching of 6H-SiC and 4H-SiC in a four-chamber QUAD 400 Series Drytek system with an electrode area of 161.3 cm^2 [12]. The purpose of their work was to obtain high etch rates and a smooth, residue-free etch surface without introducing gas additives, such as, O_2 and H_2. They chose to etch the samples with pure NF_3 because it is efficiently broken into free radicals and all by-products are volatile. Etch rates of 2000 Å/min. with an unclean surface and 1500 Å/min. with a clean surface were obtained at 375 W (2.33 W/cm^2) and 250 W (1.55 W/cm^2), respectively [12]. No noticeable difference in the etch rate of the two SiC polytypes was observed.

Surface roughness, as mentioned earlier, can result in many problems in etching and in device performance. Kang and Shin performed experiments using CHF_3/O_2 followed by an O_2 ash to etch SiC in RIE systems to reduce surface roughness [6]. They achieved a 750 Å/min. etch rate with a surface roughness of only 1 Å.

The benefits of high-density plasmas (lower ion bombardment energy and higher ion flux) have encouraged much work. Wang, et. al., reported etch rates of ~3500 Å/min. for 6H-SiC in a Plasma-Therm 790 ICP system with NF_3-based chemistries [13]. They found that anisotropy was controlled by the NF_3 ratio and that both ion flux and ion energy are important parameters in determining the overall etch rate. At a high source power (750 W), they found the nature of the additive gas to be less important than the F concentration, but observed tapered sidewalls when the F concentration was high compared to the ion concentration. O_2 addition (10-35%) increases the atomic fluorine neutral concentration, but when comparing NF_3/Ar and NF_3/O_2 mixtures, etch rates were higher in Ar due to ion bombardment. They examined bottom RF and top ICP source powers and observed an increase in etch rates with increasing bottom RF power due to ion energy and an increase in ion flux energy and a decrease in ion energy with increasing ICP source power. They also observed trenching in some of their etch experiments which is a common problem in ICP etching. Trenching is said to result from glancing angle collisions of ions with the sidewall that produce enhanced etching at the foot of the sidewall [13], but the parameters associated with it are not clearly understood.

Cao, et.al., reported ICP etching of 6H-SiC in a Plasma-Therm system using a CF_4/O_2 gas mixture [14]. They found that at low O_2 concentrations, C atoms etched at lower speeds than Si atoms. The etch rate was limited by the removal of C at low O_2 concentrations and by removal of Si at high O_2 concentrations. A peak etch rate of 620 Å/min. was observed at 80% O_2/CF_4. It was observed that the C to CO or CO_2 reaction seemed to dominate at higher O_2 concentrations and the Si to SiF_4 reaction seemed to dominate at low O_2 concentration [14].

Khan, et.al., reported ICP etching of 6H-SiC in a Plasma-Therm Shuttlelock 700 ICP-RIE system [15]. They achieved an etch rate of 9700 Å/min. using a top power of 900 W and dc bias of -450 V in a SF_6 plasma [15]. This is the highest known etch rate for SiC to date. As mentioned previously, trenching at the sidewalls is a problem in ICP etching, an example of which is shown in Figure 1.7. Though this is an important problem, the causes of trenching are still only poorly understood.

Etching of SiC has also been examined to determine its affects on device performance. Kim, et. al. found that Schottky barrier diodes (SBD's) on a surface etched with SF_6/O_2 gas mixtures in a RIE system showed reduced device performance compared to those not on etched surfaces [16]. The difference was reported to be due to a non-stochiometric surface resulting from excess carbon because of the difference in volatility of the Si-related and C-related etch products. They did observe improvements in the reverse leakage current at high oxygen percentage mixtures due to the improved surface stochiometry [16]. Cao, et.al., reported minimal changes in the electrical properties of Au Schottky barrier diodes in ICP etching using a SF_6:O_2 gas mixture (gas ratio of 10:5) when using practical etch rates (~2500 Å/min.) and reasonable powers (ICP coil power of 500 W and a dc bias under -35 V) [17]. At higher dc bias conditions they observed a reduction in breakdown voltage and the ideality factor of the diodes due to lattice damage caused by increased ion bombardment energy [17]. Li, et. al., also examined ICP etching effect on Au Schottky barrier diodes [18]. They used a CF_4:O_2 gas mixture (gas flow of 20:9 sccm) and top power of 700W. They reported that a dc bias of -50 V provided good diode characteristics. At higher dc bias, a reduction in the breakdown voltage and ideality factor was observed which again was thought to be due to increased lattice

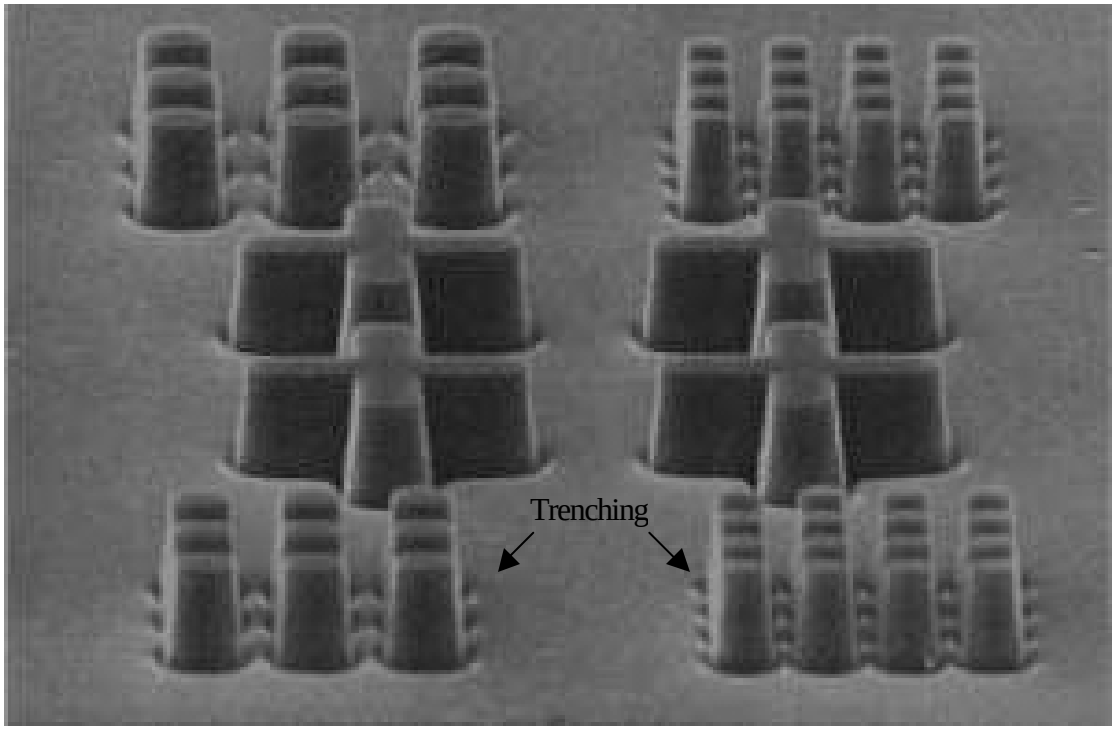

Figure 1.7 A scanning electron microscope (SEM) image of 7.5 μm deep structures etched in 6H-SiC exhibiting trenching at the sidewalls After [15]

damage. At lower dc bias, they observed increased leakage currents in the diodes, which they suggested was due to a C-rich surface or polymer on the surface that was not efficiently removed by the chemistry or ion bombardment at reduced dc bias [18].

Many groups are developing trench SiC JFETs because they are easier to fabricate than lateral structures and easier to pinch off the conduction channel than vertical structures not having trenches [19]. Gupta, et. al., reported the development of JFET's with 3-6 μm deep trenches [20]. The devices demonstrated a blocking voltage of over 600 V with -30 V on the gate and a specific on-resistance of 5 mΩ-cm^2 with 0 V on the gate. Zhu and Chow reported the development of JFETs with 3 μm deep trenches [19]. Simulation results show that a blocking voltage as high as 1600 V and a specific on-resistance as low as 1.2 mΩ-cm^2 is possible, but at the time of publication had not been achieved. When considering the fabrication of these vertical trench JFETs, etching is an important issue. As mentioned earlier, trenching at sidewalls is a problem during etching. Koo, et. al., examined trenching effects which can occur during the etching of the trenches for JFETs [21]. When etching 4.5 μm deep trenches, trenching at the bottom of the trench next to the sidewall was observed to be 0.2 – 0.3 μm deep. The effect of this phenomenon on the device was to produce SIT-like (static inductor transistor) or triode characteristics at low drain voltages.

Scope and Organization of Thesis

Though much work has been done in the area of SiC etching, no work has been reported on SiC etching in a Lam TCP 9400SE II system. This work focuses on SiC etch development in the Lam TCP 9400SE II system. Various parameters (carrier type,

pressure, gas additives, gas flow, and bottom electrode power) are studied. The work is divided into five main sections. Chapter One provides a brief overview of SiC and the status of SiC technology. In Chapter Two, dry etch fundamentals, etch parameters, and a comparison of inductively coupled plasma (ICP) systems and reactive ion etch (RIE) systems are provided. Etch development for SiC is discussed and the experimental results from the development are provided in Chapter Three. In Chapter Four a discussion of the etch results are given. Chapter Five concludes the work.

CHAPTER II

PLASMA (DRY) ETCHING

Introduction

Fabrication of semiconductor devices involves repeatedly putting down films in selected areas, and/or selectively removing films from certain areas on the wafer. The films can be deposited by evaporation or etched with chemical solutions in beakers which are designed to selectively etch some films while not etching others, or they can be deposited and etched using a plasma-assisted process. Using chemical solutions to etch is generally referred to as wet etching, while using a gaseous source of chemicals in plasma is often referred to as dry etching.

Plasma processing has many advantages over wet and non plasma-assisted dry processes. Plasmas can be used to create and accelerate ions. They can also be used to replace the high-temperatures needed to crack molecules or increase chemical reaction rates. Photoresist (a hydrocarbon-based photo-sensitive polymer used to create patterns on the wafer) that has been exposed to harsh conditions is more thoroughly cleaned from the substrate surface using an oxygen plasma rather than liquid chemicals, such as, acetone and stripper [22]. Unlike evaporation systems, the plasma sources in sputtering systems allow alloy sources to be deposited onto materials while maintaining their original compositions, allow step coverage to be improved by adding bias to the

substrate, and allow compound films to be deposited by adding a gas that reacts with the sputtered metal [22]. Traditional chemical vapor deposition (CVD) systems require high temperatures unlike the plasma enhanced chemical vapor deposition (PECVD) systems, which allow films to be deposited at a much lower temperature [22].

When specifically considering the etch process, plasma (dry) etching has many benefits over wet etching. Wet etching is isotropic (etches in all directions at the same rate), so line width is difficult to control and can result in bubbles of wet chemicals etching under the masked areas, which results in catastrophic failure during the etch. Dry or plasma etching allows anisotropic etching, reduced chemical consumption, cleaner processing, precise pattern transfer and compatibility with automation [23].

These benefits are very important in semiconductor processing, so while in the past most semiconductor processing steps were chemical (carried out in either liquid or gas phase), today the cleaning, deposition, and etching processes are based on the chemistry and physics of plasmas. In the following sections a brief overview of plasma etching will be provided.

Plasma Etching

The production of gaseous products from the removal of solid material from a wafer surface with gaseous reactants is known as dry etching [24]. The generic reaction for dry etching is shown by the following equation:

$$S(s) + R(g) \rightarrow P(g) \tag{2.1}$$

where S is the solid (s) substrate to be etched, R are the gaseous (g) reactants, and P is the gaseous products [24].

Chemistry

Typical reagents for dry etching silicon nitride and silicon dioxide are CHF_3, C_4F_8, and CF_4 and O_2 and H_2O for photoresists and organics [6]. Fluorinated gas mixtures are effective in etching SiC [2]. Common fluorinated gases are CHF_3, CF_4, C_2F_6, SF_6, and NF_3. NF_3 is a highly toxic gas, but commonly used because of the high concentration of fluorine radicals that can be generated [2]. These reagents are typically not reactive with the materials at room temperature but when introduced in a plasma chamber where radio frequency (RF) or microwave (MW) discharges cause the reagents and atomic and molecular ions in the chamber to dissociate and ionize, they readily attack certain materials [24].

The trends observed in etching Si are very similar in SiC etching [2]. Both CF_x and SiF_x form by the reaction of F with SiC. This reaction can occur chemically but is greatly enhanced when a bias is applied to the substrate resulting in ion bombardment [2]. The addition of O_2 enhances the etch rate of SiC as it does Si by not only increasing the fluorine concentration but by also reacting with the carbon in the SiC [2].

For both silicon and SiC, the etching of the silicon component in fluorine is normally accomplished through the following reaction:

$$Si + 4F \Rightarrow SiF_4 \qquad (2.2)$$

In the case of SiC, before Si can be etched the SiC bond must be broken, and this is normally accomplished through ion bombardment, elevated temperature, or increased plasma density. Once the SiC bond is broken, the Si is etched with the reaction above, and carbon is etched through one of the following mechanisms:

$$C + xO \Rightarrow CO \text{ or } CO_2 \qquad (2.3)$$

$$C + xF \Rightarrow CF_4 \text{ or } CF_2 \quad (2.4)$$

or ion bombardment. Not surprisingly, the SiC etch rates are much slower than for pure Si.

Etch Process

The following steps generally occur when etching in a chamber which has been pumped down to a low pressure.

1. Feed gas is introduced (such as CF_4, NF_3, SF_6,…) and is broken into chemically reactive species by the plasma.
2. Species diffuse to the wafer surface and are adsorbed.
3. Species may move about surface until they react with the exposed film.
4. The reaction product must be desorbed, diffuse away from the wafer and be transported by the gas stream out of the chamber.

Many systems, such as a reactive ion etch system (RIE), rely not only upon the plasma etch process described above, but also ion bombardment of the wafer surface which assists in breaking bonds and increasing the etch rate of the material. Possible typical reactions that occur in the steps of plasma etching are shown in Table 2.1.

Plasma etching begins by taking a molecular gas, establishing a glow discharge and creating a reactive species [23]. The most important species in plasma processing are created when electrons collide with neutral gas molecules [22]. Dissociation, ionization and excitation are the processes that can result from the collision. Low energy processes are favored in etching; therefore dissociation is preferred over ionization [23]. When dissociation occurs relatively unreactive etch gas molecules are converted into very

Table 2.1

Possible Steps in Plasma Etching

After [6]

Event	Example
Reactive species formed by ionization (I) or dissociation (D)	$Cl_2 + e^- \rightarrow 2Cl + e^-(D)$ $Cl_2 + e^- \rightarrow Cl_2^+ + 2e^-(I)$
Surface adsorption of reactive species	$Cl(g) \rightarrow Cl(s)$
Chemical reaction on surface	$\equiv Si(s) + Cl(s) \rightarrow \equiv Si - Cl(s)$
Ion-assisted removal of surface species	$\equiv Si\langle_{Cl}^{Cl}(s) + M^+(g) \rightarrow M^+(g) + SiCl_2(g)$
Thermal desorption from surface	$SiCl_4(s) + Heat \rightarrow SiCl_4(g)$
Product dissociation by plasma	$SiCl_4(g) + e^- \rightarrow SiCl_2(g) + 2Cl(g) + e^-$

reactive radicals (molecules with an unpaired outer electron which is available to form a covalent bond) [25] which accomplish the most important plasma-surface chemistry in lower density plasmas [23]. In higher density, low-pressure plasmas such as those created in ICP systems, the ions can dominate the radicals. Because of electrostatic considerations, negative ions usually can not reach the surfaces so they do not play a significant role in etching. Radicals tend to be more abundant in discharges because they are generated at higher rates than ions and have longer lifetimes in the plasma [23]. In low density plasmas, it is important that the plasma only partially ionize the gas because the etch rate is greater with ions (or radicals) and neutrals in the plasma than with ions (or radicals) alone [26]. Neutrals are important because electrons collide with them. Little energy is transferred to a neutral when an electron collides with it but the collision transforms the directed energy an electron gains from accelerating in the electric field to random thermal energy which causes the electron to heat up and have more energy to cause dissociation or ionization [22].

The plasma potential and self-bias voltage both play a significant role in the etch process. Plasma potential is defined as the potential of the plasma in steady state relative to a wall or electrode with which it is in contact [25]. Self-bias voltage is a time-average bias produced by systems with asymmetrical electrodes and resulting in a negative voltage on the smaller electrode [22]. The plasma potential helps reactive species diffuse toward the surface of materials being etched while the self-bias voltage accelerates those positive reactive species toward the surface to provide energetic ion bombardment [22]. Ion bombardment helps increase the adsorption of reactive species to the surface of the materials, the reaction rate between those species and the materials being etched, and the

desorption and removal of the reaction products [22]. It is important to choose a chemistry that has a reactive species that reacts with the material being etched to form a volatile product with a high vapor pressure which can be easily pumped away. Otherwise dissociation of the product will occur and redeposition can take place [22].

From a gaseous electronics point of view, the ion bombardment plays a huge role in these issues. If the ion bombardment is too energetic it will result in poor etch selectivity, contamination, and lattice structure damage to the semiconductor materials [22]. Lower ion energies are desired, but they result in lower etch rates and reduced anisotropy. The etch rates can be restored by using higher ion fluxes and the anisotropy can be restored by operating at lower pressures [23]. ICP systems offer the solution by having high reactive species densities, high process rates, a low and controllable sheath voltage, and a low operating pressure (on the order of 1 mTorr to 100 mTorr) [27].

Parameters of Plasma Etching

The input and output parameters of etching are important in controlling and evaluating the etch process. Table 2.2 provides input and output parameters to consider when etching. Masking issues, substrate temperature, loading effects, pressure, gas additives, power, gas flow, aspect ratio, etch directionality, and damage are discussed in the following sections.

Masking Issues

In order to etch a selected area of a material, a mask has to be used that will either be much thicker than the area being etched and/or be selective (etch at a much slower rate than the etch surface) to the area being etched. Methods to achieve etch selectivity are

Table 2.2

Typical Input and Output Parameters of Plasma Etching

Input Parameters	Output Parameters
1) Pressure	1) Etch Rates
2) Reactant Flow	2) Selectivity
3) Reactant Flow Ratio	3) Uniformity
4) RF or MW Power (s)	4) Critical Dimensions (CD's) or Aspect Ratios
5) Wafer Temperature	5) Profile Angle
	6) Defect Levels
	7) Surface Damage
	8) Surface Morphology

- Selective formation of an etch inhibiting layer on the masking material versus the material to be etched due to the differences in chemical processes occurring on the masking material with respect to the material being etched;
- Non-reactivity of the masking material versus the material being etched in a chosen plasma;
- Non-volatility of reaction products on the masking material versus volatile species formation on the material being etched [22].

The masking material is most often removed once the etch is completed leaving only the etched area of the material being processed; therefore it is important to choose a masking material that can be easily removed without damaging the material being left behind.

Common materials used as etch masks are photoresist, silicon dioxide, silicon nitride, or metal. Photoresist requires fewer processing steps than the other materials so it is often used wherever possible.

Silicon Dioxide as a Mask

When using silicon dioxide (SiO_2) as a mask it is important to remember that it is slowly etched by fluorine (F_2) radicals even at room temperature and without ion bombardment because there is a net energy loss in the reaction between fluorine and SiO_2 as shown in the following energy balance equation [28]:

$$F \underline{\vee} F + Si \underline{\vee} O = Si - F + (-5 kcal / mole) \tag{2.5}$$

Despite this fact, it can still be used as a selective mask for Si and other materials. In a pure fluorine beam, the selectivity of Si to SiO_2 is approximately 50:1 and 100:1 when the wafer is held at room temperature and -30 ^oC, respectively [28]. Pure F_2 can be used as the etch gas for these materials, but it is highly toxic and therefore undesirable; so CF_4, C_2F_6, and SF_6 are commonly used as etch gases because they produce large concentrations of free F.

Silicon Nitride as a Mask

Silicon nitride (SiN) is also a masking material that can be etched selectively over SiO_2 and Si, but can not be selectively etched simultaneously over both due to its intermediate position in terms of bond strength and electronegativity [28]. A fluorine rich plasma, such as CF_4:O_2, allows selective etching of SiN over SiO_2. A CF_4:H_2 mixture allows selective etching of SiN over Si [28].

The selectivity of the masking material over that of the material being etched can be increased by adjusting the chemical composition of the plasma which is discussed in a following section.

Substrate Temperature

Since surface coverage of chemisorb species (species which chemically bind onto the surface of another substance) is temperature dependent and the rates of many chemical reactions increase with temperature, then substrate temperature can increase the etch rate [29]. Even though increased temperature favors etching, variations in temperature throughout the etch process can make it difficult to obtain consistent and

uniform etch rates. Therefore, it is necessary to provide cooling for the substrate to maintain a consistent temperature.

Loading Effects

If the area of exposed film being etched is increased then the etch rate tends to decrease due to the depletion of reactive species in the plasma [28]. This tendency is known as the loading effect and described by the equation

$$R = \frac{R_o}{1 + kA} \tag{2.6}$$

where Ro is the empty chamber etch rate, A is the area of the exposed film to be etched, and k is a constant that can often be reduced by fixing the reactor pressure and increasing the flow of the etch gases [28].

Pressure

Generally, as gas pressure is increased a decrease in the mean free path of the plasma components is observed which produces more free radicals and ions in which to etch the material resulting in an increased etch rate [30]. In high density plasmas, the lower pressures reduce the scattering of ions, thereby increasing directionality [5]. At higher pressures, it is more probable that higher molecular weight species form which can result in polymers on the surface, thereby decreasing the etching rate of the material [30].

Gas Additives to Plasmas

The addition of gas additives, such as oxygen (O_2), hydrogen (H_2), argon (Ar), and helium (He) have many affects in plasmas. The addition of O_2 to a fluorinated plasma enhances the etch rate by reacting with unsaturated fluoride species generating

reactive F atoms [5]. When higher percentages of O_2 are added to fluorinated plasma the O_2 dilutes the mixture resulting in a reduced etch rate [5].

When specifically considering the etching of Si and SiO_2 in a CF_4 plasma, the addition of O_2 in small amounts will increase the etch rate of both Si and SiO_2 because the O_2 reacts with C to form carbon dioxide (CO_2), which is a volatile product that is quickly pumped out of the etch system [28]. This reaction creates a fluorine rich plasma in which the etch rate of Si dramatically increases over that of SiO_2. The problem with this process is that the resulting Si etch may not be anisotropic [28]; but anisotropic etching can be encouraged through polymer formation on the sidewalls, which will be discussed in Chapter 2. At higher O_2 concentrations, O_2 is chemically adsorbed in the Si surface making it appear as SiO_2 and greatly reducing the selectivity from of Si to SiO_2 [28].

When considering SiC etching, the addition of O_2 in fluorinated plasmas somewhat follows the trends observed in Si etching, such as, an initial increase in etch rate due to an increase in reactive F and a reduction in etch rate due to dilution. However, the trend of O_2 addition in specific fluorinated gases differs in SiC compared to Si due to reactions occurring with the C component of SiC. As mentioned in Chapter 1, O_2 reacts with the C component in SiC to enhance etching but its specific benefits vary depending on the fluorinated gas used to etch and the efficiency in which C reacts with O_2 or F under different conditions.

Hydrogen is often added to slow the etch rate, as well as to increase anisotropic etching through the use of sidewall polymerization. The addition of H_2 encourages polymerization because it scavenges the fluorine resulting in a carbon rich or fluorine

deficient plasma [28]. This process has the opposite affect of O_2 addition resulting in a lower Si to SiO_2 selectivity (as compared to 1:2 for $Si:SiO_2$ at 50% O_2 concentration) [28]. Therefore, an anisotropic Si etch with good selectivity (for example, 1:1.5 for $Si:SiO_2$) can be obtained. The addition of H_2 in a CF_4 plasma causes the etch rate of both Si and SiO_2 to decrease, but at moderate H_2 concentrations the etch rate of SiO_2 exceeds that of Si allowing SiO_2 to be selectively etched over Si [28]. This occurs because H_2 reacts with the fluorine radicals to produce HF, which etches the SiO_2 but not the Si, and because ion bombardment on the SiO_2 surface breaks the bonds to produce O_2 which reacts with the carbon and forms volatiles [(carbon monoxide) CO and CO_2] which are quickly pumped away [28]. The anisotropy also increases at moderate H_2 concentrations, because of the nonvolatile fluorocarbon film that is deposited.

The addition of noble gases such as Ar and He (whether to stabilize plasmas by modifying the electrical characteristics enabling more efficient power deposition throughout the plasma [31] or for cooling purposes) may significantly change the etch reaction [22]. They have been shown to result in anisotropic etching because of inert ion bombardment of the surface but their effects are not fully understood [22].

Power Input

An increase in power input can increase ion bombardment and free radicals and increase the thermal energy available to increase reaction rates on the surface. It can also increase the energy of secondary electrons creating more free radicals for etching [30].

Gas Flow

Gas flow is another parameter of concern. An increase in the gas flow can significantly increase the etch rate if it is below the critical flow rate to adequately supply reactants to the plasma [30]. A less noticeable difference in etch rate is observed if the flow rate is increased significantly over the critical rate because the additional precursors can be pumped away before having time to react [30].

Etch Rate Dependence on Aspect Ratio

The aspect ratio is also an important consideration in etching and is define as the ratio of the depth/width of a feature. The etch rate decreases as the aspect ratio increases. For widths less than 1 um, the etch rate decreases linearly [22] making mask selectivity more of an issue. The dominant mechanism of this effect had not been established but has been attributed to the consumption of reactants on the trench sidewalls, the lack of diffusion of reactants to the bottom of the trench, and the diverging electric field in the trench [22].

Etch Directionality

Etches can either be isotropic or anisotropic as shown in Figure 2.1. Isotropic etches result in etching in both the horizontal (x) and vertical (d) direction and anisotropic etches result in etching in only the vertical (d) direction. The following equation gives a method of measuring the isotropy or anisotropy of an etch:

$$A = \frac{d}{x} \text{ [30]} \tag{2.7}$$

In isotropic etches and anisotropic etches A=1 and A=8, respectively.

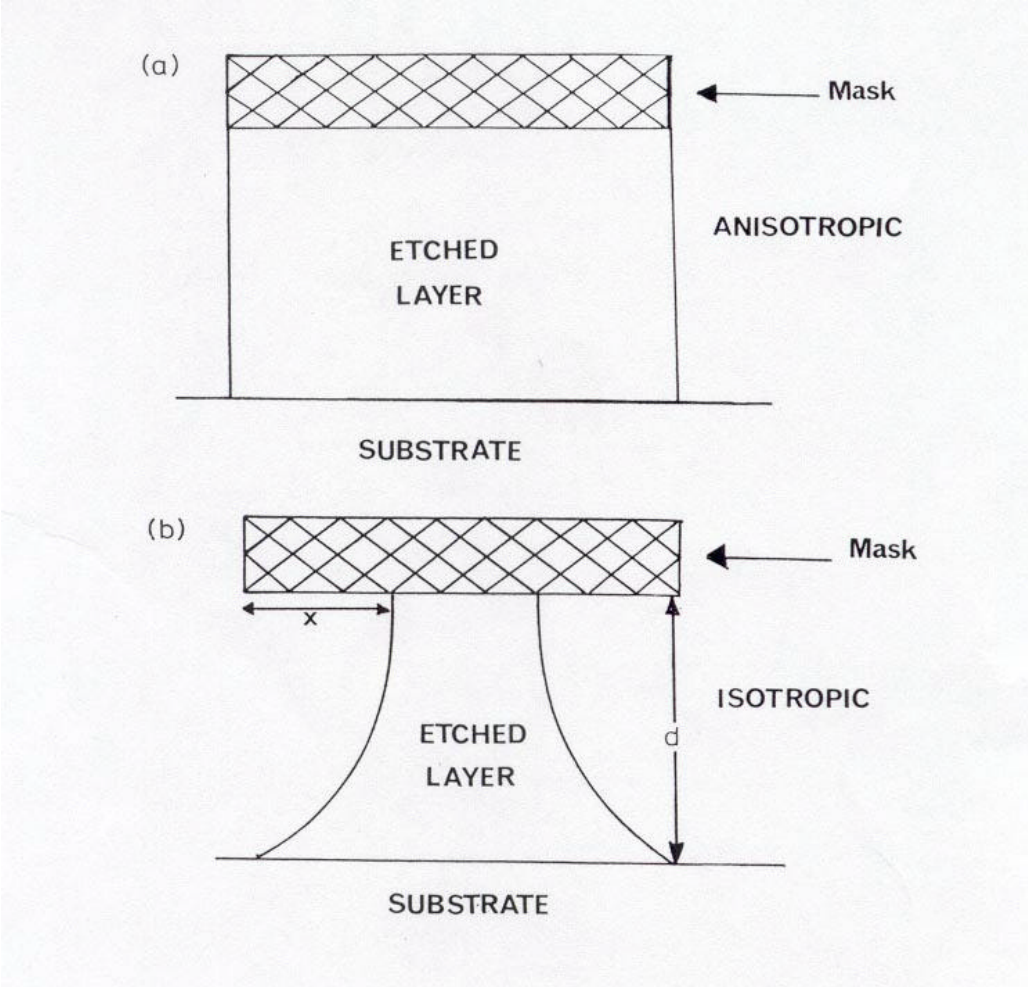

Figure 2.1 Schematic of a) anisotropic and b) isotropic etches After [30]

Etch directionality is a major factor in determining the resulting profile angle of an etched surface. It is achieved through directed energy applied to an etching reaction at a surface. This is specifically accomplished through energetic ion bombardment in an RIE system, but it can also occur through electron or photon bombardment of a surface exposed to a chemical etchant [22].

Primary models for enhanced etching due to ion-induced reactions are the chemically enhanced physical sputtering model, the damage model, and the chemical sputtering model [22]. Sputtering is the removal of an atom from a surface by bombardment with atoms in a discharge. In chemically enhanced physical sputtering, a surface layer sputters more readily after chemically reacting with an etchant than areas of unreacted material. In the damage model, the reaction rate of etchant species with the material is increased due to dangling bonds exposed by ion bombardment. In the chemical sputtering model, energy is supplied to the surface to increase reaction rates through ion collision cascades.

Sidewall passivation (polymerization formation on the sidewalls) also promotes etch directionality and is useful for etching materials that normally exhibit isotropic etching in certain chemistries [22]. Polymerization is the process of producing nonvolatile species that reduce the etch rate [28]. The polymer is typically a fluorocarbon film that deposits over the entire material being etched. It can only be removed by ion bombardment. The ion velocity follows the electric field, which is nearly normal to the surface. The resulting ion sputtering of the fluorocarbon film on the normal surface enables the etching of the surface and not the sidewalls. This process is illustrated in Figure 2.2.

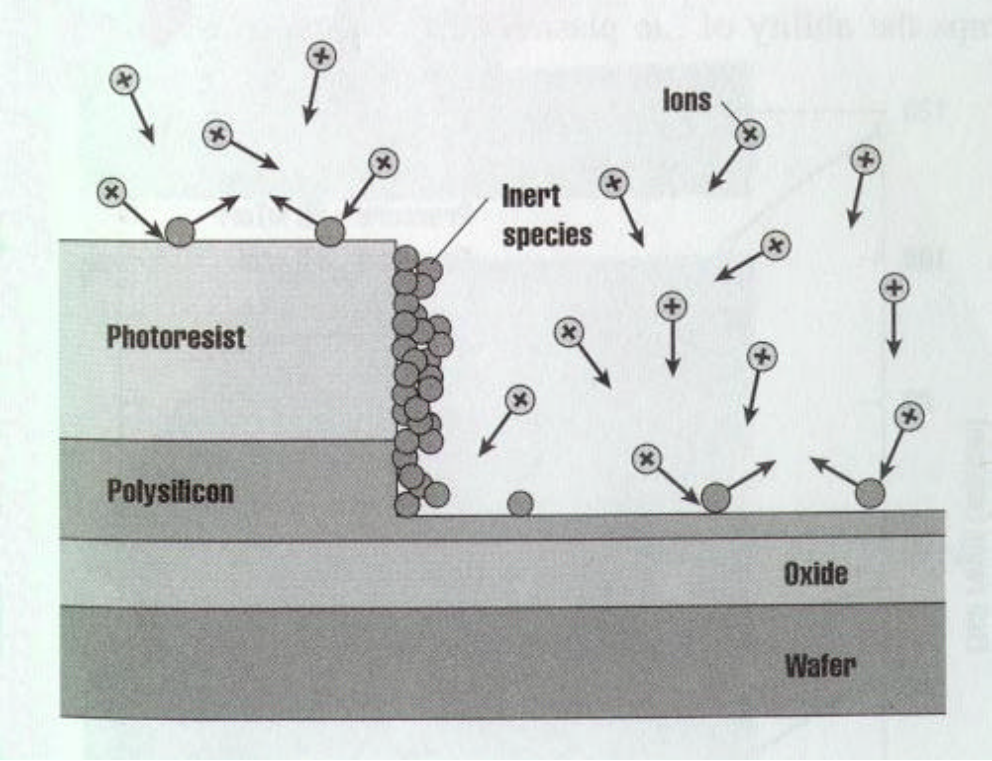

Figure 2.2 Schematic diagram of a high pressure anisotropic etch showing the formation of sidewall passivating films After [28]

As previously mentioned, the addition of H_2, for example in a CF_4 plasma, encourages polymerization because it scavenges the fluorine resulting in a carbon rich plasma [28]. The use of a photoresist mask can also encourage polymerization because many of the etch products from the photoresist are hydrocarbons.

In fluorocarbon systems, the polymerization process depends on the fluorine to carbon ratio [28]. If the carbon concentration in the feed gas mixture is greater than half of the fluorine concentration, after accounting for HF, CO, CO_2, and other scavenging compound formation, then polymerization occurs [28]. Figure 2.3 shows the increasing concentrations of NF_3 and the resulting etch of SiO_2. At 100% NF_3, a fast etch of SiO_2 is obtained but substantial undercutting is observed because of the lack of polymer formation on the sidewalls [28].

Plasma Etch Damage

Damage due to ion bombardment and surface contamination during plasma etching are both areas of concern because they can affect the electrical properties of devices. Damage types include:

- Surface residues from processes intrinsic to the etch, such as, fluorocarbon films or involatile product formation.
- Surface residues from processes extrinsic to the etch, such as residue from the etching chamber configuration like aluminum electrodes.
- Impurity penetration from implantation or diffusion during the etch process.
- Lattice damage such as point defects or extended defects.

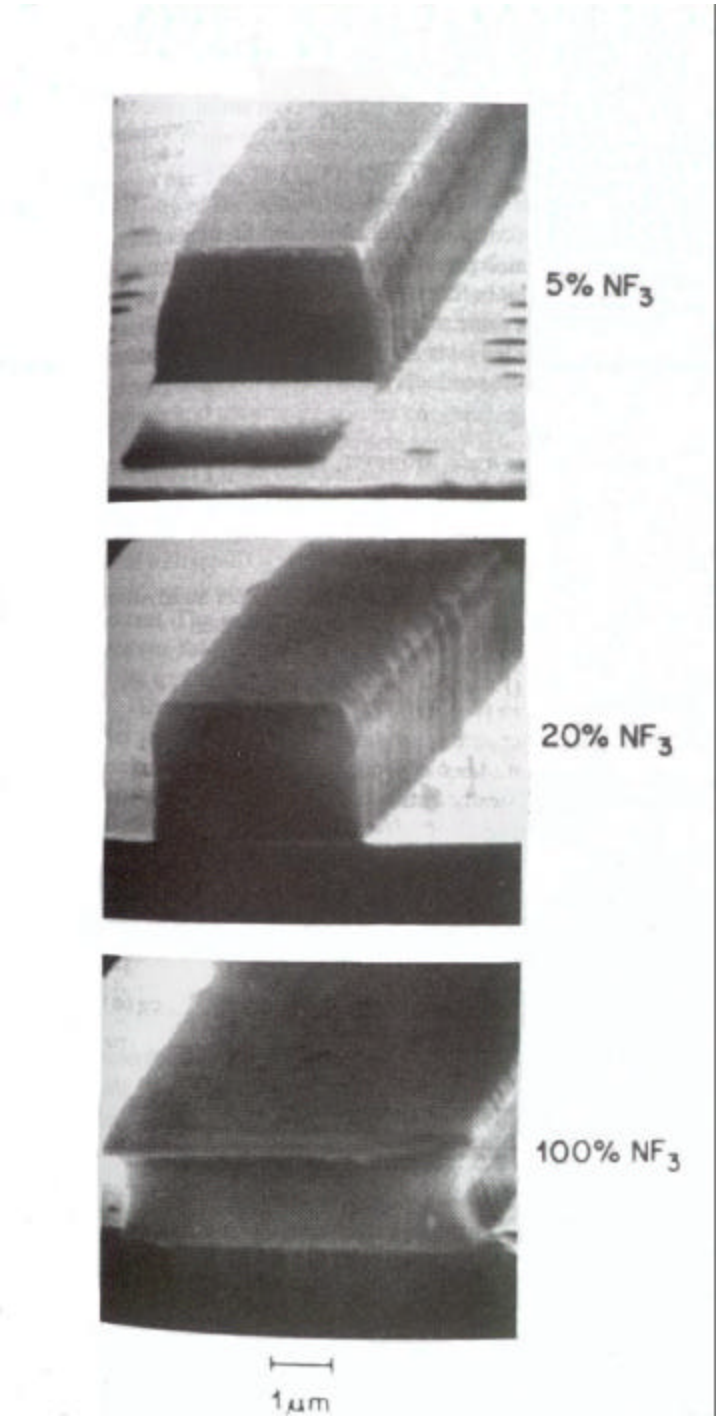

Figure 2.3 Etch profiles of SiO_2 with increasing concentrations of NF_3 After [28]

- Dopant loss from chemical interaction in the plasma.
- Heavy metal contamination from metal parts in the chamber.
- Mobile ion contamination from material in the chamber, such as, teflon electrodes which contain sodium.
- Surface roughness from micromasking (extrinsic to the etch process), and the etching of rough overlayers which replicate the roughness into
- underlayers (intrinsic to the etch process) [22].

ICP and RIE Comparison

Two basic systems used in SiC etching are reactive ion etching (RIE) systems and inductively coupled plasma (ICP) systems, shown in Figures 2.4 and 2.5, respectively. An ICP system differs from traditional RIE systems in that it uses two RF power supplies instead of one, resulting in a much denser plasma. The denser plasma provides capability for high etch rates without the need for high ion bombardment, which should reduce surface damage.

RIE systems rely on high-energy ion bombardment, unlike ICP systems [23] which rely on high ion flux with low energy to etch instead of simply high ion energy [13]. In ICP systems, the ion flux and ion energy can be separately controlled with the top and bottom powers, respectively. Typical operating pressures are 10 – 300 mTorr and 1-2 mTorr in RIE and ICP systems, respectively [13]. Typical ion flux is $=10^{9}$ $cm^{-2}s^{-1}$ and $=10^{13}$ $cm^{-2}s^{-1}$ for RIE and ICP systems, respectively [13]. This higher ion flux of reactive species to the substrate makes ICP systems much more efficient in etching than RIE systems [32].

A typical RIE system has parallel plates and uses 13.56 MHz RF power. This frequency is used because it is greater than the plasma frequency (frequency at which electrons oscillate about positive charges) therefore the flux responds only to the self-biased voltage [22]. If the frequency was lower than the plasma frequency then it would be shielded out and the electrons would not respond. The parallel plates can be either symmetrical (the same size) or asymmetrical (different sizes). The areas of the electrodes are important when controlling ion bombardment on the surface of the cathode. If they are symmetrical, the potential difference is the same for each [28]. If they are asymmetric, the potential difference can be determined using the following equation, assuming current is conserved through the plasma,

$$\frac{V_1}{V_2} \approx \left[\frac{A_2}{A_1}\right]^4 \tag{2.8}$$

where $V_1 \equiv V_{plasma} - V_{top}$, $V_2 \equiv V_{plasma} - V_{bottom}$, and A_1 and A_2 are the areas of the top and bottom electrodes, respectively [28]. In order to maximize the ion bombardment energy on the lower electrode, the area of the upper electrode should be increased [28]. This is accomplished in practice by connecting the top electrode to the chamber walls (making the effective area equal to the sum of the chamber wall area and the top electrode area) and bonding it to dc ground (for safety reasons).

An ICP systems also uses a 13.56 MHz RF power source; but instead of parallel plate electrodes, it has a coil (which has one end attached to a RF source and the other end floating) surrounding the chamber and an electrode. The coil couples the plasma through a quartz plate under which the sample is sitting on an electrode. The uniformity of etch rate over a large area is superior in an ICP system compared to an RIE due to the

minimization of edge effect on the periphery of the electrodes because of the use of the coil [32].

The basis for a RIE system is capacitive (or voltage) coupling, while for an ICP system it is inductive (or current) coupling [33]. RIE systems require high capacitance between the electrode and plasma and large amplitude RF voltages. ICP systems require high mutual inductance between the electrode and plasma, usually achieved through the use of a coil.

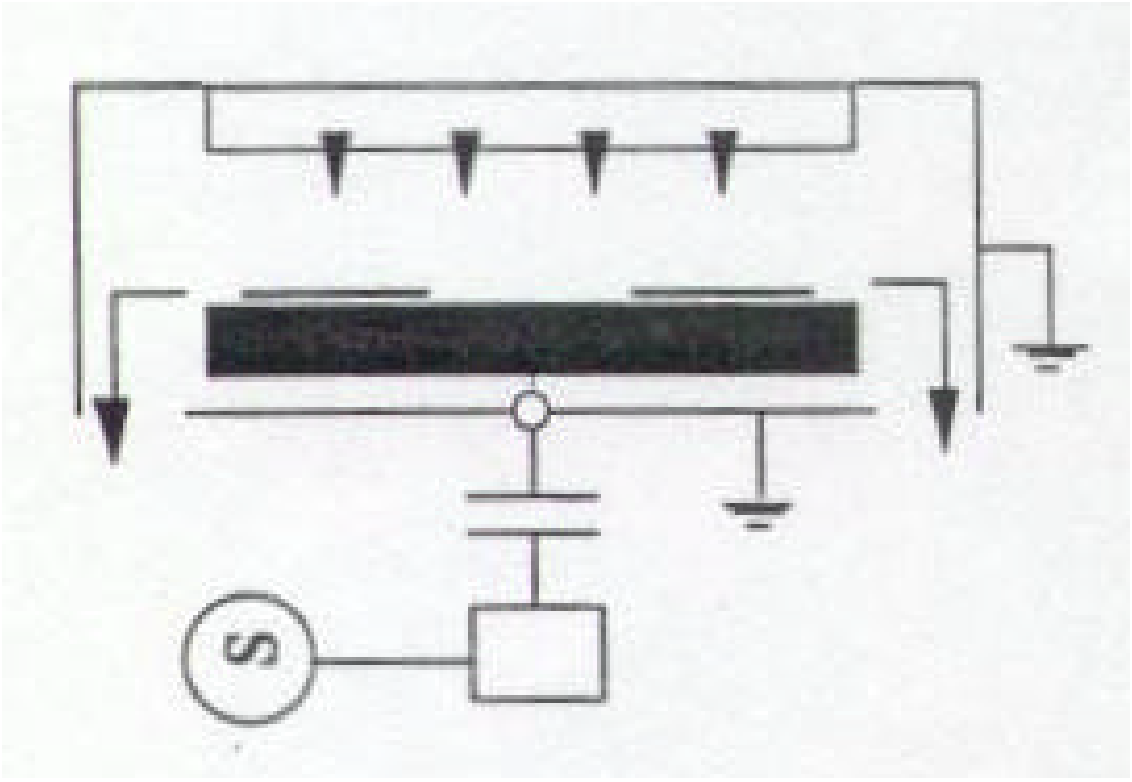

Figure 2.4 Layout of a basic RIE system After [5]

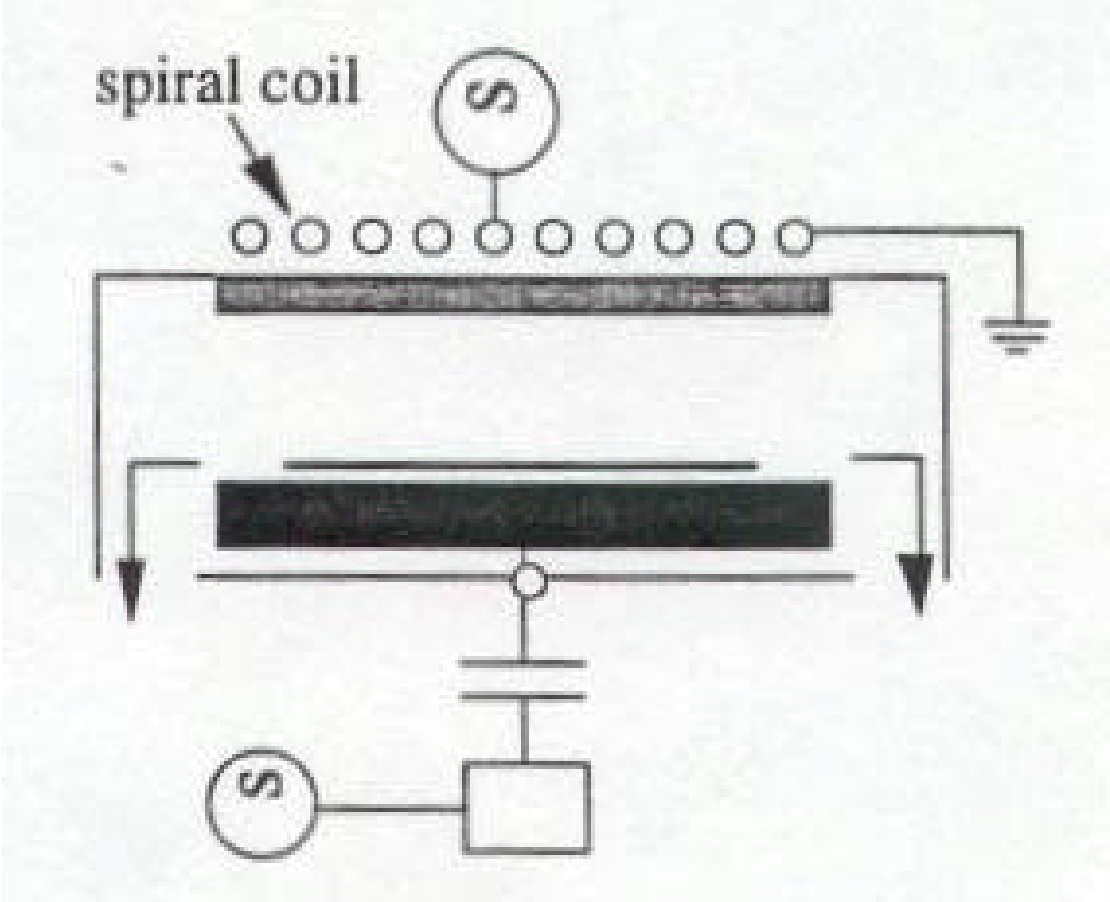

Figure 2.5 Layout of a basic ICP system After [5]

CHAPTER III

ETCH DEVELOPMENT

The focus of this work is the etching of single crystalline SiC using a Lam TCP 9400SE II etch system. TCP refers to Transformer Coupled Plasma, which is more commonly known as Inductively Coupled Plasma (ICP) etching. This system, described in Appendix B, was developed for etching polysilicon and was modified to work for SiC etching in this work by creating an 8" carrier with five 2" pockets to hold the SiC substrates. As previously mentioned, SiC can be etched using fluorinated as well as chlorinated gases and mixtures. For example, CF_4/O_2, CF_2Cl_2, CF_3Cl, $SF_6/O_2/Cl_2$, $Cl_2/H_2/C_2F_6/CCl_4$, C_2ClF_5/O_2, Br_2SiF_4/O_2, NF_3, ClF_3, CCl_4, CCl_3F_5, C_2ClF_5/SF_6, C_2F_6/CF_3Cl, CF_3Cl/Br_2. In this work with the Lam TCP 9400SE II system, NF_3, CHF_3, CF_4, SF_6, O_2, H_2, Ar, and He are available.

After examining the parameters, a trench etch was examined for VJFETs. As mentioned in Chapter 1, much work is being done in VJFET device development which requires a 3 to 6 μm deep SiC etch. This etch is the most critical fabrication step for such devices because trenching at the sidewalls or slanted sidewalls can greatly impact the fabrication of the device and the device performance. In this chapter, the experimental results will be presented. A more detailed discussion of the results is provided in Chapter 5.

Experimental Setup

Silicon-faced 4H-SiC wafers with a n-type doping of approximately $8x10^{18}$ cm^{-3} were patterned using AZ1518 photoresist with a mask having 1 mm squares. The samples were then masked with evaporated nickel that was 2000 Å thick and cut into approximately 1 cm square etch samples. A matrix of 10 minute etches on a graphite carrier with an electrode temperature of $10^{o}C$ was used to investigate the effects of gas pressure, gas flow rate, electrode power, and gas additives on the etch rate. The matrix is presented in Table 3.1. The etch rate was determined by measuring the differential height between the masked and unmasked regions using a Tencor Dektak profilometer system. The etch damage and sidewall profile was examined in a scanning electron microscope (SEM).

SiC Experimental Etch Results

SiC Versus Graphite Carrier

Before completing the etch matrix (Table 3.1), etches using a CHF_3:O_2 gas mixture with the O_2 concentration being varied was performed on a SiC carrier and then repeated on a graphite carrier to determine which carrier provided the highest etch rates. Figure 3.1 shows the etch rate versus O_2 concentration on both the SiC and graphite carriers. The etch rates on the graphite carrier ranged from approximately 50 Å/min. to 250 Å/min. higher than on the SiC carrier. The maximum etch rate obtained on the SiC carrier was 908 Å/min. and on the graphite carrier was 1106 Å/min. This difference is explained by the difference in the etch rate of SiC and graphite (carbon), and the decision was made to use the graphite carrier. This is explained in more detail in Chapter 5.

Table 3.1

Etch Matrix for Pressure, Gas Additives, Gas Flow Rate, and Electrode Power

Gas	Additive	Top Electrode . Power (W)	Bottom Electrode Power (W)	Pressure (mTorr)	Total Flow Rate (sccm)	Variable
SF_6	He & O_2	750	250	Varying	20 (10:9:1)	Pressure (2-50)
SF_6	He & O_2	750	250	Varying	30 (15:13.5:1.5)	Pressure (2-50)
CHF_3	O_2	750	250	25	30	O_2 Concentration (0-90%)
SF_6	O_2	750	250	25	30	O_2 Concentration (0-60%)
NF_3	O_2	750	250	25	30	O_2 Concentration (0-50%)
NF_3	O_2	750	250	2	30	O_2 Concentration (0-50%)
CHF_3	H_2	750	250	25	30	H_2 Concentration (0-45%)
NF_3	Ar	750	250	25	30	Ar Concentration (0-50%)
NF_3	Ar	750	250	2	30	Ar Concentration (0-50%)
NF_3	He	750	250	2	30	He Concentration (0-50%)
SF_6	None	750	250	25	Varying	SF_6 Flow (0-120)
CHF_3	None	500	Varying	25	30	Bottom Electrode Power (50-250)

Pressure Variation

After the carrier was selected, the next parameter of interest was the pressure. The effects of pressure on the etch rate are examined and shown for a SF_6:He:O_2 plasma in Figure 3.2. Two gas ratios, 10:9:1 and 15:13.5:1.5, of the gas mixture with a total flow of 20 and 30 sccm, respectively, are used. The pressure is varied from 2 to 50 mTorr. The etch rate increases up to 25 mTorr, and then decreases. For both cases the peak etch rates are 3283 Å/min for a total gas flow of 30 sccm and 2503 Å/min for a total gas flow of 20 sccm. Figures 3.3 and 3.4 are SEM images of samples etched at 2 mTorr with a total flow of 20 and 30 sccm, respectively. The etch profile is very anisotropic, as evident by the vertical sidewalls. Slight amounts of residue are around the sample mostly due to the sample being cut to fit the SEM. Figures 3.5 and 3.6 are SEM images of samples etched at 15 mTorr with a total gas flow of 20 and 30 sccm, respectively. The etch profiles are again very anisotropic but trenching appeared on both samples. Figures 3.7 and 3.8 are SEM images of samples etched at 25 mTorr with a total gas flow of 20 and 30 sccm, respectively. The etch profiles are again very anisotropic but trenching also appeared.

Gas Additives

The next parameters of interest were gas additives. The effects of O_2 in CHF_3, SF_6, and NF_3 plasmas, H_2 in CHF_3 plasmas and noble gases (Ar and He) in NF_3 plasmas are examined. The results are given in the following sections.

Oxygen in CHF_3, SF_6, and NF_3 Plasmas

Figure 3.9 shows the etch rate versus concentration of O_2 in a CHF_3 plasma. The maximum etch rate, 1254 Å/min., was observed at 60% O_2 concentration. Figures 3.10, 3.11, and 3.12 are SEM images of samples etched with 20%, 40%, and 60% O_2 concentration, respectively. The etch profile is anisotropic on all samples but trenching was observed at the higher O_2 concentration beginning at 60% O_2. Figure 3.13 shows the etch rate versus O_2 concentration in a SF_6 plasma. The maximum etch rate, 4314 Å/min. was observed at 20% O_2 concentration. The SEM image of this sample is shown in Figure 3.14. Severe trenching and mask degradation were observed. Figure 3.15 shows the etch rate versus O_2 concentration in a NF_3 plasma at 2 and 25 mTorr. The maximum etch rates, 1893 Å/min. and 1255 Å/min., are observed at 0% O_2 concentration at 2 mTorr and approximately 30% O_2 concentration at 25 mTorr, respectively. Figures 3.16 and 3.17 are SEM images of samples etched with 10% O_2 concentration at 2 and 25 mTorr, respectively. The etches are very anisotropic and produce good surface morphology. Very pronounced trenching was observed on the sample etched at 2 mTorr with only slight traces of trenching observed on the sample etched at 25 mTorr. Figures 3.18 and 3.19 are SEM images of samples etched with 50% O_2 concentration at 2 and 25 mTorr, respectively. The etches are again very anisotropic and produce good surface morphology. Slight trenching was observed on the sample etched at 2 mTorr. No trenching was observed on the sample etched at 25 mTorr.

Hydrogen in CHF_3 Plasmas

Figure 3.20 shows the etch rate versus concentration of H_2 in a CHF_3 plasma. The maximum etch rate, 894 Å/min., was observed at 10% H_2 concentration. Figures 3.21, 3.22, and 3.23 are SEM images of samples etched with 7%, 17%, and 60% H_2 concentration, respectively. Slight undercutting of the mask was observed on the samples etched with 17% and 60% H_2 concentration but the surface morphology was good. Severe trenching was observed on the sample etched with 17% H_2 concentration. Polymerization is severe on the sample etched with 60% H_2 concentration resulting in a poor surface morphology and slow etch rate.

Noble Gases (Ar and He) in NF_3 Plasmas

Figure 3.24 shows the effects of Ar on etch rate in a NF_3 plasma. The maximum etch rates, 1195 Å/min. at 2 mTorr and 1978 Å/min. at 25 mTorr, were observed at 0% and 10% Ar concentration, respectively. A small addition of Ar (up to approximately 15%) in a NF_3 plasma at 25 mTorr seemed to enhance the etch rate while no enhancement was observed at 2 mTorr. Increases in Ar beyond 15% in a NF_3 plasma at 25 mTorr results in a decrease in the etch rate as a result of the dilution of the reactive gas. Figures 3.25 and 3.26 are SEM images of samples etched in 10% Ar concentration at 2 and 25 mTorr, respectively. The surface morphology is good and the etch profile is anisotropic on both samples but trenching is observed on the sample etched at 2 mTorr. Figure 3.27 shows the effects of He on etch rate in a NF_3 plasma. As with the Ar at 2 mTorr, the maximum etch rate, 1195 Å/min., is observed at 0% He concentration; therefore, the addition of He did not seem to enhance the etch rate at all. Figures 3.28

and 3.29 are SEM images of samples etched in 10% and 20% He concentration, respectively. The surface morphology is good, and the etch profile is very anisotropic. No trenching was observed on either sample.

Gas Flow

The effects of SF_6 gas flow rate on the etch rate were also examined and the results are shown in Figure 3.30. The etch rate increases with increasing gas flow up to 30 sccm and then saturates. An etch rate of 3867 Å/min. is observed at 30 sccm of SF_6 flow.

Power Effects

The effect of the bottom electrode power was also examined. The etch rates versus bottom electrode power are shown in Figure 3.31. The increase in etch rate was approximately linear up to 150 W where it then saturated. The etch profile of the sample etched at 50W on the bottom electrode is sloped as shown by the SEM image in Figure 3.32. Increasing the bottom electrode power improved the etch profile until it became completely vertical (anisotropic) at 250W on the bottom electrode as shown by the SEM image in Figure 3.33. The surface morphology was good on all samples.

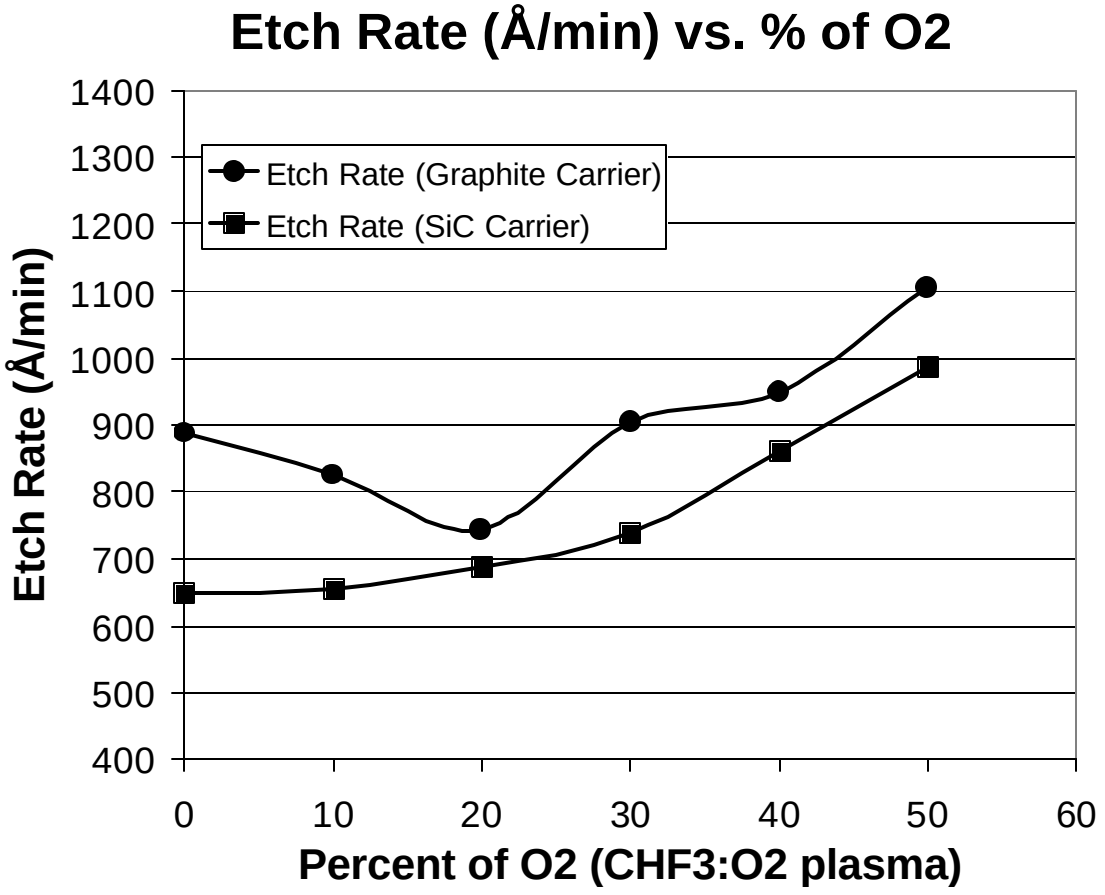

Figure 3.1 Graph showing the etch rate versus O_2 concentration in a CHF_3:O_2 plasma using a SiC and graphite carrier

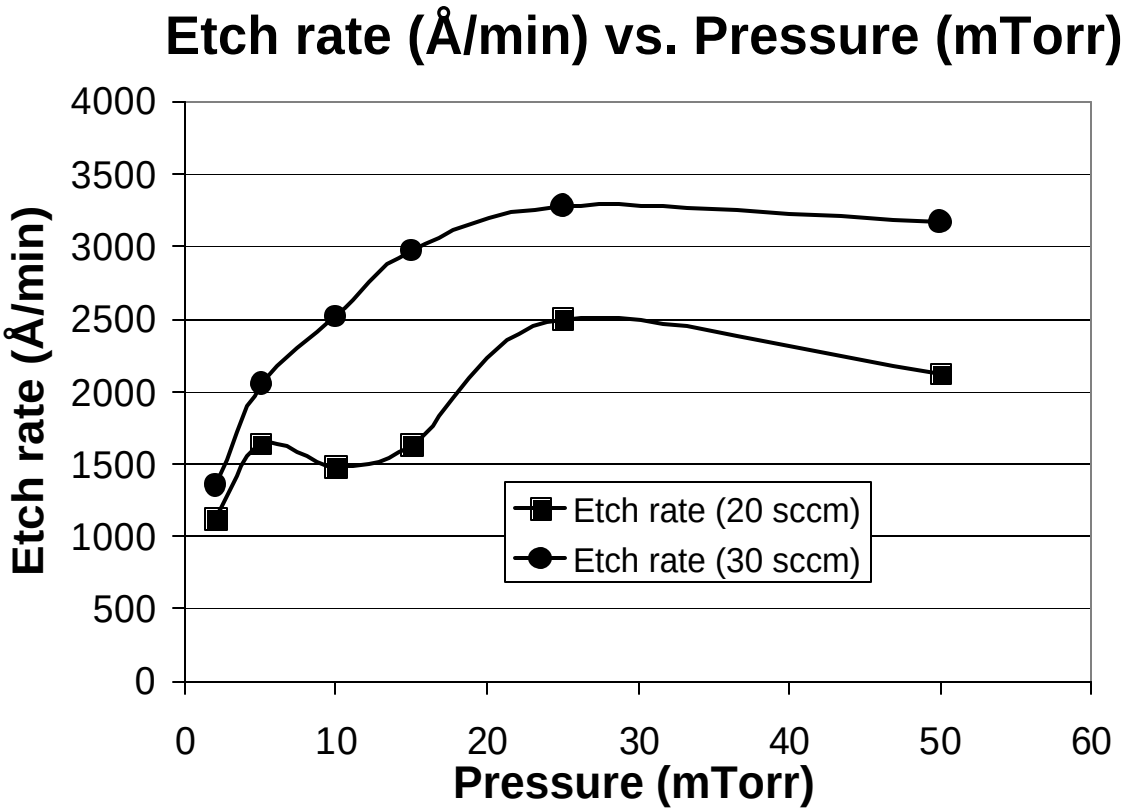

Figure 3.2 Graph showing the etch rate versus pressure in a SF_6:He:O_2 plasma

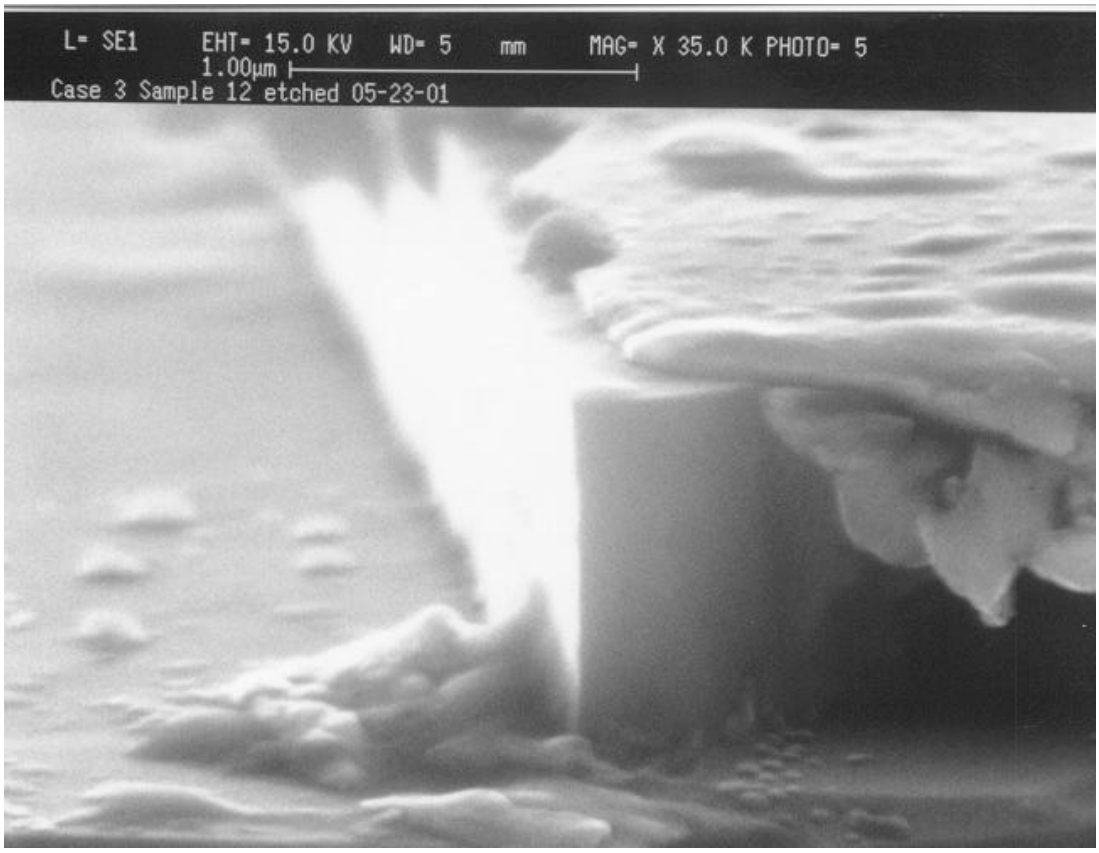

Figure 3.3 SEM showing etch profile of a sample etched in SF_6:He:O_2 - 10:9:1 sccm at a pressure of 2 mTorr

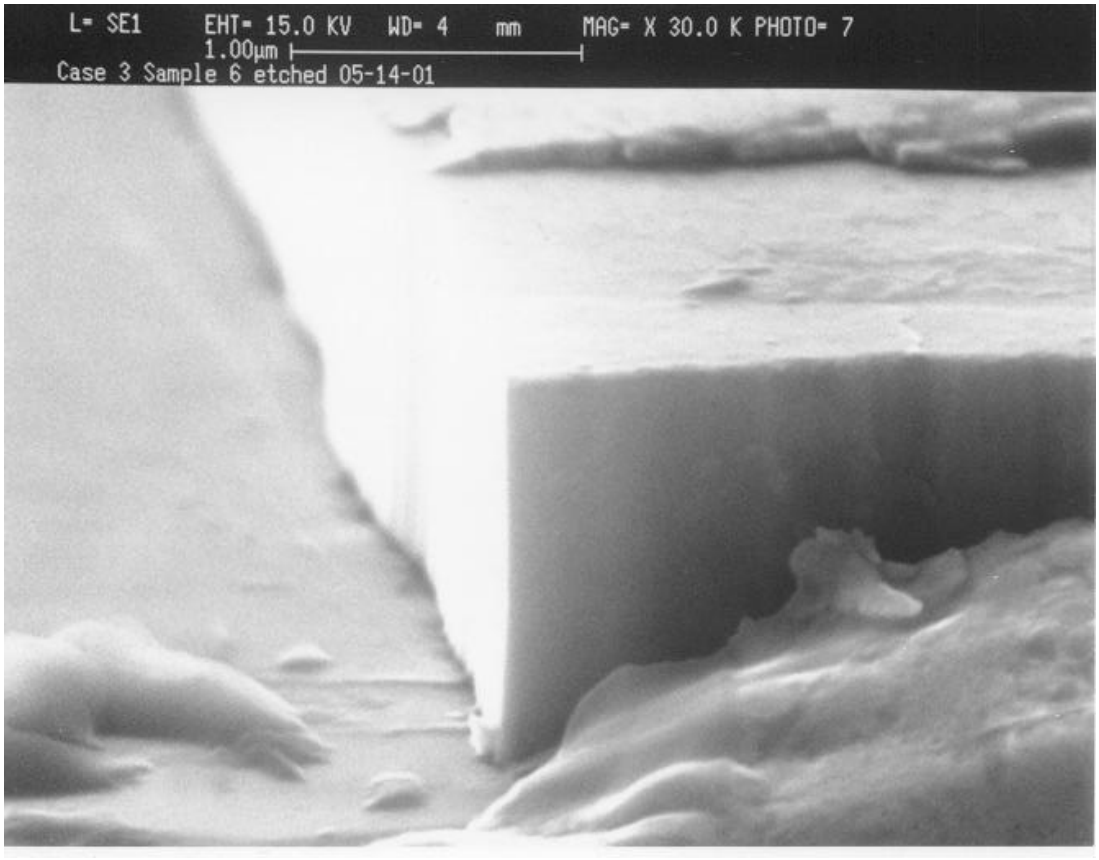

Figure 3.4 SEM showing etch profile of a sample etched in SF_6:He:O_2 - 15:13.5:1.5 sccm at a pressure of 2 mTorr

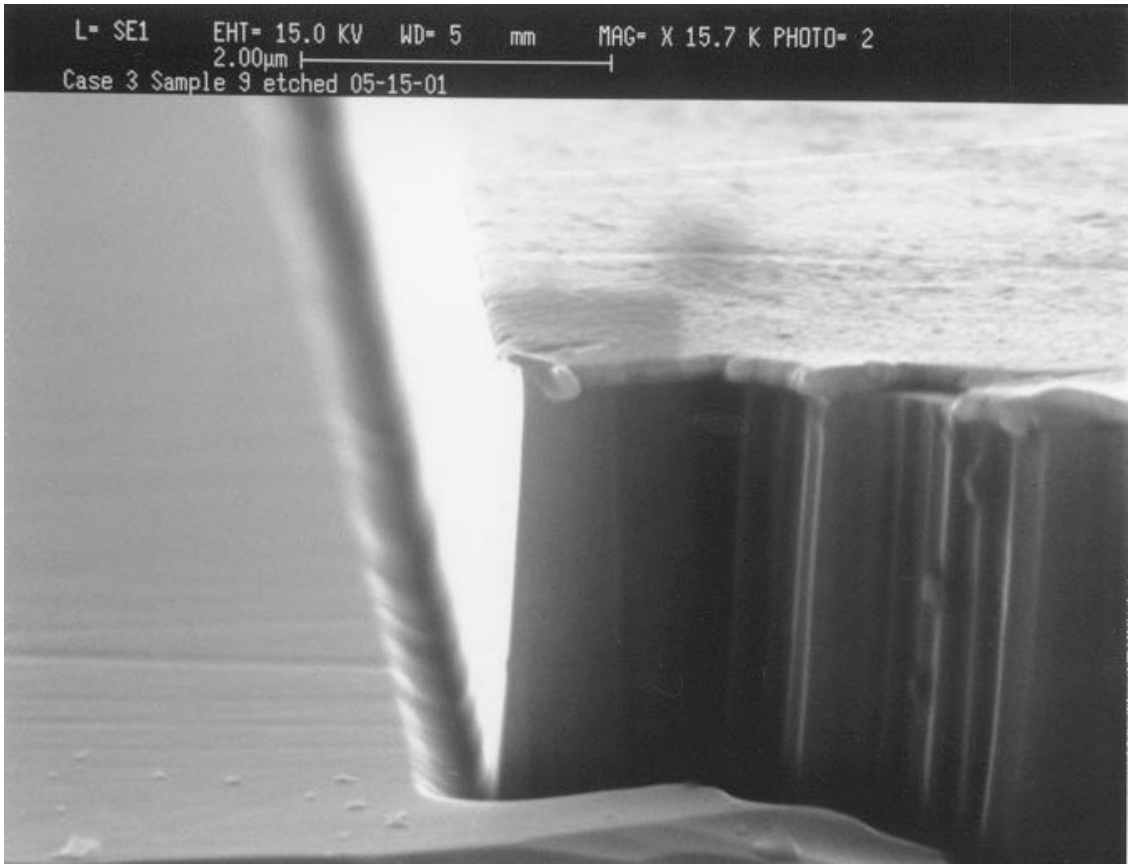

Figure 3.5 SEM showing etch profile of a sample etched in SF_6:He:O_2 - 10:9:1 sccm at a pressure of 15 mTorr

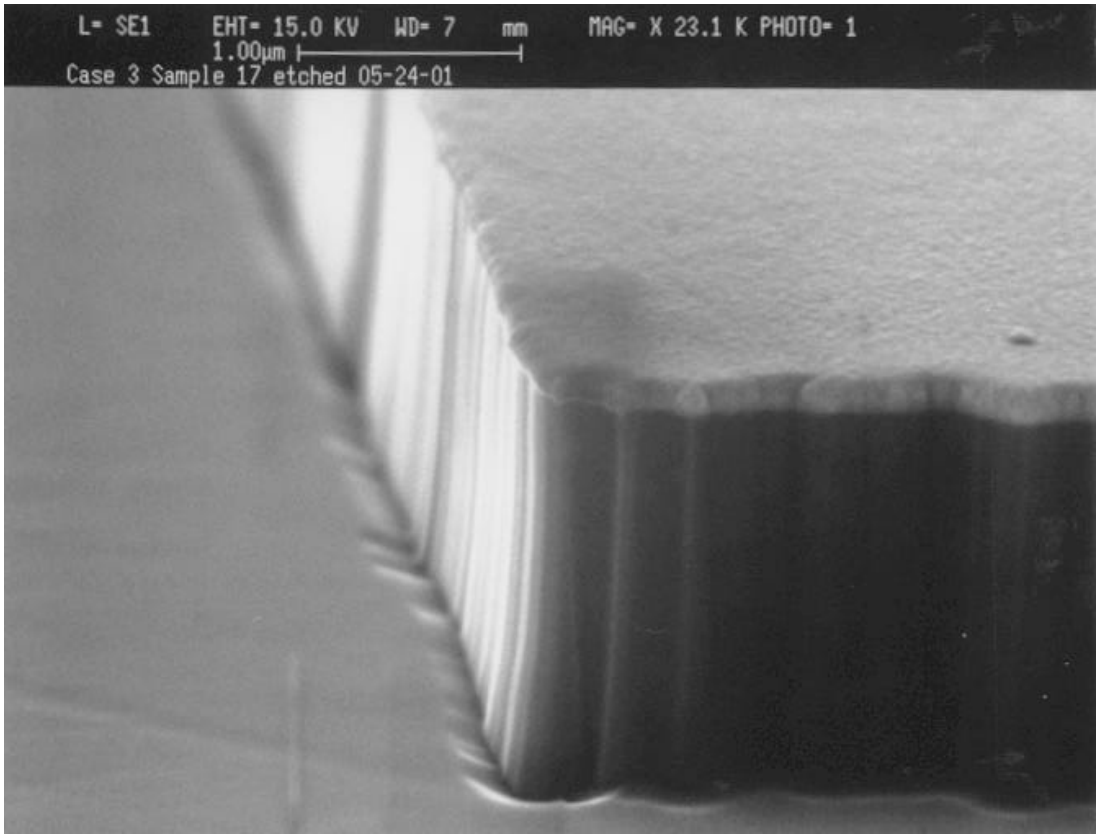

Figure 3.6 SEM showing etch profile of a sample etched in SF_6:He:O_2 - 15:13.5:1.5 sccm at a pressure of 15 mTorr

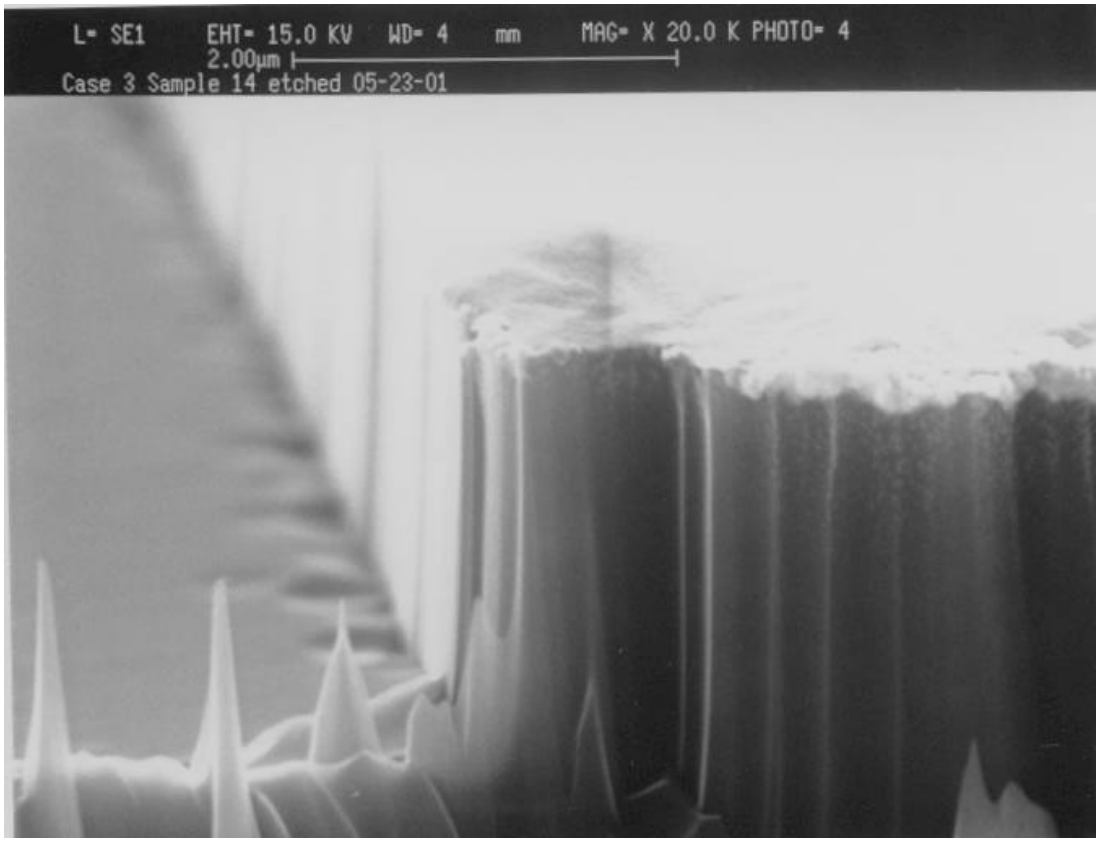

Figure 3.7 SEM showing etch profile of a sample etched in SF_6:He:O_2 - 10:9:1 sccm at a pressure of 25 mTorr

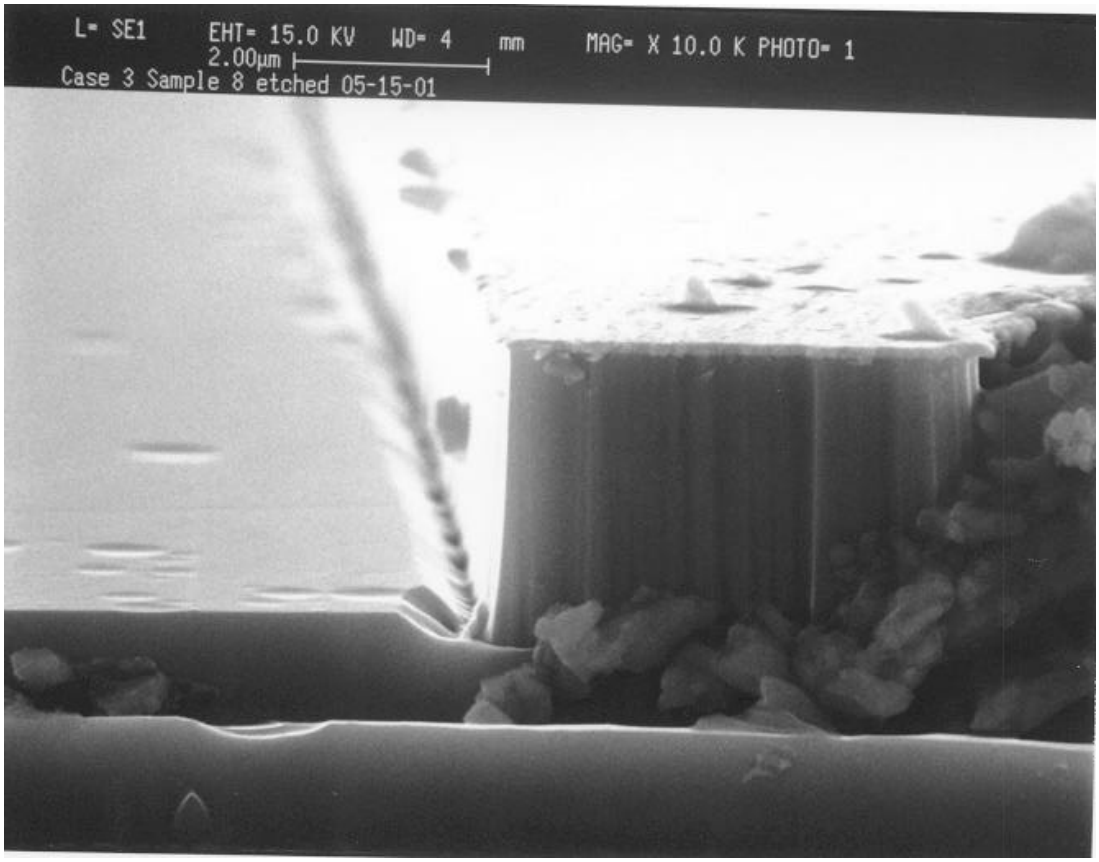

Figure 3.8 SEM showing etch profile of a sample etched in SF_6:He:O_2 - 15:13.5:1.5 sccm at a pressure of 25 mTorr

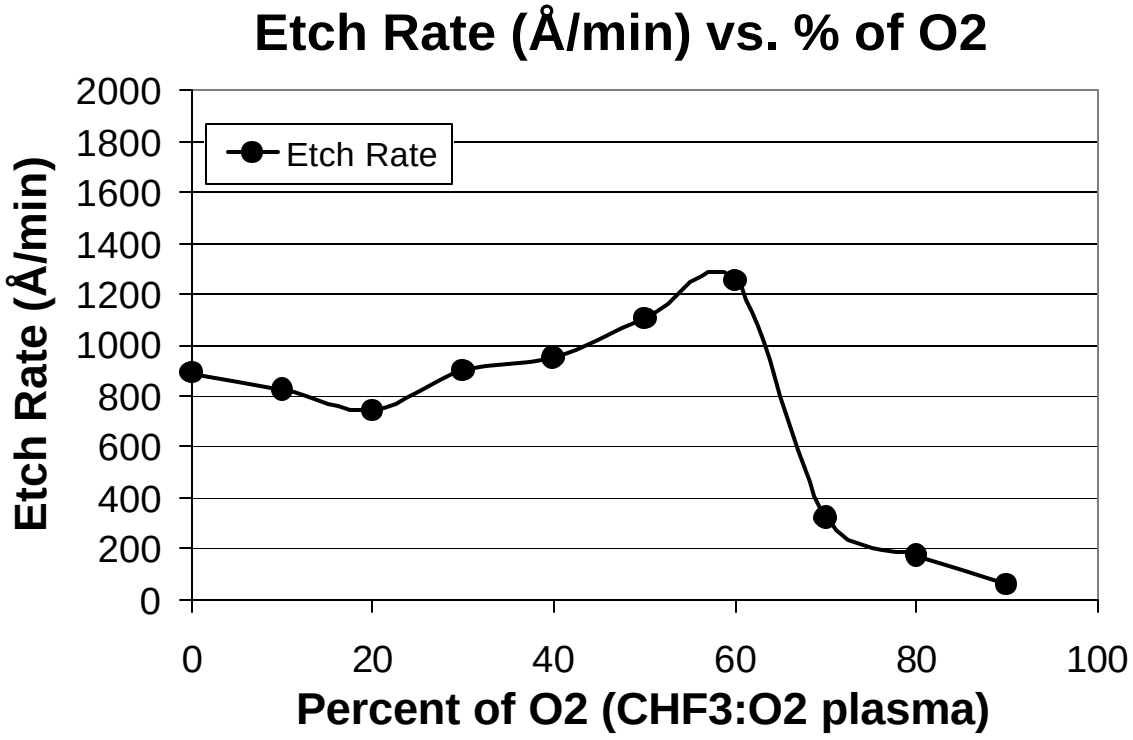

Figure 3.9 Graph showing the etch rate versus O_2 concentration in a CHF_3:O_2 plasma using a graphite carrier

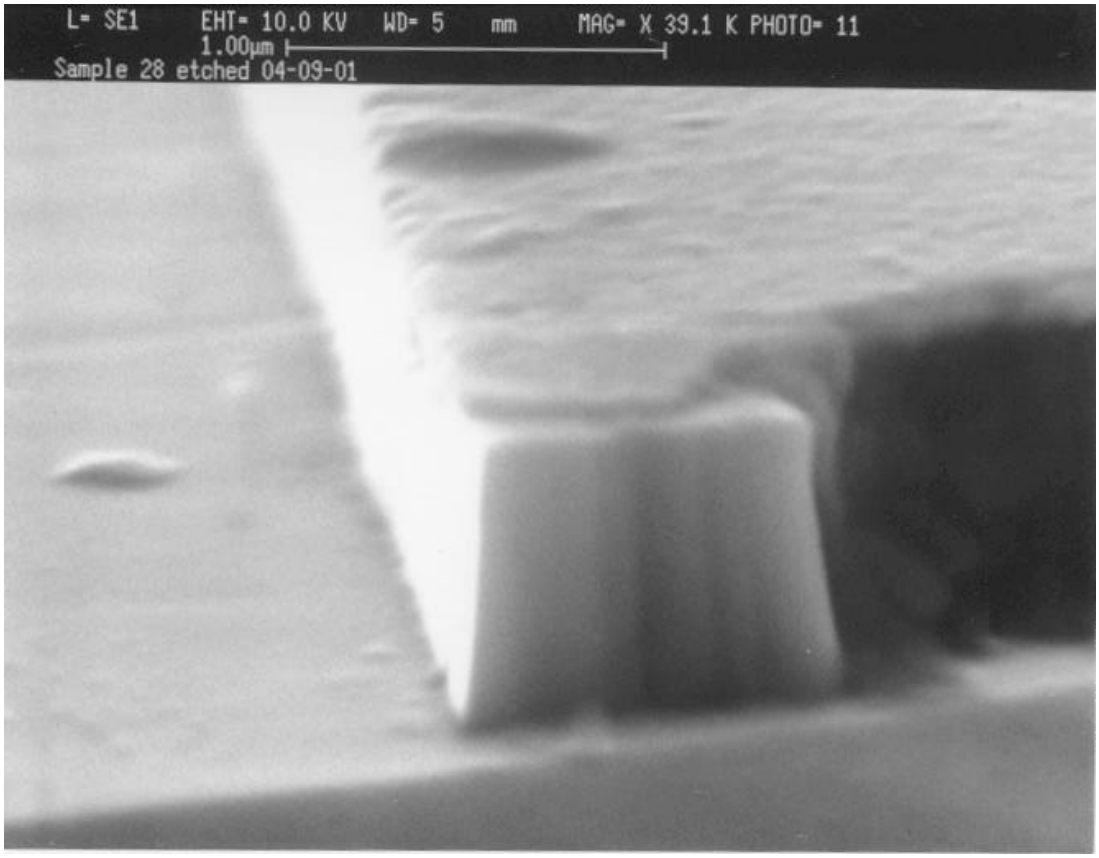

Figure 3.10 SEM showing etch profile of a sample etched in CHF_3:O_2 - 24:6 sccm at a pressure of 25 mTorr

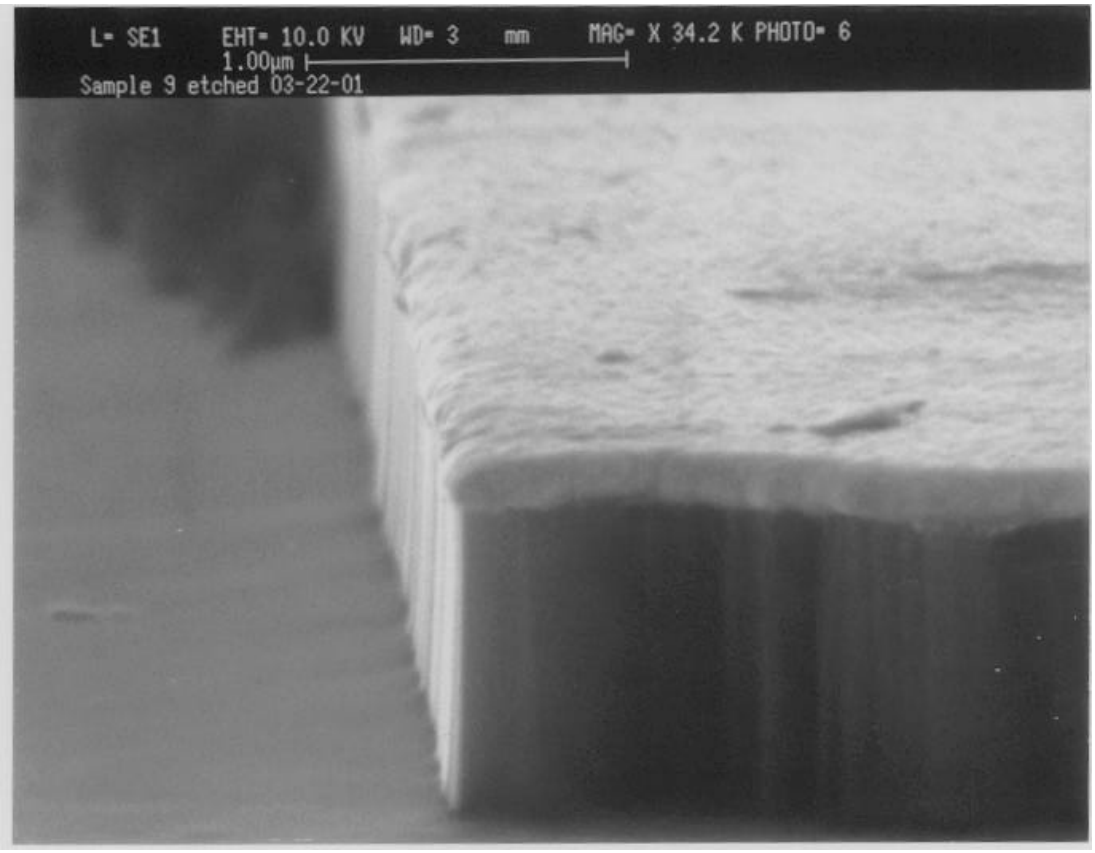

Figure 3.11 SEM showing etch profile of a sample etched in CHF_3:O_2 - 18:12 sccm at a pressure of 25 mTorr

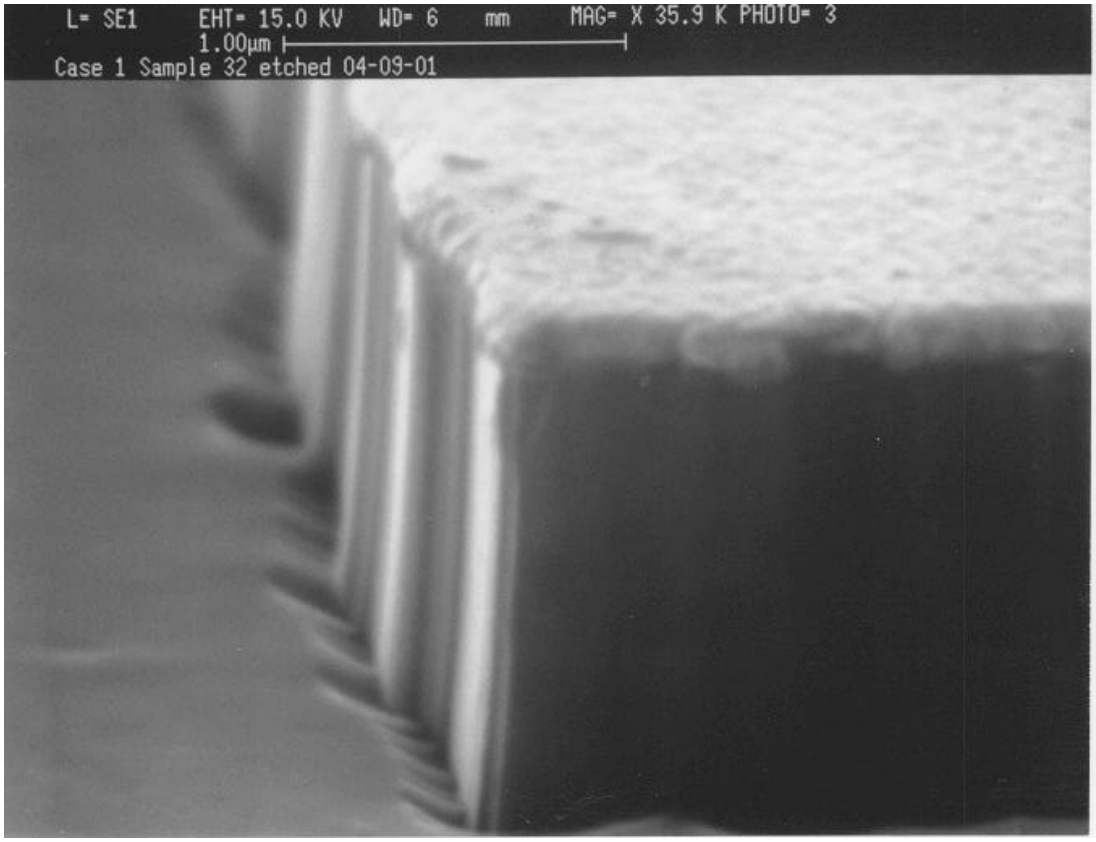

Figure 3.12 SEM showing etch profile of a sample etched in CHF_3:O_2 - 12:18 sccm at a pressure of 25 mTorr

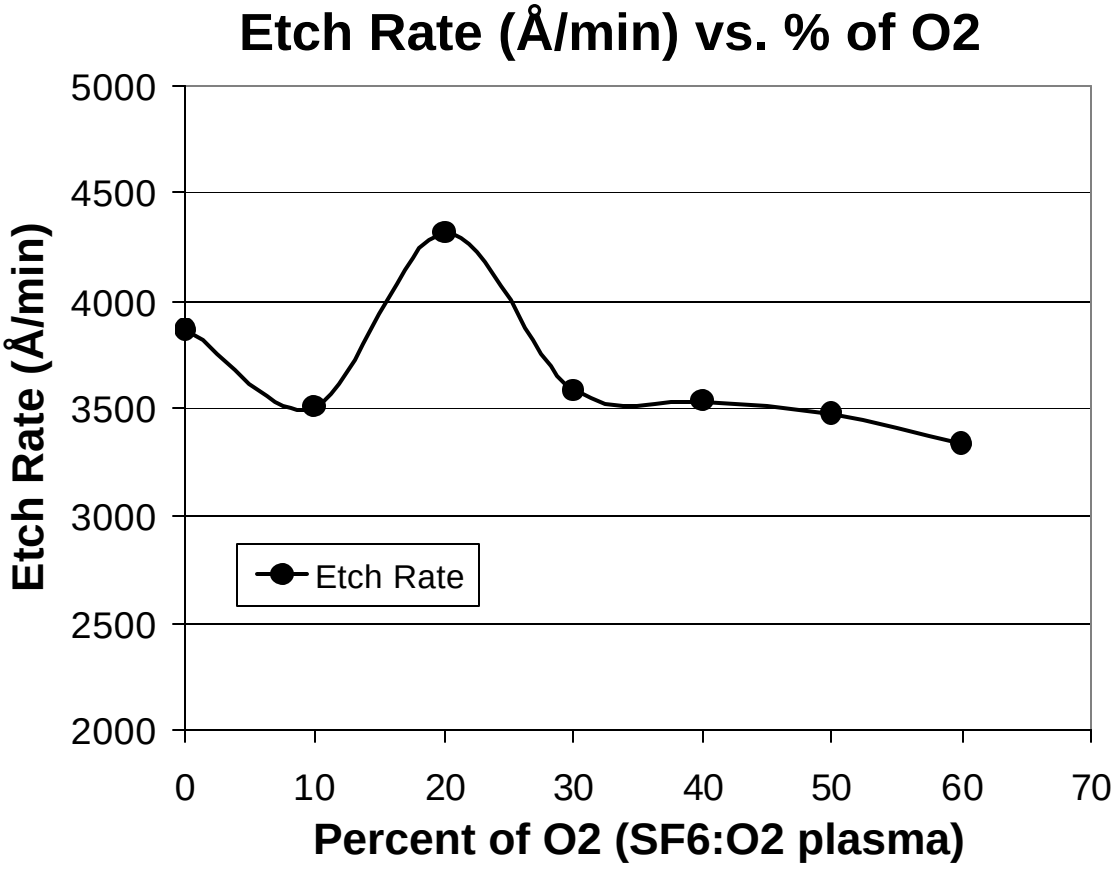

Figure 3.13 Graph showing the etch rate versus O_2 concentration in a SF_6:O_2 plasma

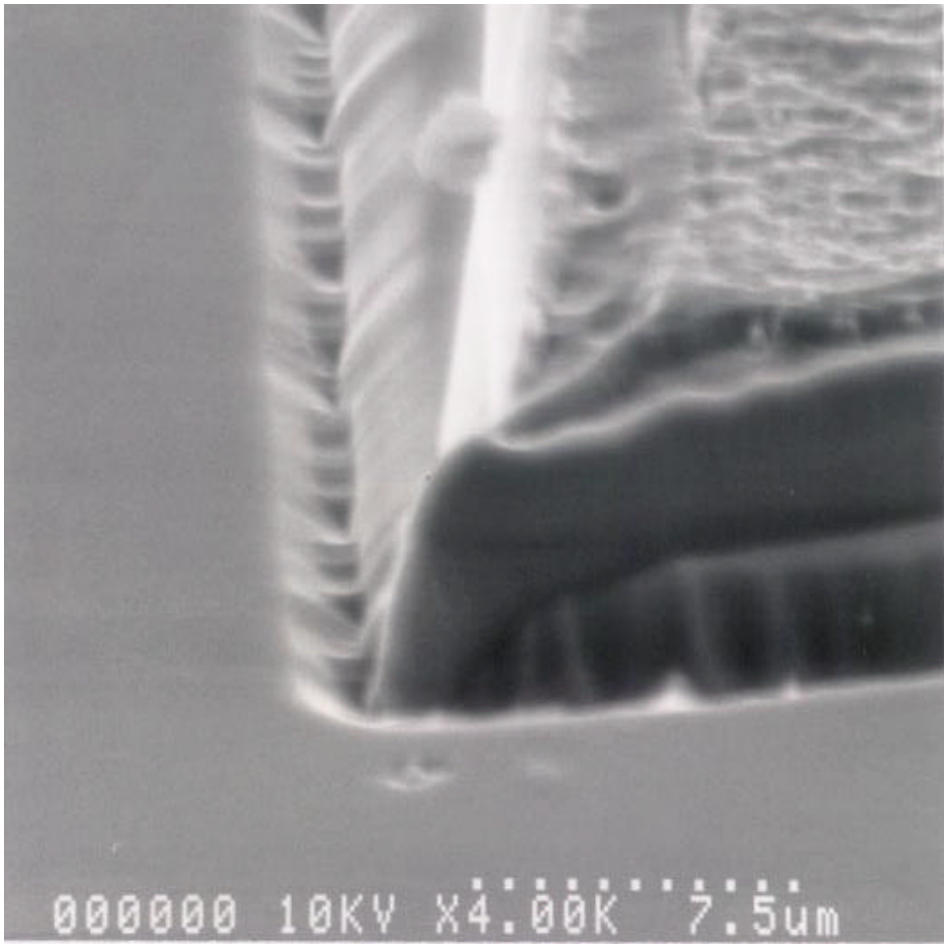

Figure 3.14 SEM showing etch profile of a sample etched in SF_6:O_2 - 24:6 sccm at a pressure of 25 mTorr

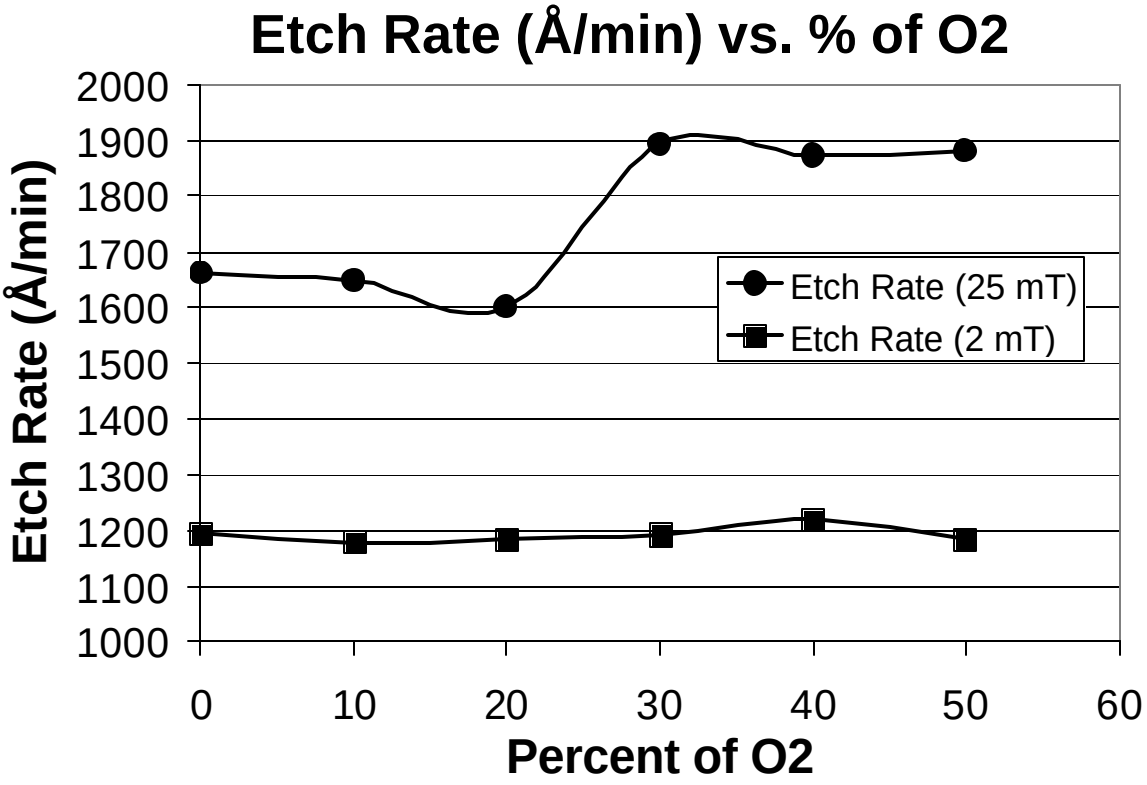

Figure 3.15 Graph showing the etch rate versus O_2 concentration in a NF_3:O_2 plasma at 2 and 25 mTorr

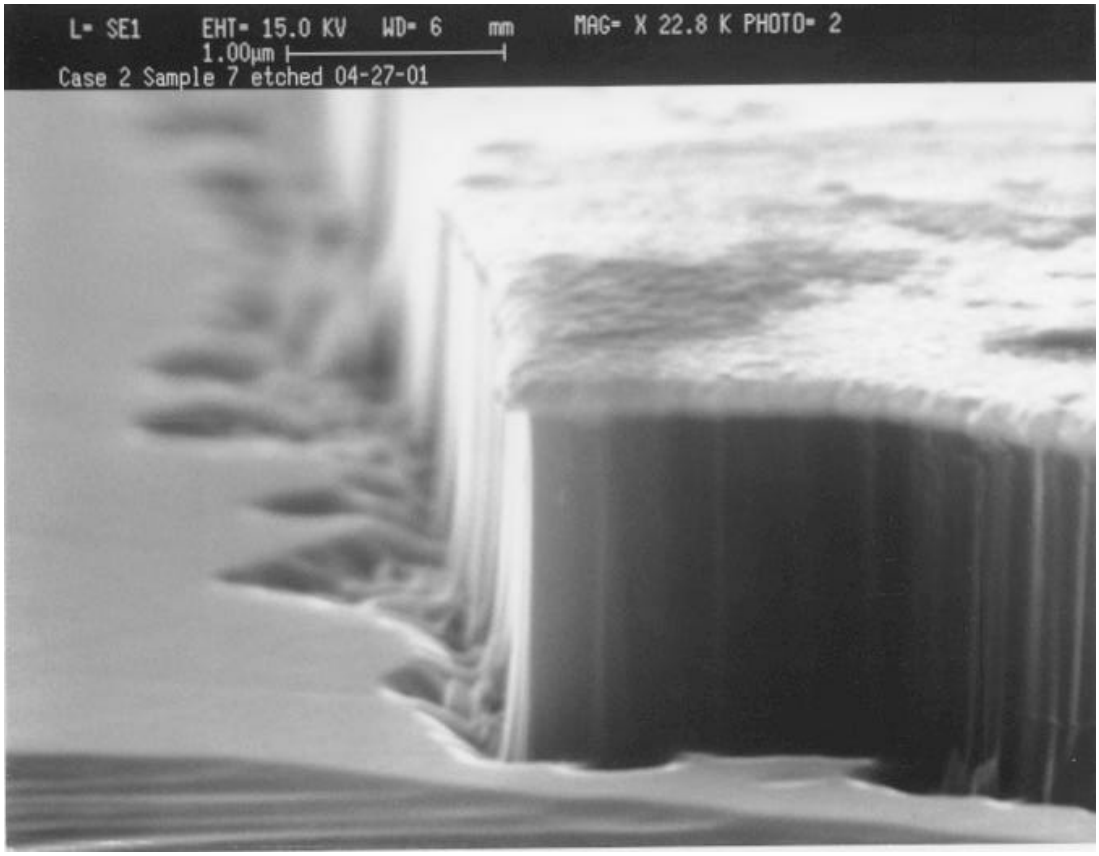

Figure 3.16 SEM showing etch profile of a sample etched in NF_3:O_2 - 27:3 sccm at a pressure of 2 mTorr

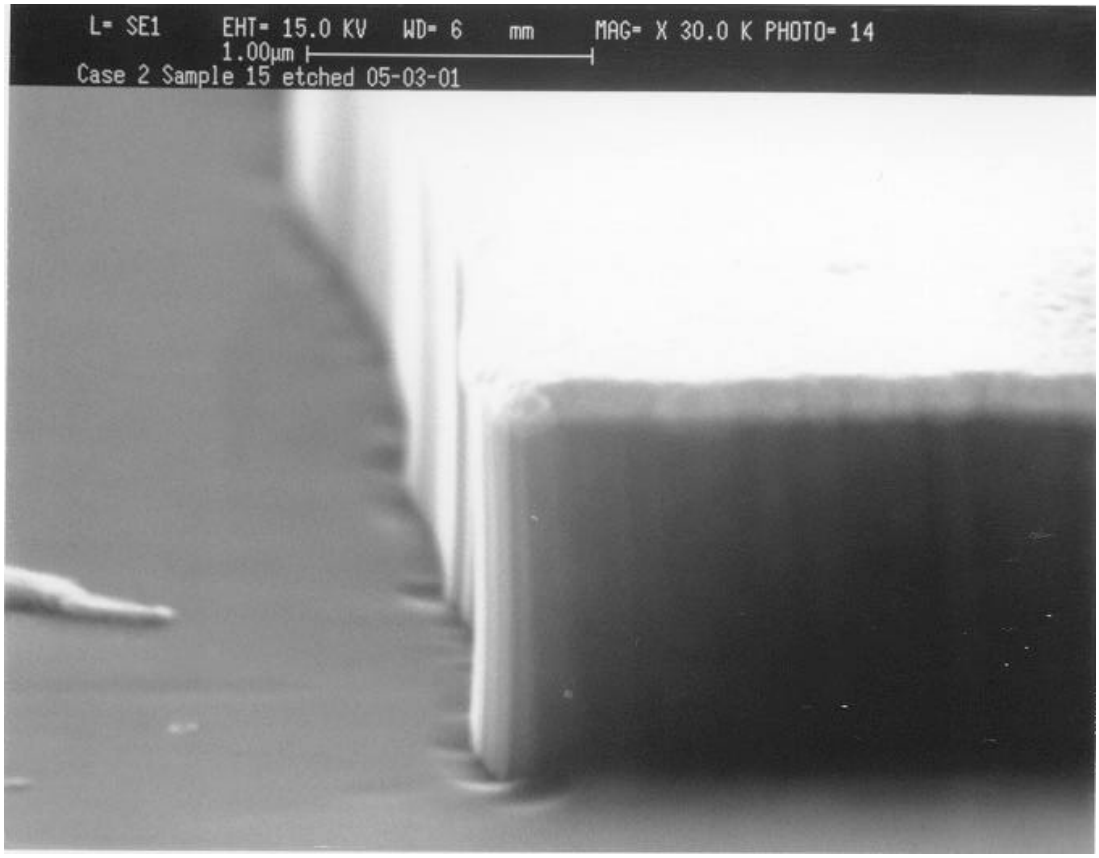

Figure 3.17 SEM showing etch profile of a sample etched in NF_3:O_2 - 27:3 sccm at a pressure of 25 mTorr

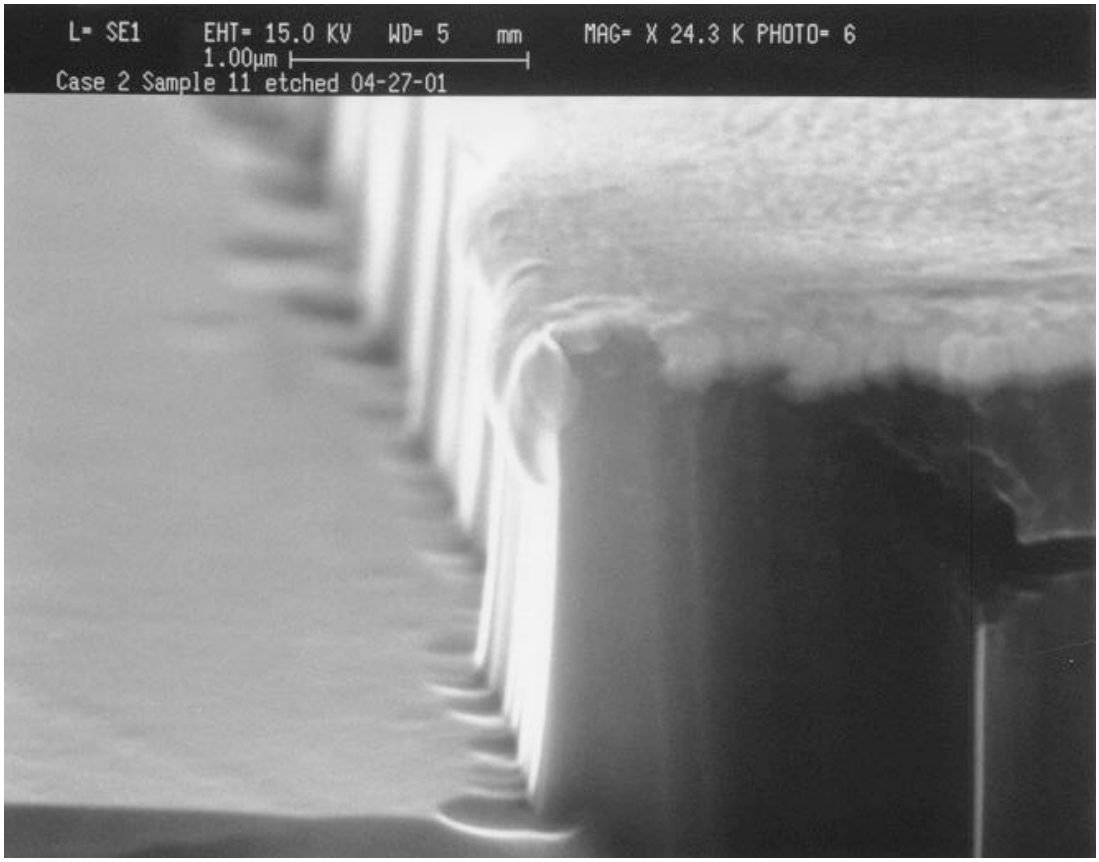

Figure 3.18 SEM showing etch profile of a sample etched in NF_3:O_2 -15:15 sccm at a pressure of 2 mTorr

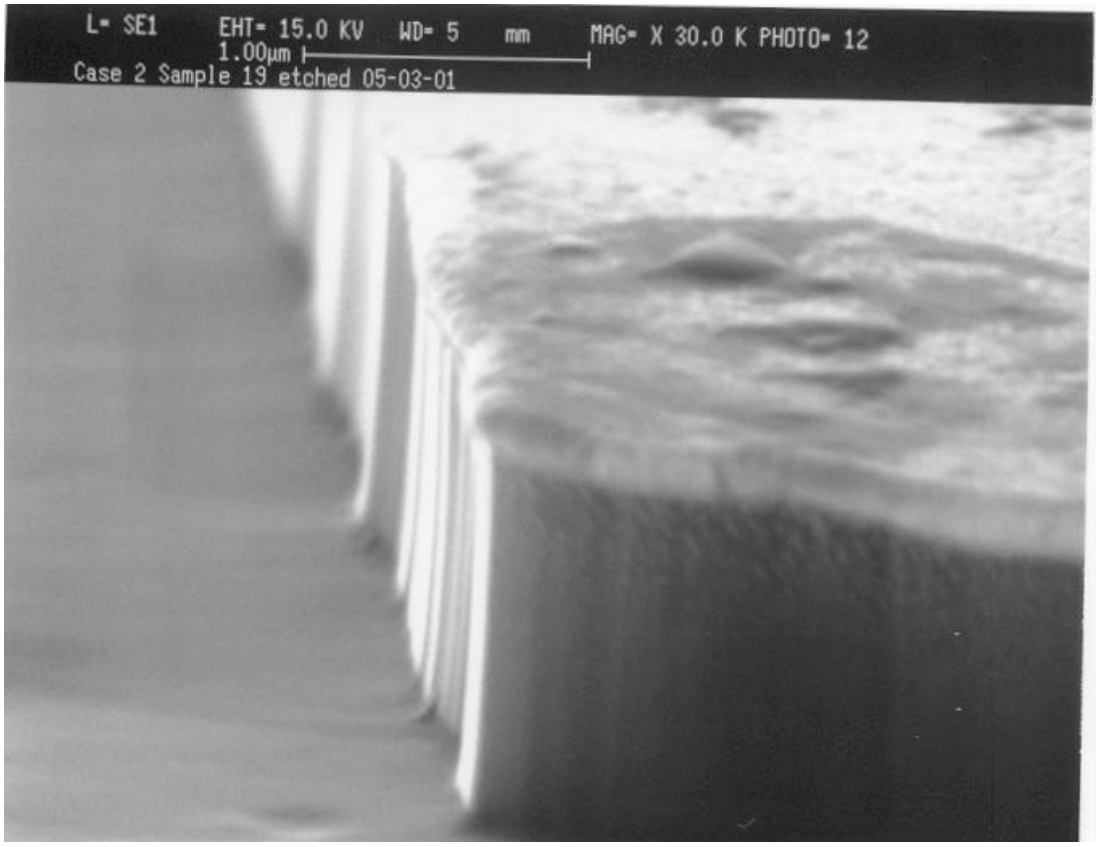

Figure 3.19 SEM showing etch profile of a sample etched in NF_3:O_2 -15:15 sccm at a pressure of 25 mTorr

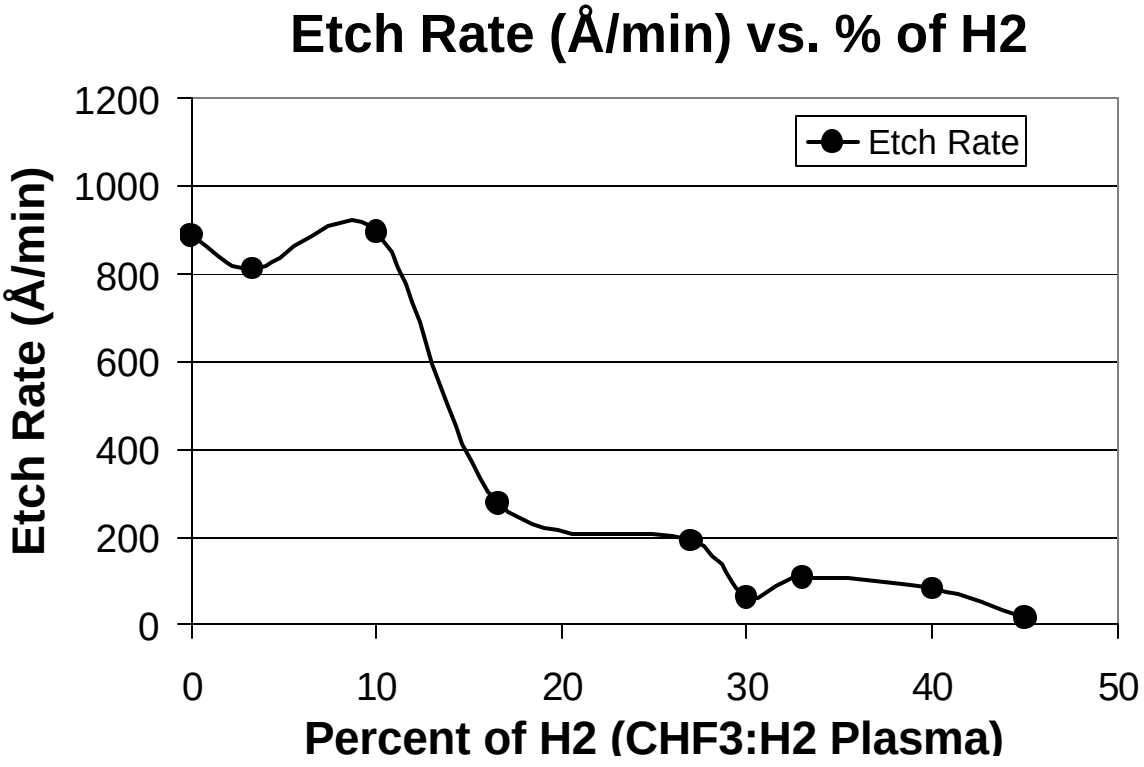

Figure 3.20 Graph showing the etch rate versus H_2 concentration in a CHF_3:H_2 plasma

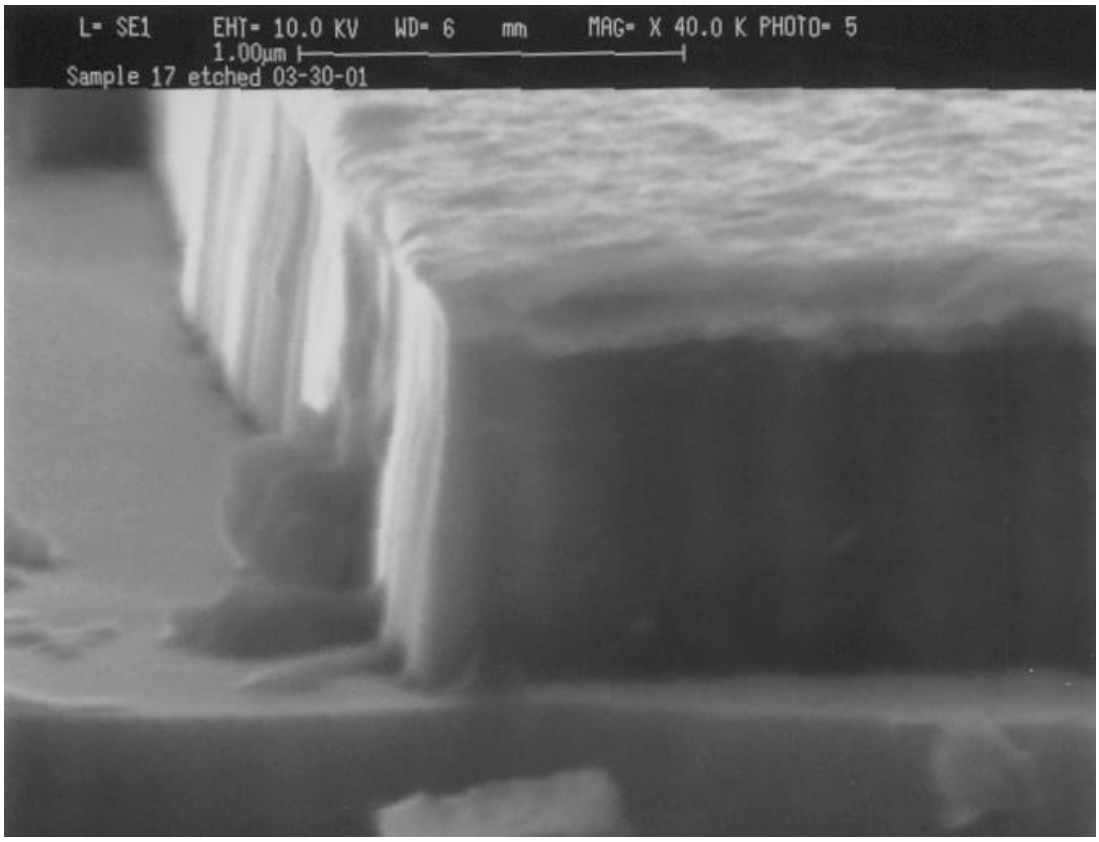

Figure 3.21 SEM showing etch profile of a sample etched in CHF_3:H_2 - 28:2 sccm at a pressure of 25 mTorr

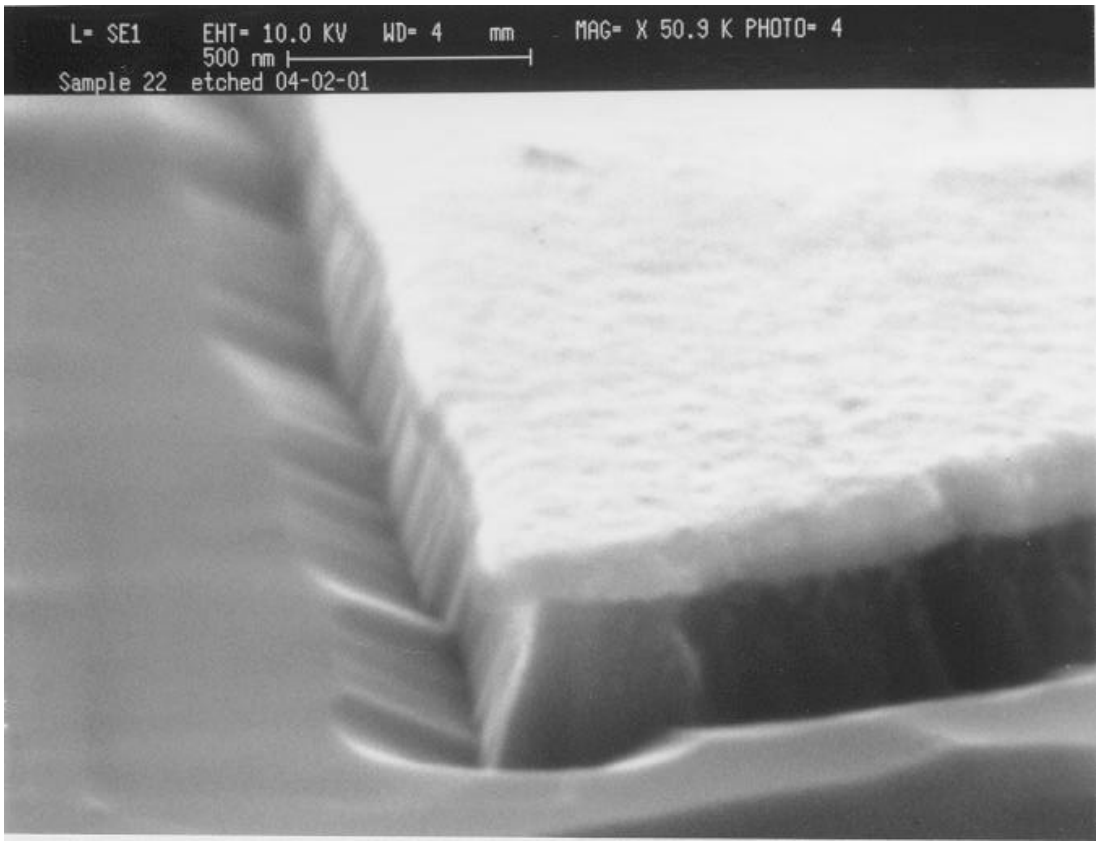

Figure 3.22 SEM showing etch profile of a sample etched in CHF_3:H_2 - 25:5 sccm at a pressure of 25 mTorr

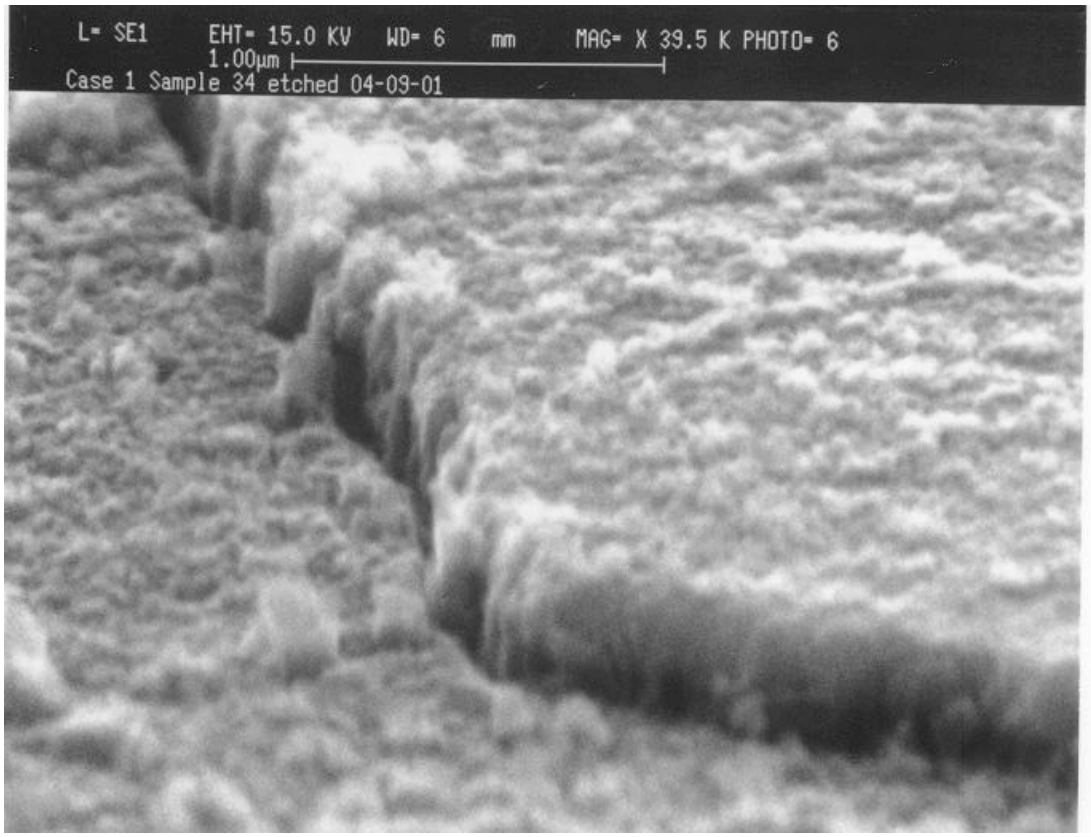

Figure 3.23 SEM showing etch profile of a sample etched in CHF_3:H_2 - 18:12 sccm at a pressure of 25 mTorr

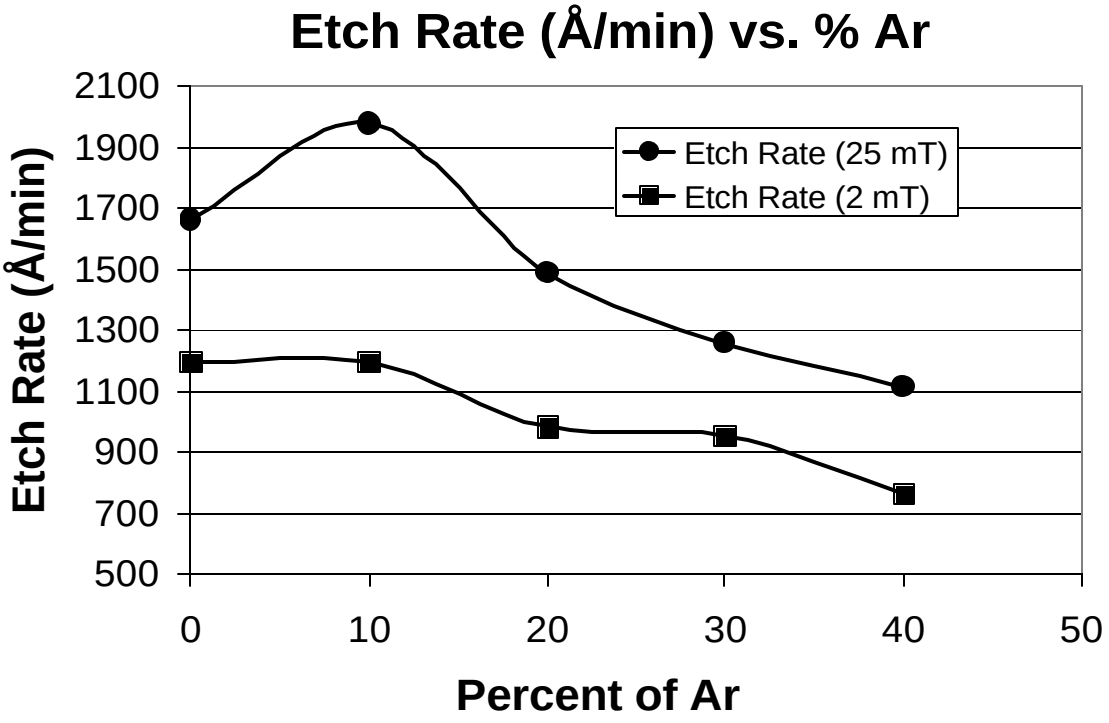

Figure 3.24 Graph showing the etch rate versus Ar concentration in a NF_3:Ar plasma at 2 and 25 mTorr

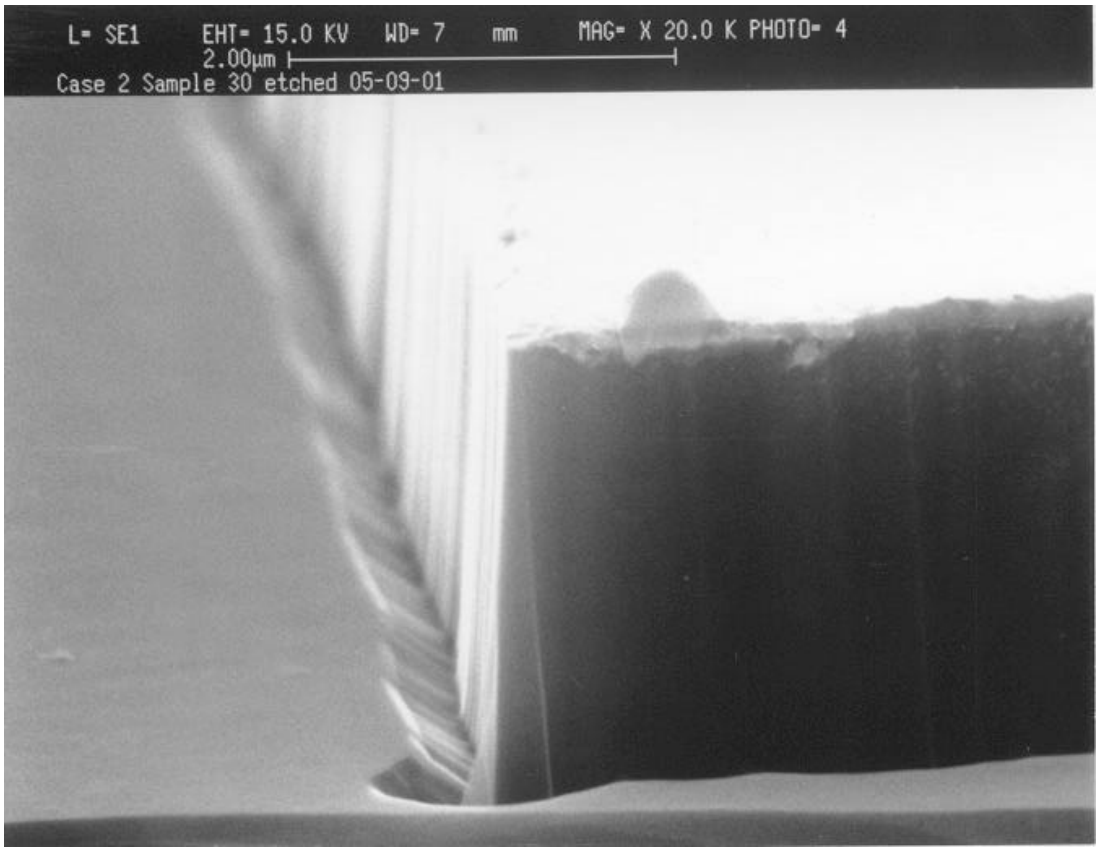

Figure 3.25 SEM showing etch profile of a sample etched in NF_3:Ar - 27:3 sccm at a pressure of 2 mTorr

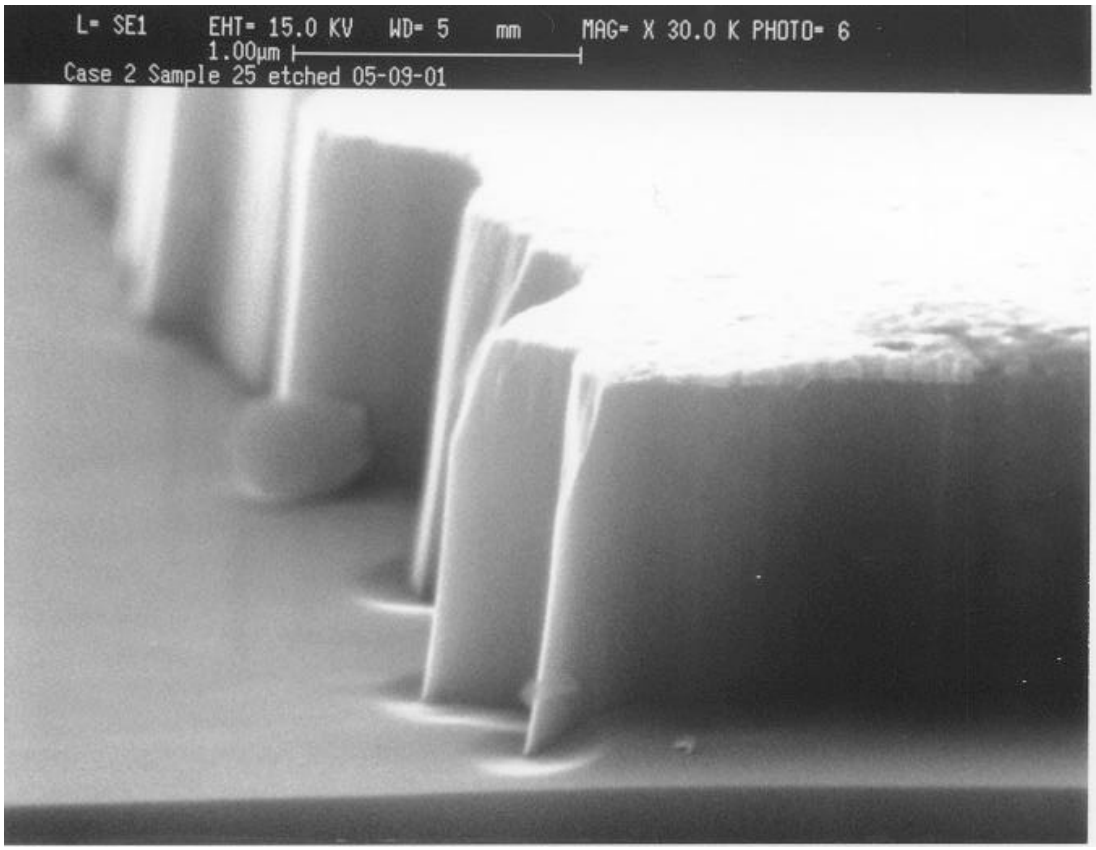

Figure 3.26 SEM showing etch profile of a sample etched in NF_3:Ar - 27:3 sccm at a pressure of 25 mTorr

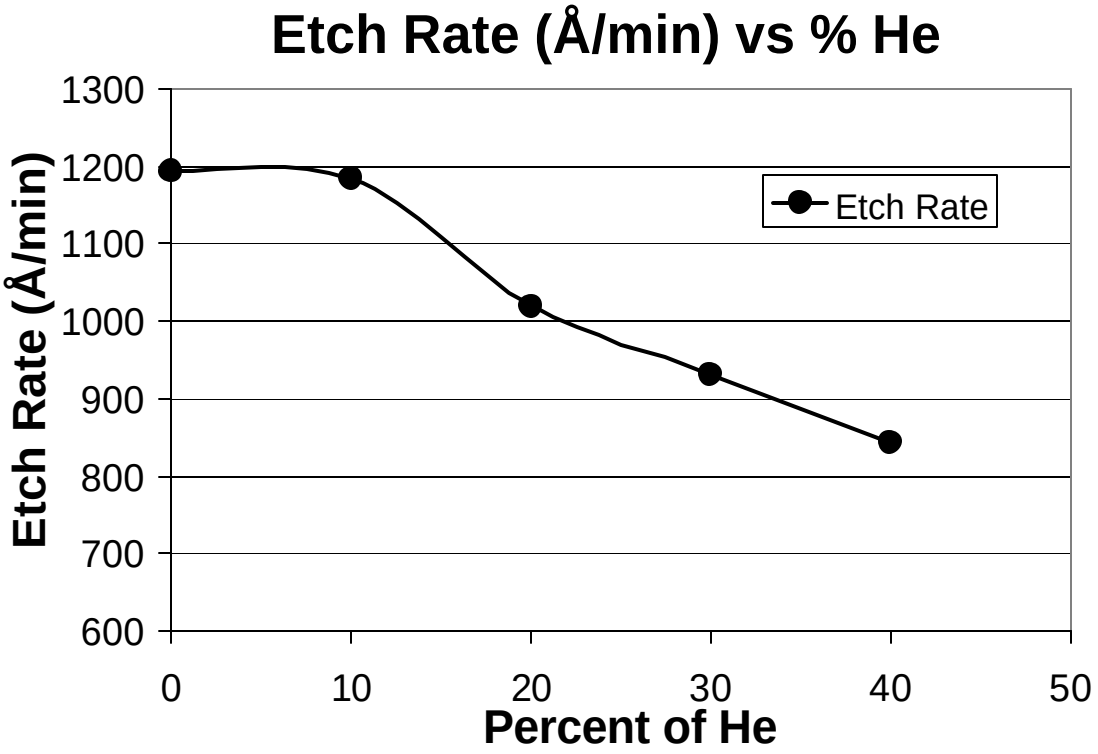

Figure 3.27 Graph showing the etch rate versus He concentration in a NF_3:He plasma

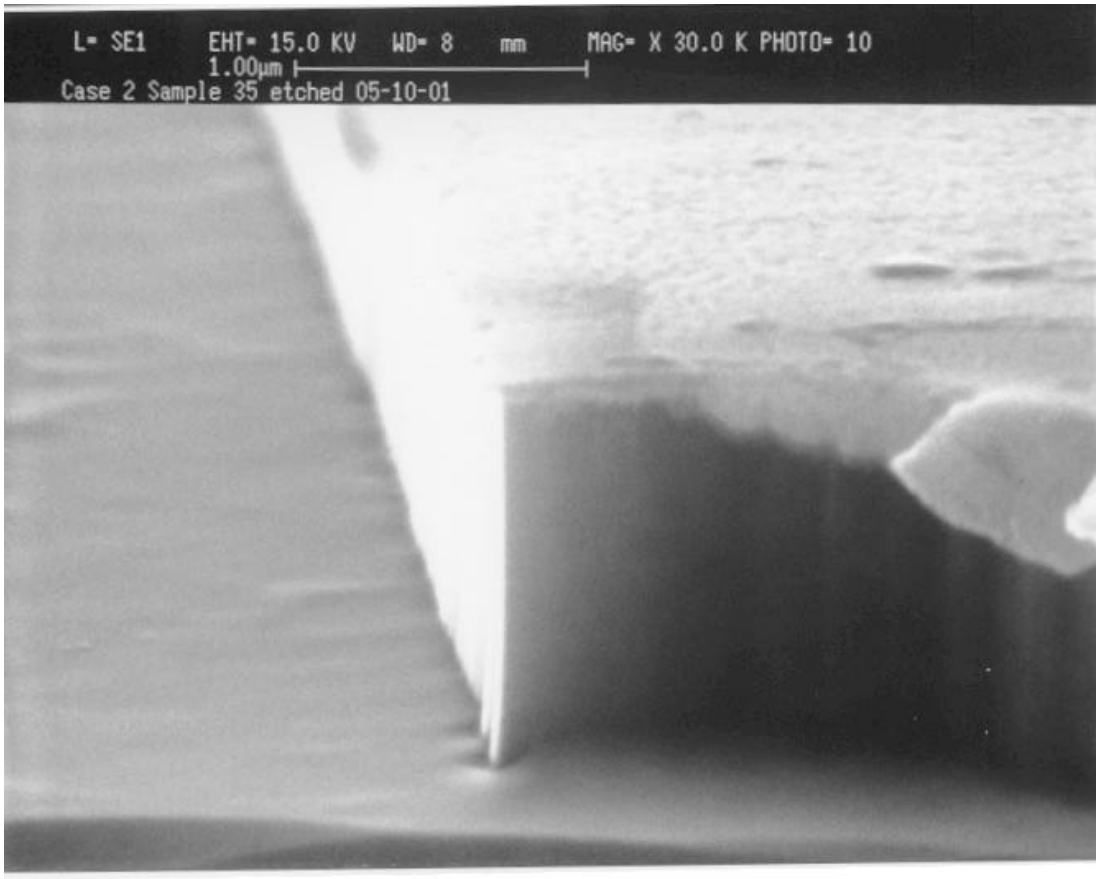

Figure 3.28 SEM showing etch profile of a sample etched in NF_3:He - 27:3 sccm at a pressure of 2 mTorr

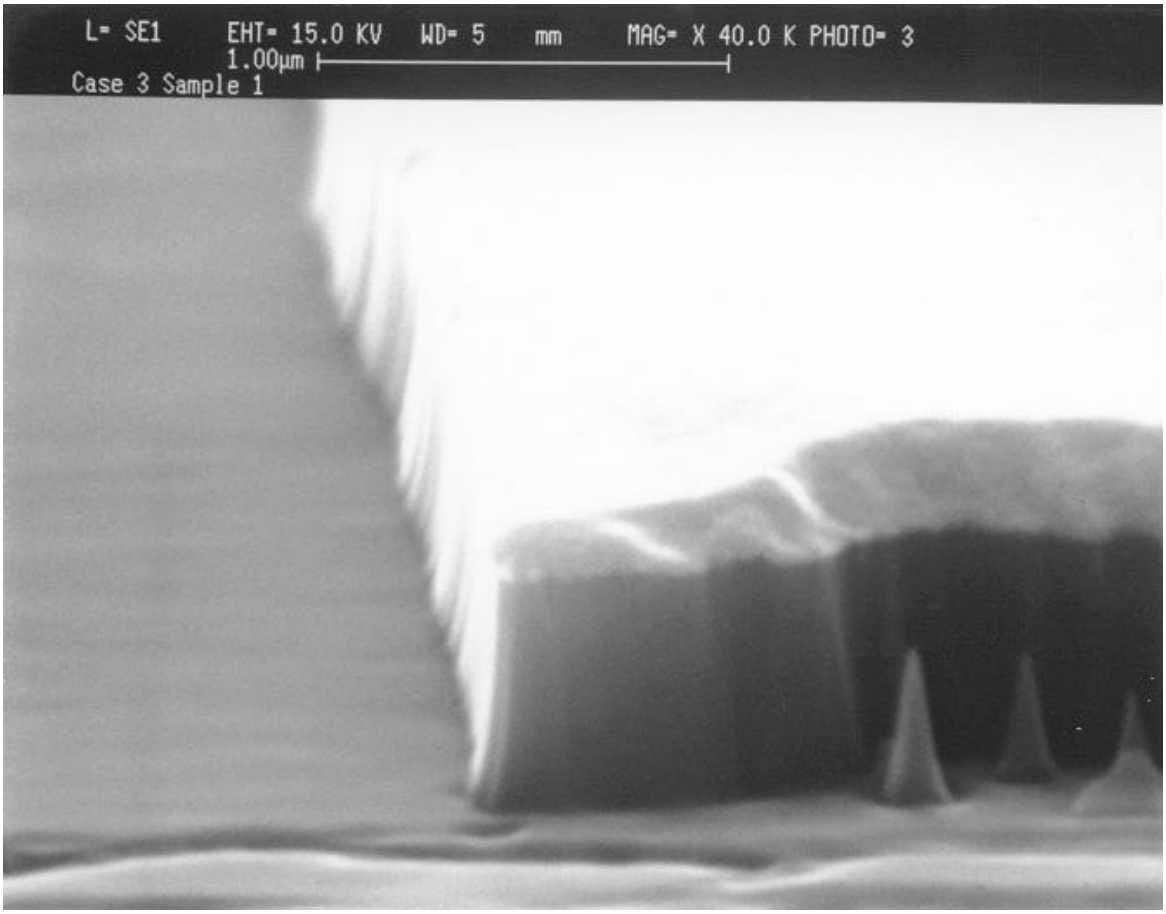

Figure 3.29 SEM showing etch profile of a sample etched in NF_3:He – 24:6 sccm at a pressure of 2 mTorr

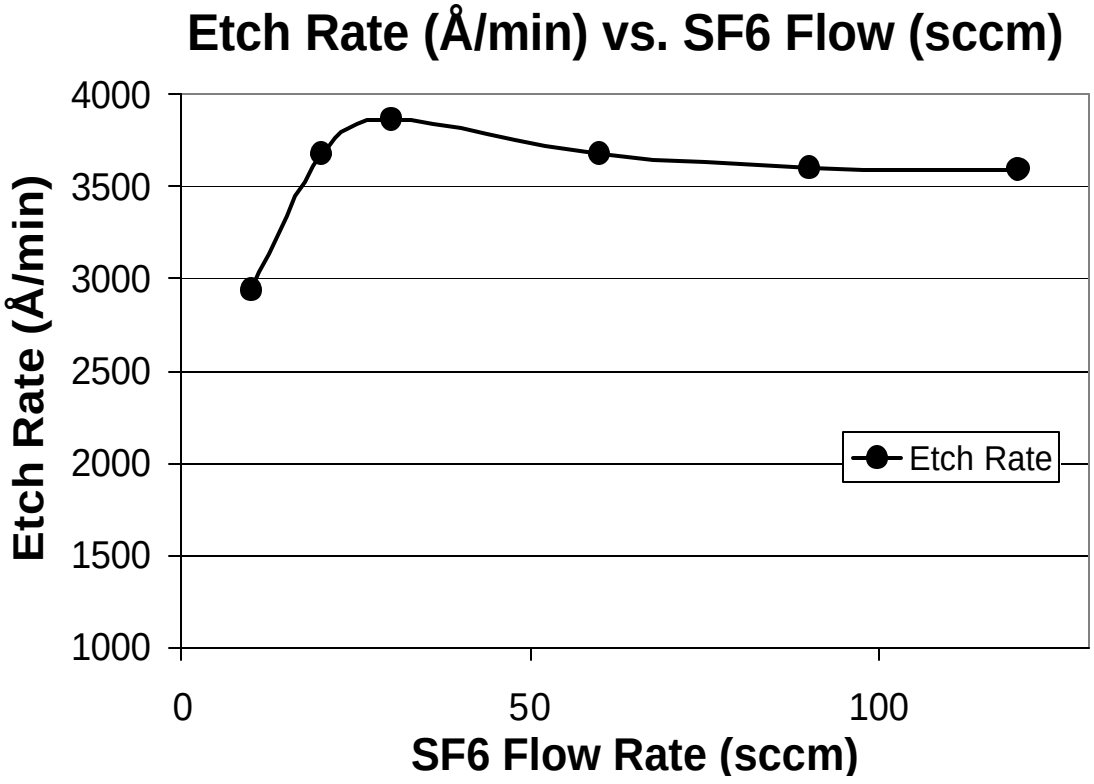

Figure 3.30 Graph showing the etch rate versus gas flow in a SF_6 plasma at 25 mTorr

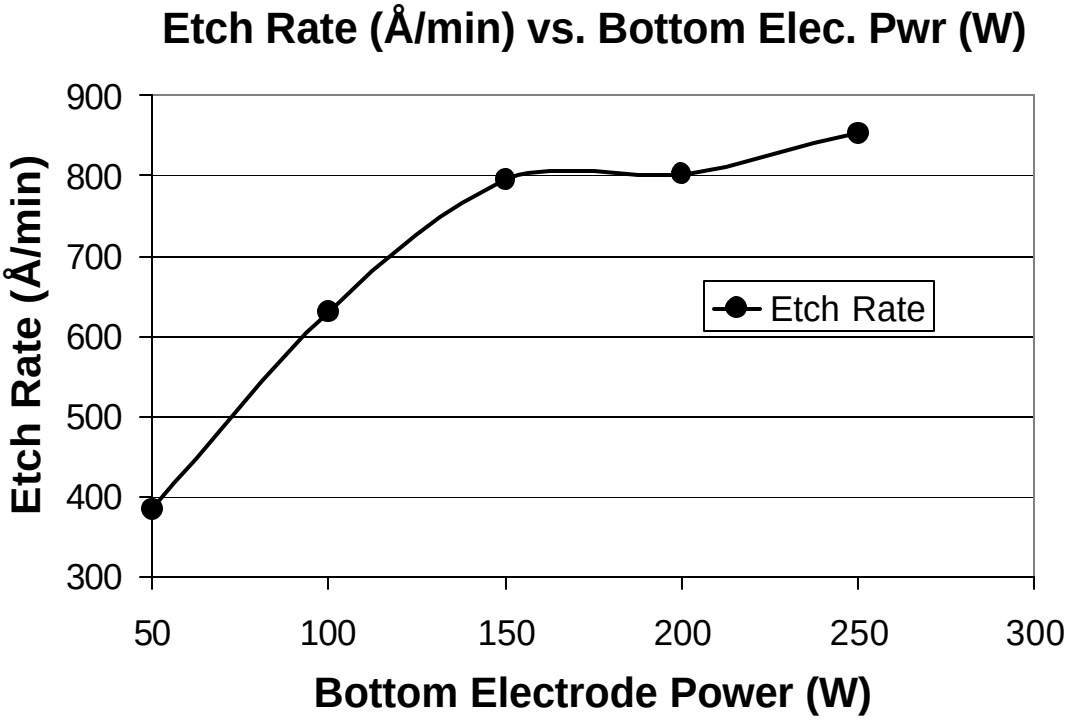

Figure 3.31 Graph showing the etch rate versus bottom electrode power in a CHF_3 plasma at 25 mTorr

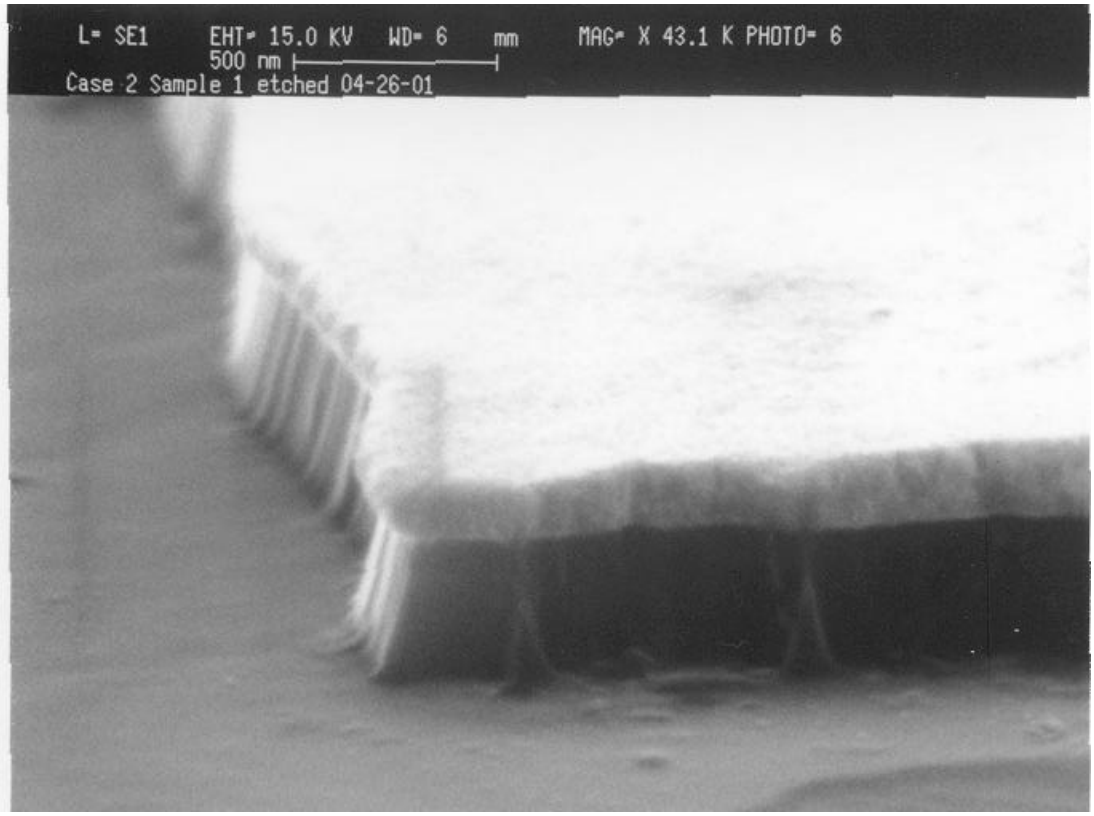

Figure 3.32 SEM showing etch profile of a sample etched in CHF_3 - 30 sccm at a pressure of 25 mTorr with a top power of 500W and a bottom power of 50W

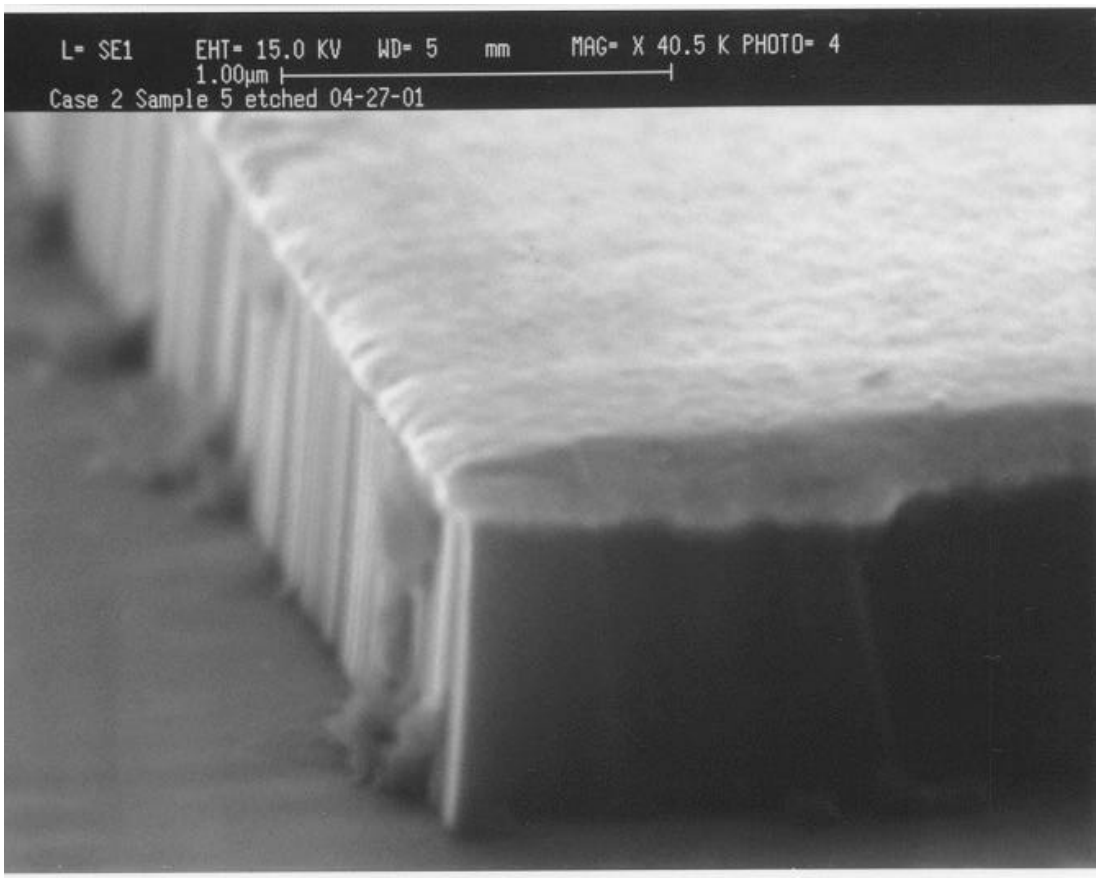

Figure 3.33 SEM showing etch profile of a sample etched in CHF_3 - 30 sccm at a pressure of 25 mTorr with a top power of 500W and a bottom power of 250W

VJFET Etch Development

In this work, a 3 μm deep SiC etch for a 2 μm wide structure spaced 1 μm apart was examined. An etch was performed at 3 mTorr in a SF_6 plasma. The gas flow was 20 sccm, the top power was 175 W and the bottom power was 150 W. The resulting etch rate was 200 Å/min. The sample exhibited small amounts of trenching at the sidewalls and a slanted sidewall as shown in Figure 3.34. Increased bottom power straighted the walls but enhanced mask erosion making it impossible to etch the depth needed. The use of NF_3 seemed to reduce mask erosion. An etch was performed at 2 mTorr in a NF_3:He plasma. The total gas flow was 20 sccm and the ratio was 10:10. The top power was 200 W and the bottom power was 75 W. The resulting etch rate was 666 Å/min. As shown in Figure 3.35, the etch produced trenching but the sidewalls were vertical. Continued work is being done to develop an etch without trenching.

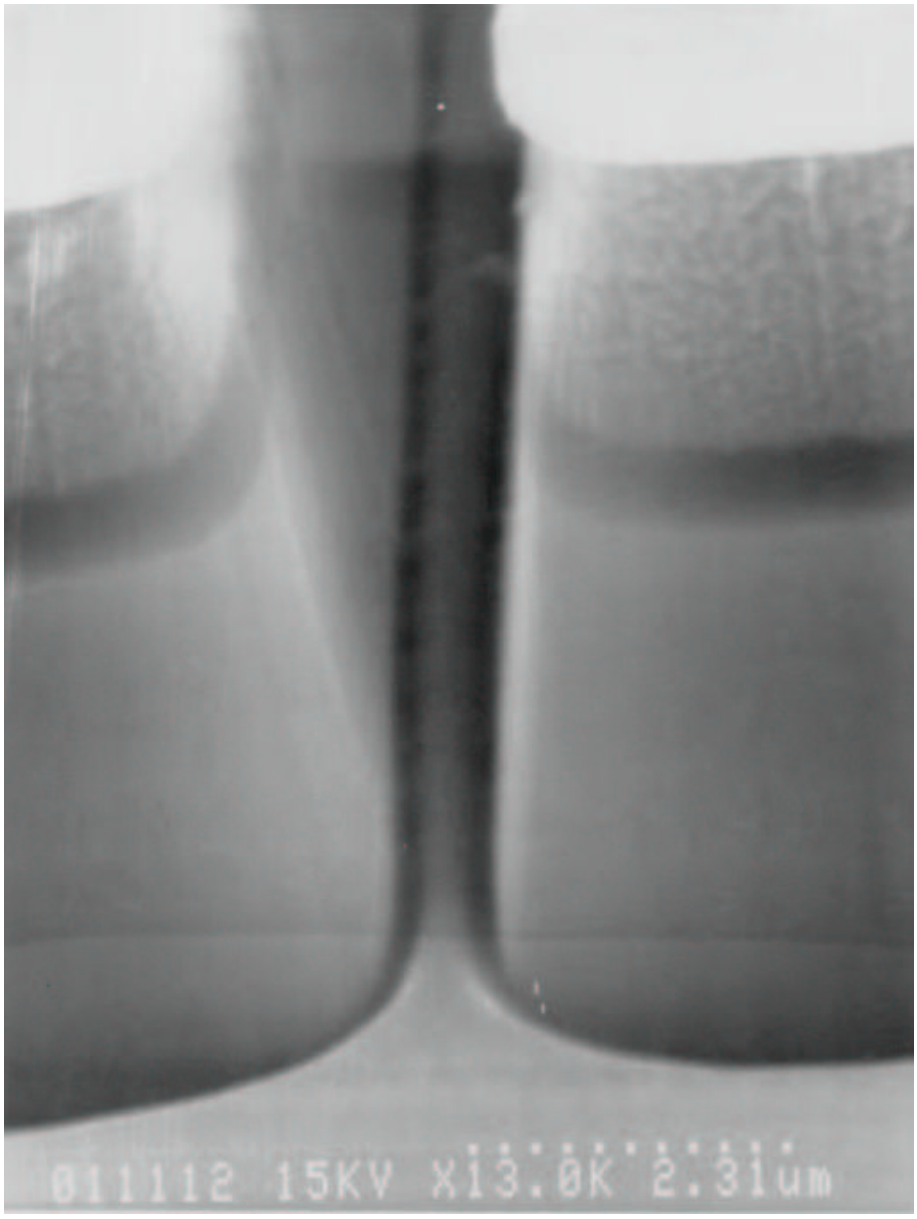

Figure 3.34 SEM showing etch profile of a sample etched in SF_6 - 20 sccm at a pressure of 3 mTorr with a top power of 175 W and a bottom power of 150 W

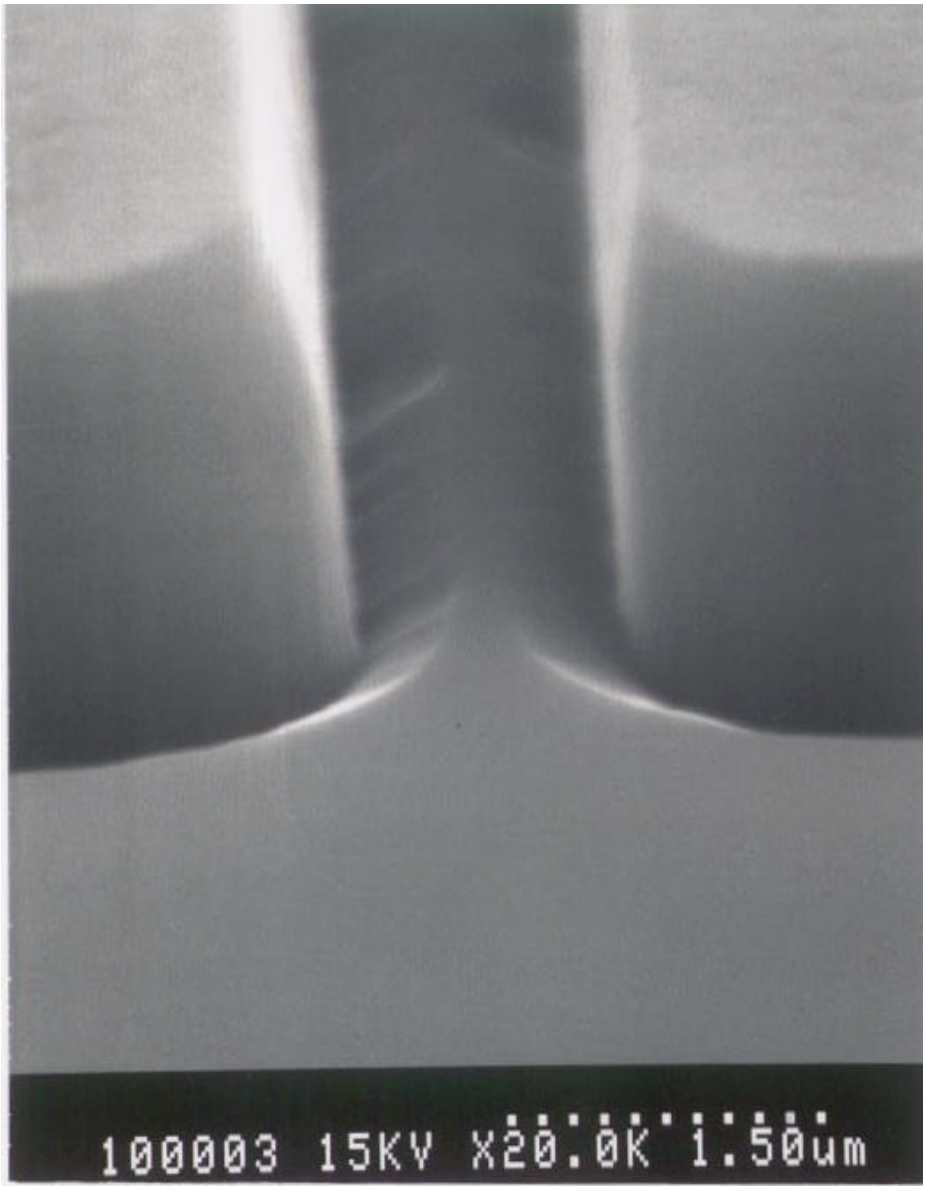

Figure 3.35 SEM showing etch profile of a sample etched in NF_3:He – 10:10 sccm at a pressure of 2 mTorr with a top power of 200 W and a bottom power of 75 W

CHAPTER IV

DISSCUSSION OF RESULTS

In Chapter 4 the experimental results of the etch work performed was provided with little discussion. In the following chapter a detailed discussion of the affects of the parameter variations and outcoming etch rates, etch profiles, and surface morphology will be provided.

Variation of Parameters

Carrier Material

As previously mentioned, the carrier material was examined, and a decision was made to use the graphite carrier instead of the SiC carrier. This decision was based on the fact that higher etch rates are obtained using the graphite carrier and since SiC is the material of interest to be etched, the loading effects are believed to be less with the graphite versus the SiC carrier. Both of these phenomenons are related to the etching behavior of graphite (carbon) and SiC. The bond energies for Si-C and C-C are 4.52 eV and 6.27 eV, respectively. Since the energy to break the C-C bonds is higher, etching occurs more favorably on SiC. In a fluorinated plasma, the use of a graphite carrier results in higher etch rates than the SiC carrier because smaller amounts of the reactive species are being consumed from the carrier material. The loading effects are also less

for SiC etching when using a graphite carrier since the etching behavior is different for the graphite carrier versus the SiC carrier with respect to the material being etched. The etch rate can vary, depending on how much SiC area is exposed to the plasma, as shown in the example given below:

Assume that 50 mm diameter SiC wafers are masked leaving only 10 mm^2 of SiC area exposed to the plasma to be etched:

A (exposed SiC) = A (carrier) – A (SiC on the carrier covered by the etch sample) + A (SiC exposed on the etch sample)

For 1 wafer: A (exposed SiC) = 32413 – 2026 + 10 = 30397 mm^2

For 2 wafers: A (exposed SiC) = 32413 – 4052 + 20 = 28381 mm^2

For 3 wafers: A (exposed SiC) = 32413 – 6078 + 30 = 26305 mm^2

For 4 wafers: A (exposed SiC) = 32413 – 8104 + 40 = 24269 mm^2

For 5 wafers: A (exposed SiC) = 32413 – 10130 + 50 = 22333 mm^2

Assuming R_o (the empty chamber etch rate) to be 1000 Å/min. and k to be $1x10^{-5}$ mm^2, the etch rates would vary as follows:

$$R_1 \text{ (etch rate of 1 wafer)} = \frac{R_o}{1+kA} = \frac{1000 \text{ Å/min.}}{1+(1x10^{-5})(30397)} = 767 \text{ Å/min.}$$

$$R_2 \text{ (etch rate of 2 wafers)} = \frac{R_o}{1+kA} = \frac{1000 \text{ Å/min.}}{1+(1x10^{-5})(28381)} = 779 \text{ Å/min.}$$

$$R_3 \text{ (etch rate of 3 wafers)} = \frac{R_o}{1+kA} = \frac{1000 \text{ Å/min.}}{1+(1x10^{-5})(26305)} = 792 \text{ Å/min.}$$

$$R_4 \text{ (etch rate of 4 wafers)} = \frac{R_o}{1+kA} = \frac{1000 \text{ Å/min.}}{1+(1x10^{-5})(24269)} = 805 \text{ Å/min.}$$

$$R_5 \text{ (etch rate of 5 wafers)} = \frac{R_o}{1+kA} = \frac{1000 \text{ Å/min.}}{1+(1x10^{-5})(22333)} = 818 \text{ Å/min.}$$

In most cases, loading affects tend to decrease the etch rate because more area of the etch material is being exposed to the plasma as additional wafers are added to the plasma resulting in a higher consumption of reactive species, but for this work the material being etched and the carrier under consideration are the same so the actual area of SiC exposed to the plasma is being reduced with the addition of more masked wafers to the system which results in a higher etch rate. While this example shows apparently only slight variations in the etch rate, it is still significant enough to result in catastrophic damage to devices when trying to precisely control the etch depth. especially over long etch times. The loading affects in this work may also be enhanced because the carrier is polycrystalline SiC compared to the single-crystalline SiC being etched. The polycrystalline SiC has a higher etch rate (resulting in higher F consumption) than single-crystalline SiC. Therefore, when the area of the carrier is reduced by adding wafers even fewer F atoms are consumed during the etch process which would tend to increase the etch rate even faster than predicted in the example.

Pressure

The operating pressure available in the Lam 9400 ranges from 1 to 99 mTorr, but for this work the pressure range varied from 2 to 50 mTorr only. This was due to the fact that a stable plasma (having no reflected power from the top and bottom electrodes and no pressure variation during the etch) was not achievable at 1 mTorr and the peak in etch rate occurred at 25 mTorr. A SF_6:He:O_2 plasma with gas ratios of 15:13.5:1.5 and 10:9:1 totaling a gas flow of 30 and 20 sccm, respectively, was used for this experiment. For

both cases the etch rate increased with pressure up to 25 mTorr and then reduced. In the case of the SF_6:He:O_2 plasma totaling 20 sccm of gas flow, a higher etch rate was observed at 5 mTorr than at 10 or 15 mTorr. This data point may be a statistical outlier, possibly due to random parameter variation in the equipment, but this cannot be confirmed since repeated etches were not performed and averaged. However, for both cases peak etch rates of 3283 Å/min. at 30 sccm of gas flow and 2503 Å/min. at 20 sccm of gas flow, were obtained at 25 mTorr.

The observed increase of the etch rate up to a particular operating pressure and then decreasing rate at higher pressures is consistent with other reports [30], but the absolute value of peak pressure depends on the particular etch system that is being used. As mentioned in Chapter 2, the mean free path of plasma components decreases with increasing pressure which produces more free radicals and ions to etch material, but at higher etch pressures polymers can form on the surface resulting in a decrease in the etch rate. A decrease in ion bombardment energy also occurs with increasing pressure which could also result in lower etch rates because the plasma components striking the surface may not have enough energy at the higher pressures to sputter a polymer or enhance chemical reactions on the surface.

Gas Additives

As mentioned in Chapter 4, the effects of O_2, H_2, and noble gases (Ar and He) were examined. A discussion of their effects on the etch rate and plasma are given in the following sections.

O_2 Addition

Oxygen was added to CHF_3, SF_6, and NF_3 plasmas and varied from 0-90%, 0-60%, and 0-50%, respectively. When etching SiC in a fluorinated plasma, the addition of O_2, as mentioned previously, can enhance the etch rate due to O_2 reacting with unsaturated fluoride compounds to form reactive F atoms and because the removal efficiency of C (as CO or CO_2) is improved. The decrease in etch rate at higher O_2 concentrations can be attributed to the dilution of the reactive gas, the efficiency of C-O reactions compared to C-F reactions, and the fluorine intensity of the species gas. It has been observed that C is removed by C-F reactions at low O_2 concentrations and by C-O reactions at high O_2 concentrations but the SiC etch rate decreases as O_2% increases above a certain level indicating that C-O reactions are not as efficient as C-F reactions [5].

In this work, the etch rate increased up to 60% O_2 concentration to 1254 Å/min. and then decreased as additional O_2 was added in a CHF_3 plasma. The initial increase in etch rate is explained by the increase in reactive F atoms and removal efficiency of C. The decrease in etch rate is explained by the dilution of the reactive gas (reactive F concentration) and lower C-O reaction efficiency. The peak etch rate occurring at a high (60%) O_2 concentration is due to the fact that CHF_3 is a low fluorine intensity gas. High etch rates have been reported in low fluorine intensity gases at high O_2% (60 to 80%) [5]. While C-O reactions are less efficient than C-F reactions, the higher rate of C-O reactions compared to C-F reactions in low fluorine intensity gases can be the cause for the increase in etch rate up to high O_2 concentrations. In contrast, the etch rate may not increase at an O_2 concentration in high fluorine intensity gases.

O_2 addition in high fluorine intensity gases, such as SF_6 and NF_3, was also examined. The etch rate increased up to 20% O_2 concentration in SF_6 to 4314 Å/min. and up to 30% O_2 concentration to in NF_3 to 1255 Å/min. (at 25 mTorr) and then decreased as additional O_2 was added. The increase and eventual decrease of the etch rate is again believed to be related to the increase in reactive F and removal efficiency of C and the dilution of the reactive gas and lower C-O reaction efficiency, respectively. The peak in etch rate at lower O_2 concentrations (compared to 60% in CHF_3) is due to the fact that SF_6 and NF_3 are high fluorine intensity gases. High etch rates at low percent O_2 in CF_4, NF_3, and SF_6 have been observed because these gases produce high fluorine intensity [5]. This can be attributed to the large number of C-F reactions at the lower O_2% and their efficiency. In the case of the NF_3 plasma at 2 mTorr no increase was observed with the O_2 additive. This can be due to the etch process being dominated by physical mechanism as compared to chemical mechanisms.

H_2 Addition

The addition of H_2 in the CHF_3 plasma resulted in a slight increase of etch rate at 10% H_2 concentration to 894 Å/min., beyond this point the etch rate decreased to a low of 16 Å/min. at 45% H_2 concentration. The addition of H_2 results in a decrease in the etch rate because the H reacts with F atoms reducing the amount of reactive species in the plasma to etch the material. The further reduction in etch rate is likely due to increased polymer formation on the etch surface from fluorocarbon species, as was discussed in Chapter 2.

He and Ar Addition

The addition of He and Ar into the NF_3 plasma in this work had little or no affect on the etch rate. Other work [13] has reported few affects from gas additives in NF_3 at a high top power (ICP coil power) of 750 W. This is believed to be due to the relatively high dissociation of NF_3 at these high power levels which makes the additive less important [13]. Maximum etch rates of 1195 Å/min. at 2 mTorr and 1978 Å/min. at 25 mTorr were observed at 0% and 10% Ar concentration, respectively. No increase of etch rate was observed when He was added to NF_3 at 2 mTorr.

The addition of diluent gases at low pressure conditions (2 mTorr, for example) will typically not provide the benefit they afford at higher pressures [32]. Noble gases (Ar and He) are beneficial due to the modification of the gas phase chemistry occurring in the volume of the plasma; more specifically, the change in the electric field to number density ratio (E/n) [32]. At higher pressures (25 mTorr, for example) the addition of noble gases can increase the discharge E/n resulting in an increase of desired fragments of the gases (F versus SF_x, for example) which are more efficient for etching SiC [32]. At low pressures (2 mTorr, for example), E/n is large and not affected much by the addition of noble gases [32]; therefore, little or no variation of the etch rate is observed. As previously mentioned, the etch process at low pressures can be dominated by physical mechanisms instead of chemical mechanisms also resulting in less affect of gas additives. The decrease in etch rate caused by additives at both 2 and 25 mTorr is due to the dilution of the reactive gas.

Gas Flow

The etch rate increased up to approximately 30 sccm of SF_6 flow before saturating at higher gas flow rates. The peak etch rated obtained under these conditions was 3867 Å/min. As mentioned in Chapter 2, the initial increase in etch rate can be attributed the limited supply of reactants to etch the material. The additional supply from higher gas flows increases the etch rate. Once enough reactants are supplied additional gas flow rates have little affect on the etch rate, which saturates and thus indicates that other rate limiting processes are at work. This is due to the gas exiting the system before having time to react. Basically, the "resident time" is not matched to the reaction rates in the reactor above certain flow rates.

Bottom Electrode Power

An increase in etch rate with increasing bottom electrode power was also observed in a CHF_3 plasma at 25 mTorr. The etch rate ranged from approximately 384 to 854 Å/min. with a power variation of 50 to 250 W. The sidewalls also became more anisotropic with increasing bottom electrode power. The increase in etch rate and anisotropy of the etch profile is attributed to the increase in bottom power which increases the ion energy to the substrate resulting in higher contribution from the physical etch mechanisms as opposed to chemical etch mechanisms and a more anisotropic pattern character of the sidewall [32] due to increased directionality of the ions.

Surface Morphology

In all cases, except with high H_2 concentration where polymerization occurred, the surface morphology was very good. Residue-free etches were obtained with many

different gas mixtures and processing parameters. One problem that was continually observed was trenching at the sidewall. As previously mentioned this, is a problem commonly observed in ICP etching. Table 4.1 summarizes the cases where trenching did and did not occur and provides suspected variables for the occurance of trenching for the conditions specified in the etch matrix which given in Table 3.1. In the SF_6:He:O_2 plasma, trenching was observed for all pressures above 2 mTorr. No trenching was observed with the CHF_3:O_2 plasma until 60% O_2 concentration. Trenching was very pronounced at 10 to 30% H_2 concentration in the CHF_3:H_2 plasma until polymerization became the dominate factor in the etch above 30% H_2 concentration. Trenching was also observed for all cases in the SF_6:O_2 plasma at 25 mTorr. No trenching was observed in the NF_3:Ar plasma with an Ar concentration range of 20% to 40% at both 2 and 25 mTorr. Trenching was more pronounced at 2 mTorr with 10% Ar concentration but not at 50% Ar concentration. Trenching occurred for all cases in the NF_3:O_2 plasma at 2 and 25 mTorr except at 40% and 50% O_2 concentration at 25 mTorr. It seemed to be more pronounced at 2 mTorr. No instances of trenching were observed in the NF_3:He plasma. It is important to point out that the aspect ratio was low on the etch samples (1/200). When the aspect ratio becomes higher (3/1 between the fingers and 3/100 at the ends of the fingers) as observed in the VJFET trench etches, it becomes more difficult to preventing trenching. Other parameters to remember when considering trenching is ion bombardment energy and those parameters which effect ion bombardment energy, such as bottom power and plasma chemistry. High ion bombardment energy is the basis for etching in a RIE system, where trenching appears to be less of a problem. In the etch matrix, trenching was observed in cases when the only parameter that was varied was the

Table 4.1

Summary of Trenching (For etch conditions specified in Table 3.1)

Plasma	No trenching	Trenching	Suspected Variables
SF_6:He:O_2 (15:13.5:1.5 and 10:9:1)	At 2 mTorr pressure	All pressures (5, 10, 15, 25, 50) above 2 mTorr	Chemistry of the plasma
CHF_3:O_2 (25 mTorr)	Up to less than 60% O2 concentration	60% to 80% O_2 concentration	Chemistry of the plasma
CHF_3:H_2 (25 mTorr)	Up to less than 10% H2 concentration	10% to 30% H_2 concentration, then polymerization became dominant process	Chemistry of the plasma
SF_6:O_2	-	All O_2 concentrations	Chemistry of the plasma
NF_3:O_2	40% to 50% O2 concentration at 25 mTorr	All O_2 concentrations at 2 mTorr and up to less than 40% O_2 concentration at 25 mTorr	Chemistry of the plasma
NF_3:Ar	20% to 40% Ar concentration	10% and 50% Ar concentration	Chemistry of the plasma
NF_3:He	All cases of He concentration at 2 mTorr	-	-

plasma chemistry. Plasma chemistry can effect ion bombardment because different chemistries result in different dc bias values (measured value which can be used to determine ion bombardment energy). It was not possible to measure the dc bias in the Lam TCP 9400SE II system; therefore, no conclusive evidence supporting this claim can be presented.

CHAPTER V

CONCLUSIONS

This work presented the results of over 90 SiC etches performed in a Lam TCP 9400SE II etch system, which was modified for SiC etching. Several etch parameters (carrier material, pressure, gas additives, gas flow, and bottom electrode power) were examined and presented. An efficient carrier material (graphite) and operating pressure (25 mTorr) to achieve peak etch rates were determined from this work for the Lam TCP 9400SE II etch system. The peak flow rate (at 25 mTorr) in the system at which gas is effectively reacting before being pumped out of the chamber was determined to be approximately 30 sccm (for a pure SF_6 plasma).

The trends observed with the variation of parameters in this work followed the predicted trends presented in other literature. For this work and particular etch system, peak etch rates of 1254 Å/min. in CHF_3:O_2, 4314 Å/min. in SF_6:O_2, and 1255 Å/min. in NF_3:O_2 plasmas were obtained at 25 mTorr with 60%, 20%, and 30% O_2 concentrations, respectively, and 1978 Å/min. in a NF_3:Ar plasma with 10% Ar concentration. Gas additives were determined to have little or no effect in enhancing the etch rate at low pressures (2 mTorr). The addition of H_2 in CHF_3 plasmas resulted in severe polymerization when the concentration of H_2 was 60% or greater. Increased power on

the bottom electrode resulted in higher etch rates from increased ion bombardment and more anisotropic etch profiles.

As mentioned, trenching is a severe problem for device fabrication and performance. It was difficult to determine the exact trend of trenching effects in this work but it was observed that no trenching occurred in SF_6:He:O_2 plasmas at 2 mTorr, CHF_3:O_2 plasmas with the O_2 concentration below 60%, CHF_3:H_2 plasmas with the H_2 concentration below 10%, NF_3:O_2 plasmas with 40% and 50% O_2 concentration at 25 mTorr, NF_3:Ar plasmas with the Ar concentration between 20% and 40%, and all NF_3:He plasmas on structures with low aspect ratios (1/200).

Specific etches were performed for a VJFET trench etch using SF_6 and NF_3:He plasmas and also found to produce trenching. It is important to note that the aspect ratio is much higher for these etches (3/1 between the fingers and 3/100 at the ends of the fingers) compared to the etch matrix (1/200). Other variables, as noted in Table 4.1, were also suspected of influencing the occurance of trenching and should be carefully controlled in future etch development.

After examining the work presented, some etch chemistries and conditions are presented in Table 5.1 which would allow SiC etches to be achieved which independently have high etch rates, residue-free surfaces, and no trenching.

Future work should include a careful study of the trench-influencing parameters to determine their exact effects on trenching. Work should also be performed to determine residues left on the surface after etching with particular gas mixtures and surface roughness resulting from the etches, which has been found to greatly impact device performance.

Table 5.1

Recommended Etch Chemistries and Conditions

Parameter	Plasma Chemistry	Etch Conditions
High etch rates	SF_6:He:O_2	Pressure: 25 mTorr, Top Power: 750W, Bottom Power: 250W, Electrode Temperature:10^{o}C, Carrier: Graphite, Total Gas Flow: 30 sccm, Gas Ratio: (15:13.5:1.5)
	SF_6:O_2	Pressure: 25 mTorr, Top Power: 750W, Bottom Power: 250W, Electrode Temperature:10^{o}C, Carrier: Graphite, Total Gas Flow: 30 sccm, Gas Ratio: (24:6)
Residue-free surface	CHF_3:O_2	Pressure: 25 mTorr, Top Power: 750W, Bottom Power: 250W, Electrode Temperature:10^{o}C, Carrier: Graphite, Total Gas Flow: 30 sccm, Gas Ratio: 0 to 50% O_2
	NF_3:Ar	Pressure: 2 and 25 mTorr, Top Power: 750W, Bottom Power: 250W, Electrode Temperature:10^{o}C, Carrier: Graphite, Total Gas Flow: 30 sccm, Gas Ratio: (27:3) and (24:6)
	NF_3:He	Pressure: 25 mTorr, Top Power: 750W, Bottom Power: 250W, Electrode Temperature:10^{o}C, Carrier: Graphite, Total Gas Flow: 30 sccm, Gas Ratio: (27:3)
No trenching	NF_3:He	Pressure: 25 mTorr, Top Power: 750W, Bottom Power: 250W, Electrode Temperature:10^{o}C, Carrier: Graphite, Total Gas Flow: 30 sccm, Gas Ratio: (27:3)
	CHF_3:O_2	Pressure: 25 mTorr, Top Power: 750W, Bottom Power: 250W, Electrode Temperature:10^{o}C, Carrier: Graphite, Total Gas Flow: 30 sccm, Gas Ratio: (15:15)

REFERENCES

[1] Yoon Soo Park, *SiC Materials and Devices, Semiconductor and Semimetals*, vol. 52, San Diego: Academic Press, 1998.

[2] Stephen J. Pearton, *Processing of Wide Band Gap Semiconductor*, Norwich: Noyes Publications, 2000.

[3] H. Morkoc, S. Strite, G.B. Gao, M.E. Lin, B. Sverdlov, and M. Burns, "Large-band-gap SiC, III-V nitride, and II-VI ZnSe-based semiconductor device technologies," *J. Appl. Phys.*, vol. 76, no. 3, 1994.

[4] H. Matsunami, "Silicon Carbide Technology in New Era," *Materials Science Forum*, vols 389-393, pp. 3-8, Switzerland: Trans Tech Publications, 2001.

[5] P.H. Yih, V. Saxena, and A.J. Steckl, "A Review of SiC Reactive Ion Etching in Fluorinated Plasmas," *Phys. Stat. Sol. B*, vol. 202, pp. 605-642, 1997.

[6] S. Yoshida, S. Nishino, H. Harima, and T. Kimoto, "Reactive Ion Etching Process of 4H-SiC Using the CHF_3/O_2 Mixtures and a Post-O_2 Plasma-Etching Process," *Materials Science Forum*, vols 389-393, pp. 949-952, Switzerland: Trans Tech Publications, 2002.

[7] Jung Gyun Song and Moo Whan Shin, "Photoelectrochemical Etching Process of 6H-SiC Wafers Using HF-based Solution and H_2O_2 Solution as Electrolytes," *Materials Science Forum*, vols 389-393, pp. 957-960, Switzerland: Trans Tech Publications, 2002.

[8] J.S. Shor, R.M. Osgood, and A.D. Kurtz, "Photoelectrochemical conductivity selective etch stops for SiC," Applied Physics Letters, vol. 60, no. 8, pp. 1001-1003, 1992.

[9] M. Kothandaraman, D. Alok, and B.J. Baliga, "Reactive Ion Etching of Trenches in 6H-SiC, " *Journal of Electronic Materials*, vol. 25, no. 5, pp. 875-878, 1996.

[10] P.H. Yih and A.J. Steckl, "Residue-Free Reactive Ion Etching of 3C-SiC and 6H-SiC in Fluorinated Mixture Plasmas," *J. Electrochem. Soc*., vol. 142, no. 8, pp. 2853-2860, 1995.

[11] P.H. Yih and A.J. Steckl, "Effects of Hydrogen Additive on Obtaining Residue-Free Reactive Ion Etching of β-SiC in Fluorinated Plasmas," *J. Electrochem. Soc*., vol. 140, no. 6, pp. 1813-1824, 1996.

[12] J.B. Casady, E.D. Luckowski, M. Bozack, D. Sheridan, R.W. Johnson, and J.R. Williams, "Etching of 6H-SiC and 4H-SiC using NF3 in a Reactive Ion Etch System," *J. Electrochem. Soc*., vol. 143, no. 5, pp. 1750-1753, 1996.

[13] J.J. Wang, E.S. Lambers, S.J. Peartion, M. Ostling, C.M. Zetterling, J.M. Grow, F. Ren, and R.J. Shul, "High Rate Etching of SiC and SiCN in NF_3 Inductively Coupled Plasmas," *Solid-State Electronics*, vol. 00, no. 0, pp.1-5, 1988.

[14] L. Cao and J.H. Zhao, "Dry Etching of 6H-SiC using Inductively Coupled Plasma," submitted to *IEEE Electron Device Letters*.

[15] F.A. Khan and I. Adesida, "High rate etching of SiC using inductively coupled plasma reactive ion etching in SF_6-based gas mixtures," Applied Physics Letters, vol. 75, no. 15, pp. 2268-2270, 1999.

[16] Bum Seok Kim, Jae Kyeong Jeong, Myung Yoon Um, Hoon Joo Na, In Bok Song, and Hyeong Joon Kim, "Electrical Properties of 4H-SiC Thin Films Reactively Ion-Etched in SF_6/O_2 Plama," *Materials Science Forum*, vols 389-393, pp. 953-956, Switzerland: Trans Tech Publications, 2002.

[17] H. Cho, P. Leerungnawarat, D.C. Hays, and S.J. Pearton, "Ultra-deep, low-damage dry etching of SiC," Applied Physics Letters, vol. 76, no. 5, pp. 739-741, 2000.

[18] Binghui Li, Lihui Cao, and Jian H. Zhao, "Evaluation of damage induced by inductively coupled plasma etching of 6H-SiC using Au Schottky barrier diodes," Applied Physics Letters, vol. 73, no. 5, pp. 653-655, 1998.

[19] Lin Zhu and T. Paul Chow, "Design and Processing of High-Voltage 4H-SiC Trench Junction Field-Effect Transistor," *Materials Science Forum*, vols 389-393, pp. 1231-1234, Switzerland: Trans Tech Publications, 2002.

[20] R.N. Gupta, H.R. Chang, E. Hanna, and C. Bui, "A 600 V SiC Trench JFET," *Materials Science Forum*, vols 389-393, pp. 1219-1222, Switzerland: Trans Tech Publications, 2002.

[21] S.-M. Koo, S.-K. Lee, C.-M. Zetterling, M. Ostiling, U. Forsberg, and E. Janzen, "Influence of Trenching Effect on the Characteristics of Buried-Gate SiC Junction Field-Effect Transistors," *Materials Science Forum*, vols 389-393, pp. 1235-1238, Switzerland: Trans Tech Publications, 2002.

[22] S.M. Rossnagel, J.J. Cuomo, and W.D. Westwood, *Handbook of Plasma Processing Technology*, New Jersey: Noyes Publications, 1990.

[23] J.W. Coburn, Plasma Etching and RIE: The Fundamentals, AVS Short Course Program, Baltimore, Maryland, 1998.

[24] Graham W. Hills, and Joel M. Cook, "Plasma Etching," *Handbook of Semiconductor Manufacturing Technology*, pp. 655-685, New York: Marcel Dekker Inc., 2000.

[25] W.N.G. Hitchon, *Plasma Processes For SemiconductorFabrication*, Cambridge: Cambridge, 1999.

[26] W. Chen, B. Abraham-Shrauner, and J.R. Woodworth, "Model etch profiles for ion energy distribution functions in an inductively coupled plasma reactor," *J. Vac. Sci. Technol. B*, vol. 17, no. 5, pp. 2061-2069, 1999.

[27] N. Forgotson, V. Khemka, and J. Hopwood, "Inductively coupled plasma for polymer etching of 200 mm wafers," *J. Vac. Sci. Technol. B*, vol. 14, no. 2, pp. 732- 737, 1996.

[28] Stephen A. Campbell, *The Science and Engineering of Microelectronic Fabrication*, pp. 259-273, New York: Oxford University Press, 1996.

[29] G. McDaniel, J.W. Lee, E.S. Lambers, S.J. Pearton, P.H. Holloway, F. Ren, J.M. Grow, M. Bhaskaran, and R.G. Wilson, "Comparison of dry etch chemistries for SiC," J. Vac. Sci. Technol. A, vol. 15, no. 3, pp. 885-889, 1997.

[30] Russ A. Morgan, Plasma Etching in Semiconductor Fabrication, Plasma Technology, vol. 1, pp. 24-36, Amsterdam:Elsevier, 1986.

[31] J. D. Scofield, P. Bletzinger, and B.N. Ganguly, "Oxygen-free dry etching of α-SiC using dilute SF_6:Ar in an asymmetric parallel plate 13.56 MHz discharge," Applied Physics Letters, vol. 73, no. 1, pp. 76-78, 1998.

[32] Dr. James Scofield, Private Communication, 10/16/2002.

[33] M.M. Moslehi, R.A. Chapman, M. Wong, A. Paranjpe, H.N. Najm, J. Kuehne, R.L. Yeakley, and C.J. Davis, "Single-Wafer Integrated Semiconductor Device Processing," *IEEE Transactions on Electron Devices*, vol. 39, no. 1, pp. 4-30, 1992.

[34] M.F. Doemling, N.R. Rueger, G.S. Oehrlein, and J.M. Cook, "Photoresist erosion study in an inductively coupled plasma reactor employing CHF_3," *J. Vac. Sci. Technol. B*, vol. 16, no. 4, 1998.

APPENDIX A

PLASMA FUNDAMENTALS

Plasma "partially ionized gas" Fundamentals

Plasma, a partially ionized gas, is a collection of electrically charged and neutral particles in which the density of negatively charged particles is equal to the density of positively charged particles [22]. Plasma used in semiconductor processing is commonly referred to as "Glow Discharge." The types of process that occur in a glow discharge are shown in Table A.1. The dissociated atoms or molecular fragments are called radicals. These species are very reactive because they have an incomplete bonding state.

The neutral gas pressure is typically 1 mTorr to 100 mTorr and the electron density, n, of the plasma is typically 10^8 cm^{-3} to 10^{12} cm^{-3} [25]. A universal characteristic of plasma is that free charges in the plasma move in such a way as to decrease the effect of any electric field applied to it [22]. Therefore, when a field is applied to plasma it only has areas of excessive positive or negative charge for a limited time before the electrons move to cancel out the charge imbalance or at least minimize the effects of the field. If a positive charge is put into a quasineutral plasma then the electrons would collect around it to cancel out its electrostatic field. The potential field around that charge will be modified from its free space values by attenuating it exponentially with a characteristic decay length of λ_D (Debye length) [22]. The Debye length is given by

$$l_D = 743\ (T_e(eV) / n(cm^{-3}))^{1/2} \qquad \text{(A.1)}$$

where Te is defined as the equilibrium temperature and n is defined as the electron concentration. The Debye length ranges from 0.01 to 1 mm for semiconductor processing plasmas [22]. This effect of shielding out a charge is called Debye shielding and characterizes how plasma responds to an electric field [22]. The process of shielding

Table A.1

Processes in a Glow Discharge

After [28]

Process	Example
Dissociation	$e^* + AB \leftrightarrow A + B + e$
Atomic Ionization	$e^* + A \leftrightarrow A^+ + e + e$
Molecular Ionization	$e^* + AB \leftrightarrow AB^+ + e + e$
Atomic Excitation	$e^* + A \leftrightarrow A^* + e$
Molecular Excitation	$e^* + AB \leftrightarrow AB^* + e$

"*" refers to a species whose energy is much larger than the ground state

is not instantaneous and occurs over a time, t_p, which is defined by

$$t_p = l_D / n = (e_o me) / (ne^2))^{1/2} \quad \text{(A.2)}$$

where v is defined as the magnitude of the electron velocity and m is defined as the electron mass [22]. The electrons tend to overshoot the Debye length and end up oscillating. The frequency at which electrons oscillate is referred to as the plasma frequency, ω_p, which is given by the equation

$$w_p = t_p^{-1} = 5.64\ x10^4 \bullet (n(cm^{-3}))^{1/2} \quad \text{(A.3)}$$

Plasma is able to screen out an oscillating field with a frequency below ω_p, but electrons can not move fast enough to shield out a field with a frequency higher than ω_p [22].

After breakdown of the gas, plasma is sustained if the rate of ionization balances the losses due to diffusion to the walls, volume recombination, electron attachment, etc [22]. Diffusion loss typically dominates. Assuming that the diffusion coefficient and ionization rate are independent of position, the steady state diffusion equation is

$$\nabla^2 n = (n_i / D) / n , \quad \text{(A.4)}$$

where ν_i is the ionization rate. At the boundary of the plasma region, n = 0, the solution requires that

$$n_i / D = 1 / \Lambda^2 , \quad \text{(A.5)}$$

where the constant Λ depends on the geometry of the plasma. If it is cylindrical with the radius (R_D) much larger than the length (h_D) then

$$\Lambda = h_D / p . \quad \text{(A.6)}$$

If it long and has a small radius then

$$\Lambda = R_D / 2.405 \quad \text{(A.7)}$$

The ability to control the plasma behavior with a higher frequency RF source and the understanding of parameters which affect and control floating potential, plasma potential and self-bias voltage allow etching of materials to be optimized for many specific applications. In the following sections, a dc glow discharge, RF glow discharge, and plasma regions will be discussed.

DC Glow Discharge

Figure A.1 shows a simple plasma reactor with two parallel plates attached to a dc supply in a vacuum system. The plasma is started by a momentarily connected high voltage source (often a charged capacitor) [28]. The gas in the chamber acts as an insulator so it will not conduct until the discharge is established. When a voltage is applied that creates a field high enough to exceed the breakdown field of the gas a glow discharge will occur [28]. This results in a large number or ions and free electrons. The ions are accelerated towards the negatively charged cathode and the electrons are accelerated towards the positively charged anode because of the electric field in the chamber. Electrons travel much faster than ions because of their small mass but ions eventually strike the cathode releasing a group of secondary electrons from the cathode material which are accelerated back towards the anode [28]. The plasma is sustained if the voltage is high enough to result in these electrons energetically striking neutral atoms in the plasma and creating more ions and free electrons [28].

Distinct regions form due to the electric field caused by the mobility difference in the electrons and ions [25]. Figure A.2 shows the positive and negative charge as well as the electric field across the plasma. The high electron mobility will cause the electron

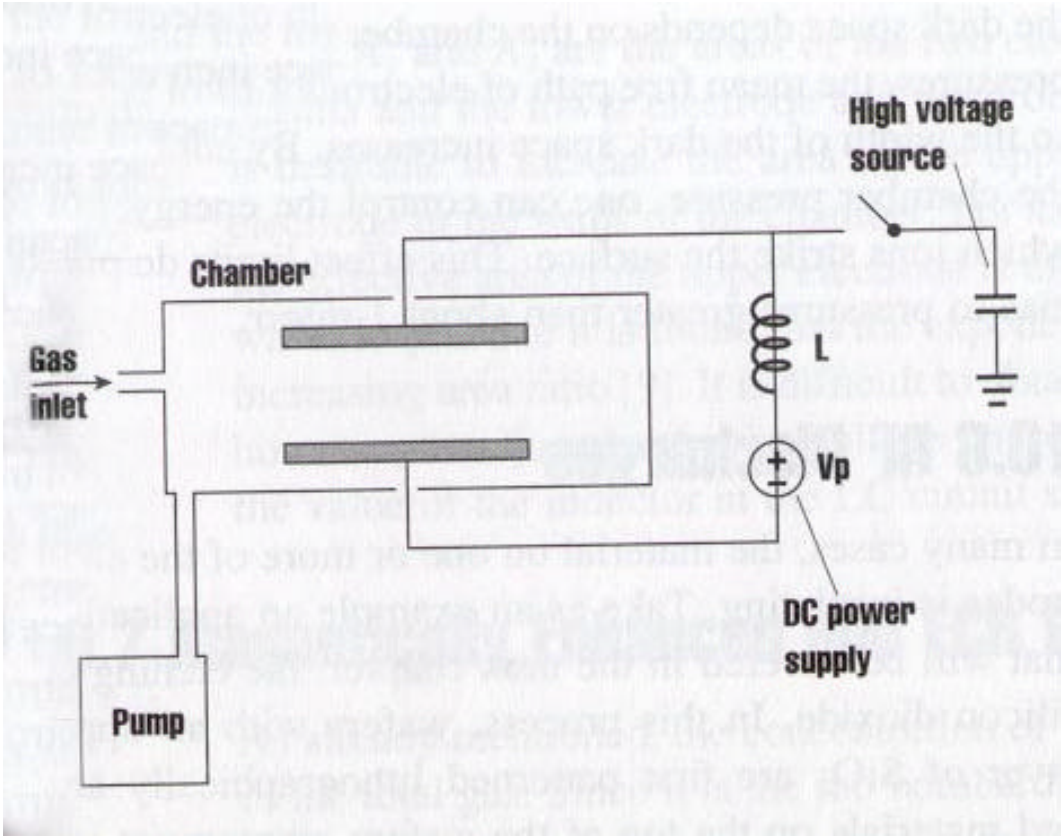

Figure A.1 DC parallel plate plasma reactor After [28]

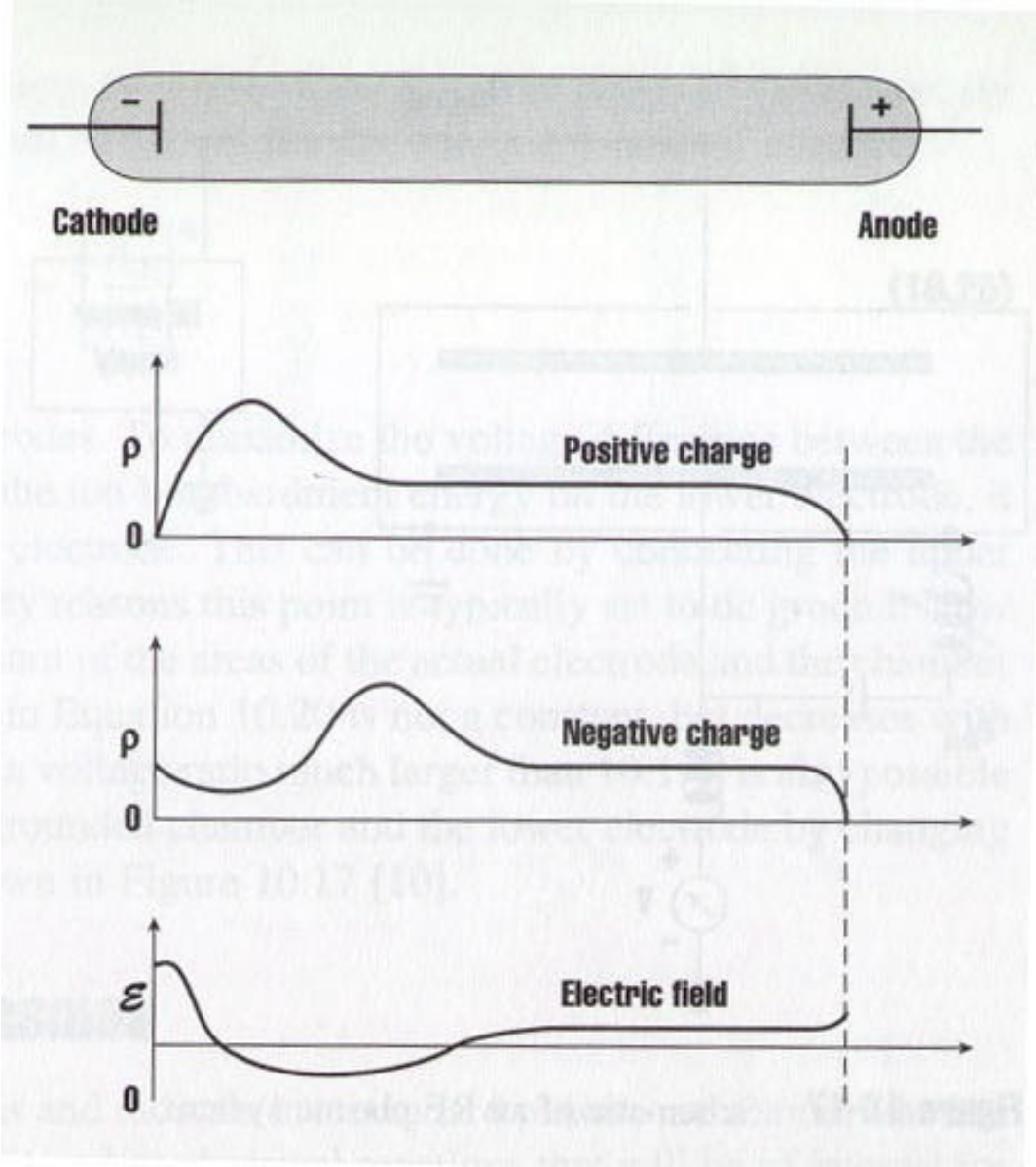

Figure A.2 Positive and negative charge densities and electric field as a function of position in a plasma After [28]

flux to be larger than the positive ion flux resulting in the walls or any insulating or unconnected surfaces in the glow discharge charging negatively [23]. The negative potential causes electrons to be repelled and positive ions to be attracted. This forms a positive region near the wall or surfaces called a "sheath." A strong electric field develops between the positive charges in the sheath and the electrons on the wall or surfaces. This field causes the arrival rates of electrons and ions from the bulk of the plasma to become equal. In the center of the plasma, the electric field is much weaker but usually points outward and helps pull the ions out toward the sheath where they are accelerated toward the surface being etched or the wall. When the electron and ion currents become equal, the plasma is in steady state [25]. The immediate flux of electrons to the wall causes the potential of the bulk plasma to become positive, but once the plasma is in steady state, it has a potential relative to the wall that is known as the plasma potential [25]. The region near the cathode has a net positive charge because the electron density is much less than the ion density due to the rapid acceleration of electrons away from the cathode [28]. The ion density increases with distance into the plasma from the cathode because electrons in the immediate region next to the cathode have enough energy to create ions; but after this peak in ion density, a lower constant ion density is observed throughout the rest of the plasma because the field and ionization rate is reduced due to the shielding affect of the positive charge at the cathode [28].

The regions that form in the plasma are shown in Figure A.3. If the energy is high the electrons strike neutral atoms to form ions. If it is moderate the electrons striking neutral atoms results in excitation instead of ionization [28]. In this case, light is emitted due to the optical emission process: electrons being excited to a higher energy

state and then decaying to their original state and releasing energy in the form of a photon. A large concentration of moderate energy electrons is required for appreciable emission [28]. At the cathode and anode no optical emission occurs so these regions are referred to as *dark spaces*. The *Crooke's dark space* is an area of very low electron energy above the cathode [28]. The *anode dark space* is an area above the anode where the electron density is too small for appreciable emission [28]. The *Faraday dark space* is the area above the cathode where the high energy electrons are causing ionization of neutral atoms instead of excitation [28].

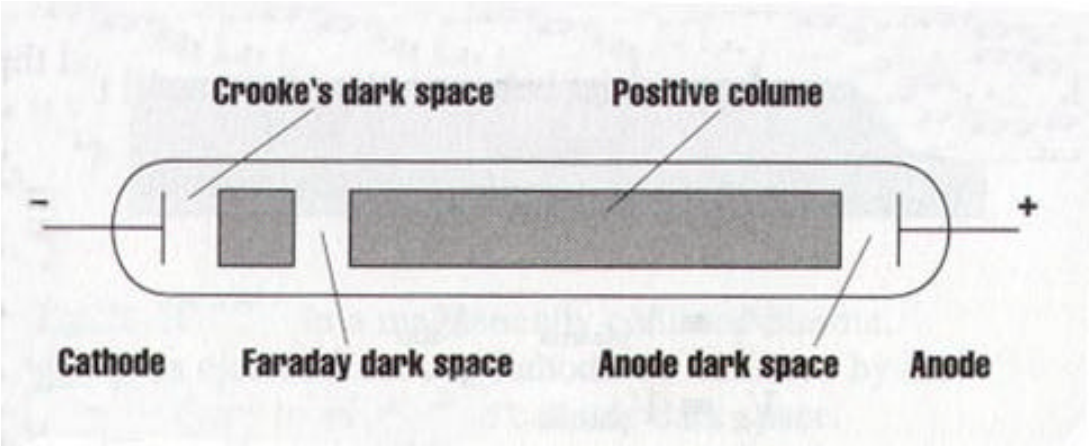

Figure A.3 Structure of a dc plasma After [28]

The *Crooke's dark space* is a region of great interest in plasma processing. A large electric field exists over this area which results in rapid acceleration of ions toward the cathode [28]. The pressure in the chamber is used to control the width of the dark space and therefore the energy which ions strike the cathode or any material placed on

the cathode [28]. With lower pressures, the mean free path of electrons increases and so the width of the dark spaces increases. In a dc plasma the pressure is limited to greater than 1 mTorr because of these effects.

RF Glow Discharge

Many electrodes or materials being etched are insulators, which become charged as ions strike them and secondary electrons are ejected [28]. A plasma in dc discharges is ultimately extinguished as charge accumulates on the surface and the field is reduced. To overcome this problem, plasmas can be driven by an ac source, which typically uses 13.56 MHz RF sources [28]. When a RF field is applied to a neutral gas, breakdown occurs from the oscillating electric field putting directed energy into electrons, which then heat up and collide with neutrals to form radicals and ions. The electric field resulting from an ac power source at frequency, ω, is

$$E = E_o \exp(j\omega t), \tag{A.8}$$

where $j = \sqrt{-1}$, and E_o is the amplitude of the field [22]. The electric field is changing directions therefore the motion and drift velocity of particles affected by the field will be oscillatory [22]. Solving the Langevin equation

$$(d/dt)(mu) = -eE - mun_N \tag{A.9}$$

results in the mobility and conductivity relations given by

$$m = e/m(n + jw), \tag{A.10}$$

and

$$s = ne^2/m(n + jw) \tag{A.11}$$

The input power (P_{in}) to the electrons is given by

$$P_{in} = ne^2 E_O{}^2 / (m n_{eff}), \quad \text{(A.12)}$$

where ν_{eff} is an "effective" collision frequency given by

$$n_{eff} = n(1 + (w/n)^2) \quad \text{(A.13)}$$

The maximum input power occurs when $\omega = \nu$ because the electrons are making approximately one collision for every cycle of the ac power which is the optimum for coupling energy from the electric field to the electrons [22].

A RF plasma system is shown in Figure A.4. The impedance between the plasma and power source are matched using a tuning network and the chamber is dc isolated from the supply using a blocking capacitor [28]. Plasma in this system follows the excitation and the width of the dark spaces pulse with the applied signal at low frequencies. At rates of excitation greater than 10 KHz, slow ions cannot follow the voltage change, but electrons are rapidly accelerated [28]. A net negative charge, with respect to the plasma, exists at both electrodes due to electrons striking each during alternate half cycles of the signal [28]. This results in dark spaces at each electrode. The dc voltage, as a function of position across the chamber, and RF signal are shown in Figure A.5. Because the plasma is conductive, the voltage drop across the glow discharge is small but it is large between the plasma and electrodes due to the electron depletion in these regions [28].

When the frequency of the RF power is higher the plasma frequency, ions have too much inertia to respond to the instantaneous electric field in the sheath region, but the electrons will respond. A time-average bias will arise due to the mobility differences in the electrons and ions and is referred to as the self-bias voltage [25]. This voltage, along

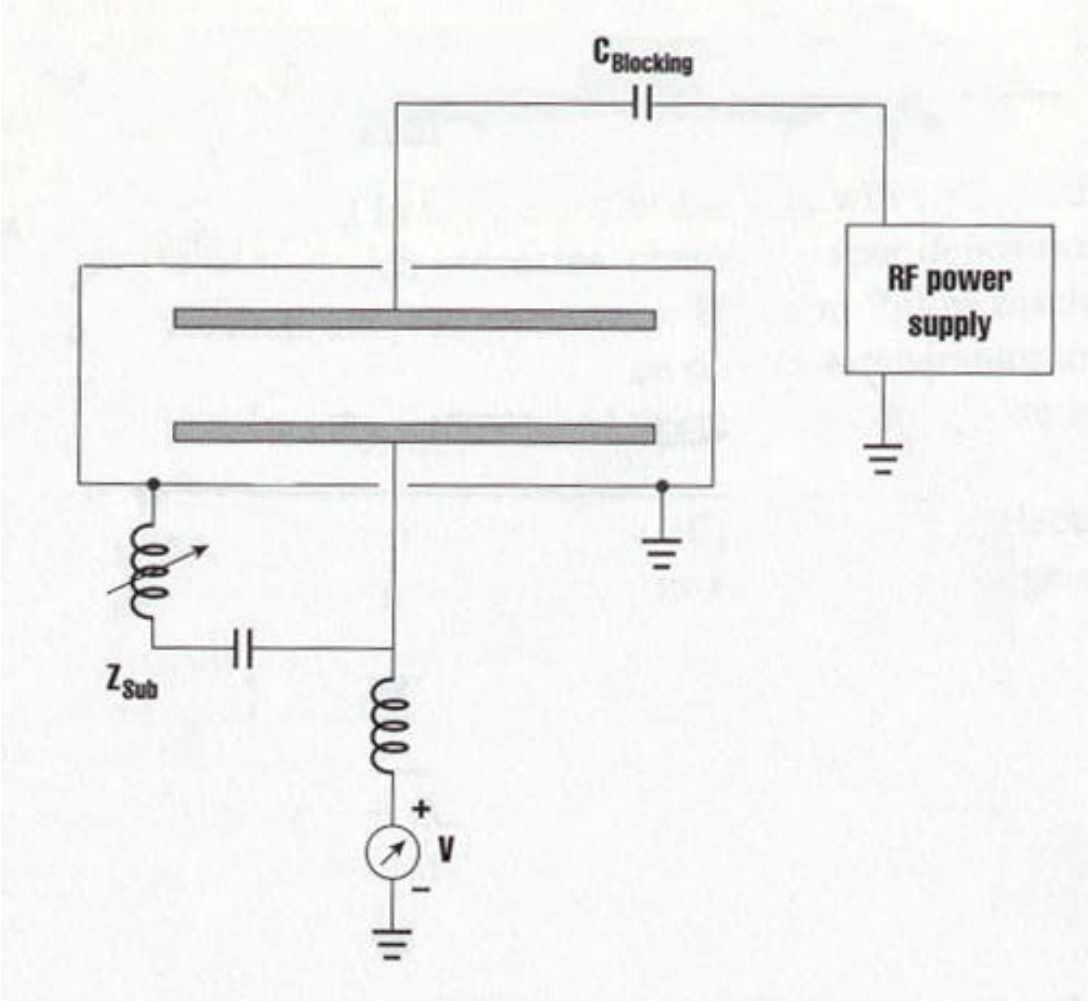

Figure A.4 Schematic of an RF plasma system After [28]

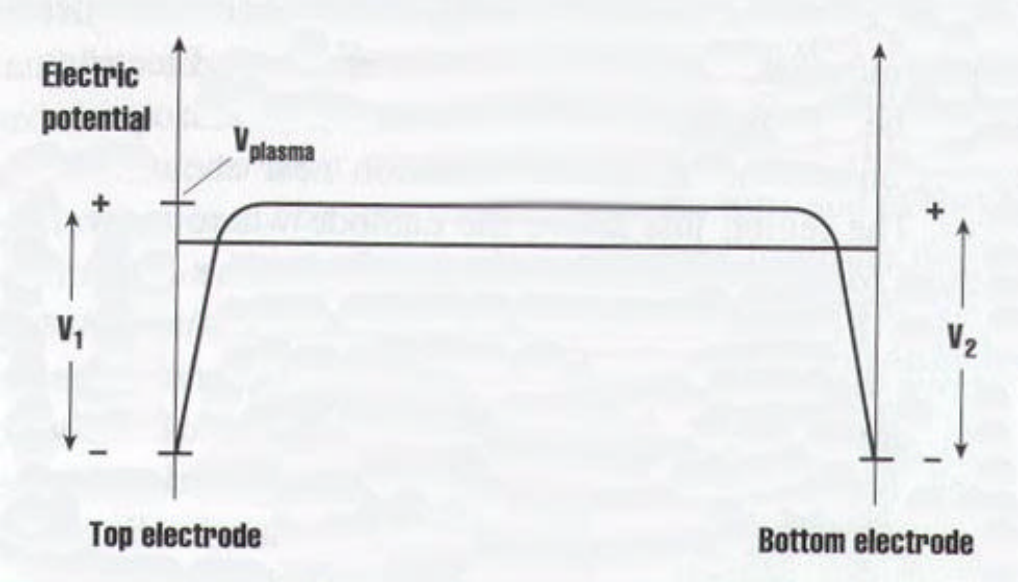

Figure A.5 Typical plot of dc voltage (with RF signal superimposed on top) as a function of position in an RF plasma After [28]

with the plasma potential, determines the ion energy present in the sheath region [34].

To better understand the chemistry of a glow discharge in a high pressure plasma etch system, it is useful to examine a practical example. In the following section the etch of silicon (Si) in a carbon tetrafluoride (CF_4) plasma is discussed since it is one of the most extensively studied systems.

Chemistry of a Glow Discharge in a High Pressure Etching Plasma

In the following prototype system example [28], it is assumed that a silicon wafer is being etched with a photoresist mask in a CF_4 plasma with a set chamber pressure of 500 mTorr. Etching occurs if silicon is volatized with a halogen which requires that Si-Si bonds are replaced with Si-halogen bonds. C-F bonds in CF_4 and Si-Si bonds require 105 kcal/mole and 42.2 kcal/mole, respectively, of energy to be broken. The sum of the two energies (~147 kcal/mole) must be less than the energy of the Si-F bond (130 kcal/mole) for silicon to be chemically etched by CF_4 at room temperature. Since the energy needed to etch the silicon is higher than the energy of the Si-F bond, it will not etch at room temperature. The equation to represent the energy balance at room temperature is shown below:

$$C\underline{\vee}F + Si\underline{\vee}Si = Si - F + 17 kcal/mole \qquad \text{(A.14)}$$

where $\underline{\vee}$ represents a bond breaking event. As previously mentioned, CF_4 will not etch silicon at room temperature but when placed in a plasma some of the CF_4 molecules are dissociated producing free molecular radicals (most commonly CF_3, CF_2, and C) and fluorine (F) atoms and resulting in the following energy balance equation:

$$Si\underline{\vee}Si = Si - F_4 = 17 kcal/mole\,. \qquad \text{(A.15)}$$

Most species in a typical plasma are unreacted gas molecules (having a density of $3x10^{16}$ cm^{-3} for this prototype example), but the density of chemically active species (which are referred to as neutral radicals) can be increased by optimizing the feed gas, chamber pressure, and plasma power. These neutral radicals are extremely reactive species and are the most common species after unreacted feed gas, making up approximately 5 to 10% of the species in the plasma. A rough estimate of the flux of radicals striking the surface of the material being etched can be determined by assuming a simple kinetic theory gas and using the following equation:

$$J_n = \sqrt{\frac{n^2 kT}{2pM}} \tag{A.16}$$

where n is electron density, k is the Boltzmann constant, T is temperature, and M is the neutral mass.

If we assume, for this example, that the radical species temperature is 500 K then the radical bombardment rate or flux due to simple diffusion is on the order of 10^{23} m^{-2}-sec^{-1}. The etch rate under these conditions, assuming that every radical that strikes the surface etches one silicon atom and that the radical flux is the rate limiting step, would be approximately 1000 Å/min. This etch rate would imply that a purely chemical process provides adequate etching, but this implication would be incorrect because not all radical species will stick to the surface to cause a reaction or even etch the silicon when present and some of the byproducts not only do not etch silicon by forming volatile species but actually diffuse to the surface. The resulting coating decreases the etch rate.

Another reaction in plasma etching is ion bombardment. Ions created in the plasma constantly bombard the surface resulting in damage. The dangling bonds that

result quickly react with radicals, which diffuse to the surface because of the concentration gradient in the plasma, and form volatile products which are pumped away. This reaction eliminates much of the energy penalty associated with the Si-Si bond breaking event; therefore energetically favoring chemical etching.

APPENDIX B

LAM 9400 TCP ETCHER

The following is a description of the 9400 etch systems manufactured by Lam Research Inc.; with a particular emphasis on the Lam 9400PTX and Lam 9400SE etch systems. Etching of polysilicon raises a number of critical issues, such as control of contamination and damage, because it is conducted on the wafer surface. Lam developed a series of high-density, poly etch systems (TCP® 9400-series) to address the issues that are critical to the poly etch process. Their chambers are ceramic-free with waferless auto cleans (WAC) which offer exceptionally clean and contamination-free processing for the industry. Higher throughput for the fab and excellent wafer surfaces are possible because of the flexible, in situ processing available with these systems. With the in situ capabilities and a single chamber. Lam systems are capable of the most advanced processes, such as rounding the top and bottom corners of isolating trenches surrounding individual transistors. Competitive systems often require separate chambers or even wet etch systems to accomplish these same results. Lam currently has more than 900 chambers installed worldwide.

The TCP 9400PTX process modules are used for all advanced poly and polysilicide gate and STI applications in device technologies down to 180 nm. The 9400PTX system has up to four process modules on an Alliance platform.

The system that was used in the etch development for this thesis is the TCP® 9400SE II. This system provides the same excellent performance for advanced gate and STI etch as the multichamber TCP 9400PTX, but is a single-chamber, standalone version of the system. Figures B.1 and B.2 are images of the TCP 9400SE II and the transport module in these systems, respectively.

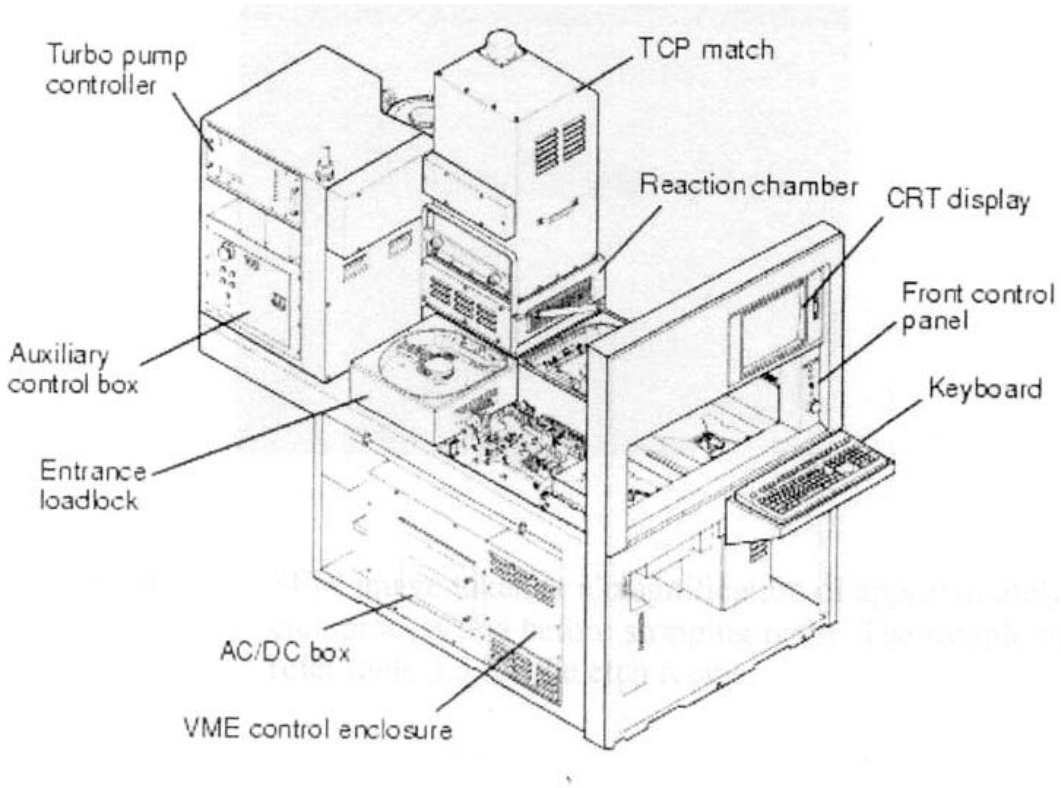

Figure B.1 Drawing of the Lam TCP 9400SE II System

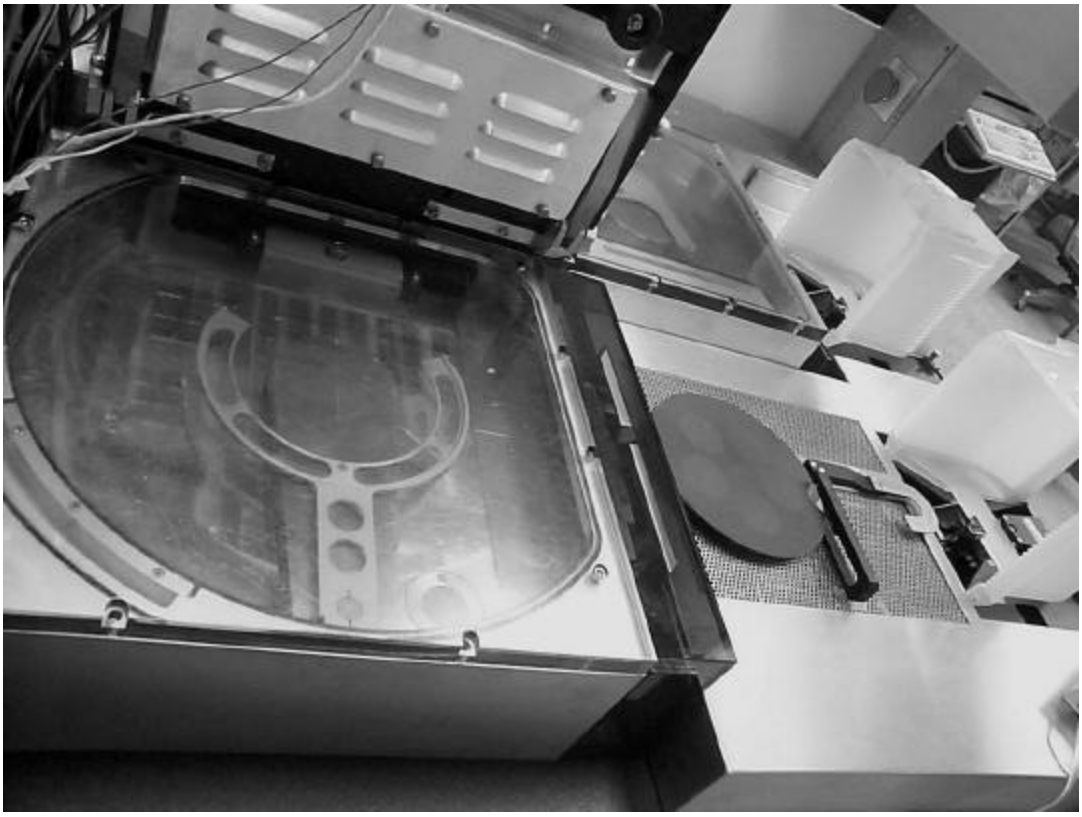

Figure B.2 Image of the Lam TCP 9400SE II Transport System

The physical dimensions and technical requirements (environmental, thermal output, power, coolant, vacuum, exhaust, nitrogen, process gases) according to the Lam manual for the Lam TCP 9400SE II system are provided in Tables B.1 thru B.9. In Table B.9, it is important to note that all gases are leak sensitive and require N_2 purge. Figure B.3 is a block diagram of the chamber and the parameters of interest in this work with the minimum and maximum ranges of operation are provided.

Table B.1

TCP 9400SE II Physical Dimensions

Equipment	Width Inch/cm	Depth inch/cm	Height inch/cm	Weight lb./kg
TCP 9400SE II	44.0/111.8	79.25/201.3	64.0/162.5	2220/999

Table B.2

TCP 9400SE II Environmental Requirements

Equipment	Temperature ^{o}C	Humidity %	Vibration Sensitivity
TCP 9400SE II	22+/-2	<50	Slight

Table B.3

TCP 9400SE II Thermal Output (BTU/hr)

Equipment	Carrier by Water	Carrier by Exhaust	Dispersed to Environment	Total Output
TCP 9400SE II	9400	8400	20,000	38,000
RF generator (two per etcher)	-	5000	3000	8000

Table B.4

TCP 9400SE II Power Requirements

Equipment	VAC	Hz	Phase	# of Cond.	Type	Power (amps) max/norm	Receptacle Required
TCP 9400SE II	208	50/60	3	5	Wye	80/63	Hardwired

Table B.5

TCP 9400SE II Coolant Requirements (Water Supply and Return)

Decription	Tube Fitting Compression	Flow	Temp ^{o}C	Pressure (PSI)	Filter μm	Type
Lower electrode (coolant-in)	1/2-inch	4 GPM	5-80	≤50	-	TCU
Lower electrode (coolant-out)	1/2-inch	4 GPM	5-80	≤50	-	TCU
Turbo cooling supply	3/8-inch	2 ± .5 LM	20 ± 10	40 ± 5	200	House
Turbo cooling return	3/8-inch	2 ± .5 LM	≤60	-	-	Non-hazard
Generator cooling supply	3/8-inch	2 GPM	20 ± 10	≤100	200	House
Generator cooling return	3/8-inch	2 GPM	-	-	-	Non-hazard

Table B.6

TCP 9400SE II Vacuum Requirements

Equipment	Connection	Pump-down time (760 to 0.1 torr)	Process Requirements		Ultimate Pressure	Pumping Volume (liters)
			Pressure	Flow @ Pressure		
Chamber	NW 40 (1.5-in tube)	≤30 sec.	≤1 torr	=250 sccm	-	22
Entrance and Exit Loadlock	NW 40 (2.0-in tube)	≤30 sec.	20 mtorr	2000 sccm	≤50 mtorr	35

Table B.7

TCP 9400SE II Exhaust Requirements

Equipment	Draw cu.ft./min (CFM)	Inches H_2O	Exhaust Connection	Hazard	Duct Size (OD) in/cm	Temp ^oC
Etcher, cabinet	300	0.5-0.7	House	-	4.0/10.2	Ambient
Etcher, gas panel	100	0.5-0.7	Scrubbed	Possible	4.0/10.2	Ambient
Upper RF match box	50	0.5-0.7	Scrubbed	Possible	4.0/10.2	Ambient

Table B.8

TCP 9400SE II Nitrogen Requirements

Description	Pressure psi	Pulsed Flow max. l/min. (LPM)	Type	Fitting Required size and type	Usage	Filter Required µm	Source
Etcher, Purge	20±5	8±2	Dry	1/4-inch VCR	Pulsed	0.05	House
Etcher, Vent	40±5	8±2	Dry	1/4-inch VCR	Pulsed	0.05	House
Turbo Pump, Ballast	20 to 100	5±2	Dry	1/4-inch compression	Pulsed	0.05	House
Etcher Pneumatic	90±20	10±4	Dry	3/8-inch compression	Pulsed	0.05	House or CDA

Table B.9

TCP 9400SE II Systems Common Process Gases and Requirements

Gas Name	Symbol	Purity %	Flow Rate (sccm)	Regulator Pressure (psi)	Filter (μm)	VCR size
Nitrogen	N	99.999	100	20	<0.05	.25-in
Argon	Ar	99.999	200	20	<0.05	.25-in
Helium	He	99.999	200	20	<0.05	.25-in
Helium (wafer cooling)	He	99.999	100	-15	<0.05	.25-in
Oxygen	O_2	99.995	200	20	<0.05	.25-in
Hydrogen	H_2	99.999	50	20	<0.05	.25-in
Sulfur Hexafluoride	SF_6	99.996	200	20	<0.05	.25-in
Nitrogen Trifluoride	NF_3	99.999	200	20	<0.05	.25-in
Trifluoromethane	CHF_3	99.999	50	20	<0.05	.25-in
Carbon Tetrafluoride	CF_4	99.999	200	20	<0.05	.25-in

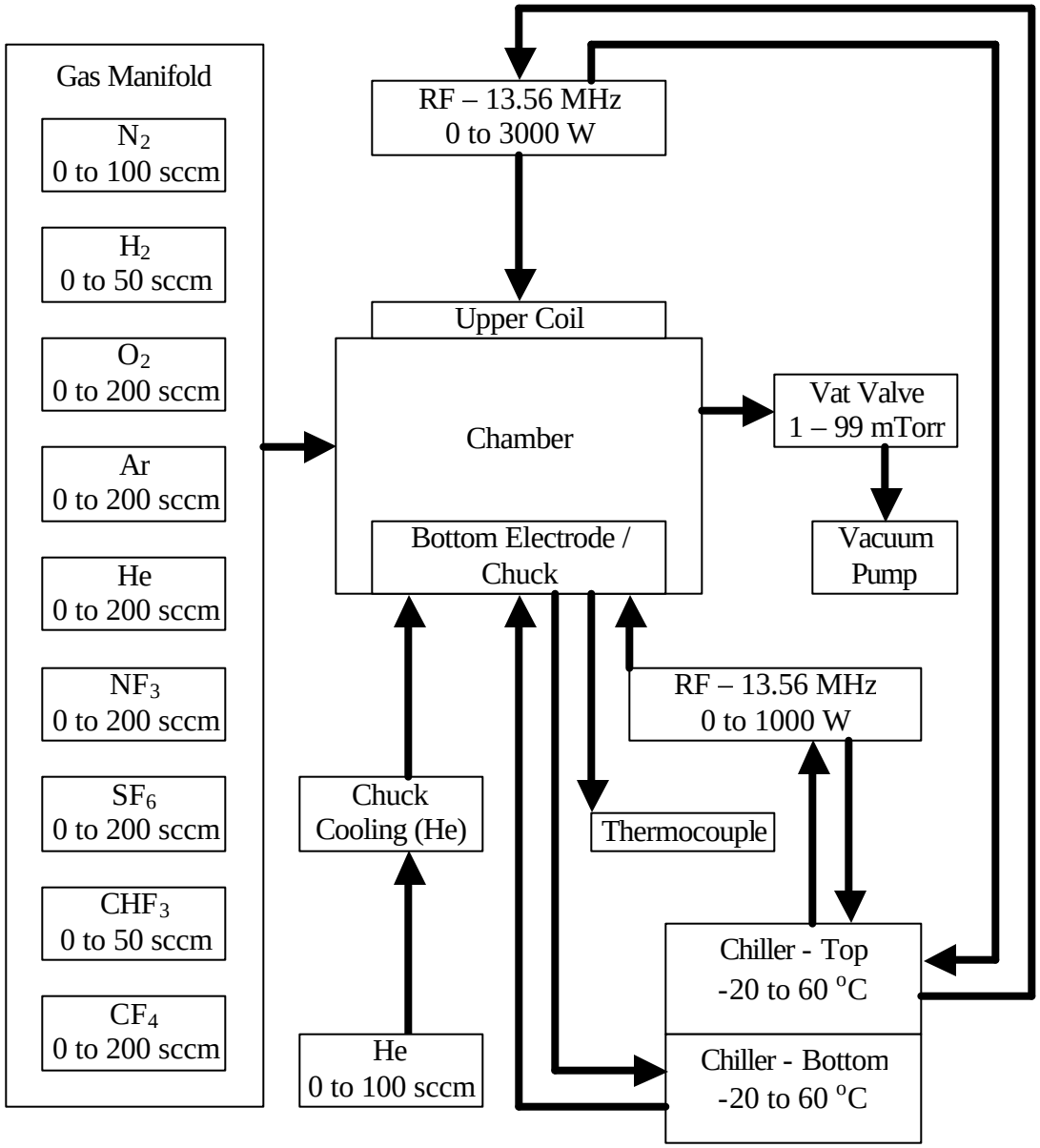

Figure B.3 Block Diagram of Parameters Associated with the Chamber of the TCP 9400SE II system